Osmosis in groundwater

Chemical and electrical extensions to Darcy's Law

Osmosis in groundwater

Chemical and electrical extensions to Darcy's Law

PROEFSCHRIFT

ter verkrijging van de graad van doctor
aan de Technische Universiteit Delft,
op gezag van de Rector Magnificus Prof. dr. ir. J.T. Fokkema,
voorzitter van het College voor Promoties,
in het openbaar te verdedigen op 4 oktober 2005 om 10.30 uur
door

Samuel BADER

doctorandus in de natuurkunde
geboren te Breda.

Dit proefschrift is goedgekeurd door de promotor

Prof. dr. ir. S.M. Hassanizadeh

Toegevoegd promotor

dr. R.J. Schotting

Samenstelling promotiecommissie:

Rector Magnificus,	voorzitter
Prof. dr. ir. S.M. Hassanizadeh,	Technische Universiteit Delft, promotor
Dr. R.J. Schotting,	Technische Universiteit Delft, toegevoegd promotor
Prof. dr. ir. P.A.C. Raats,	Wageningen Universiteit
Prof. dr. ir. P.H. Groenevelt,	University of Guelph
Prof. dr. ir. A. Leijnse,	Wageningen Universiteit
Dr. ir. J.P.G. Loch,	Universiteit Utrecht
Prof. dr. ir. F.B.J. Barends,	Technische Universiteit Delft
Prof. ir. C.P.J.W. van Kruijsdijk,	Technische Universiteit Delft, reservelid

Copyright © 2005 by S. Bader

Dit onderzoek kwam tot stand met steun van NWO

All rights reserved. No part of the material protected by this copyright notice may be reproduced or utilized in any form or by any means, electronic or mechanical, including photocopying, recording or by any information storage and retrieval system, without the prior permission of the author.

ISBN 90-9019900-4

Author email: samuelbader@gmail.com

"The wines were too various. It was neither the quality nor the quantity that was at fault. It was the mixture. Grasp that and you have the root of the matter. To understand all is to forgive all." Evelyn Waugh - Brideshead Revisited

Contents

1 Introduction **1**
- 1.1 Background . . . 1
- 1.2 Thesis outline . . . 4

2 Theory **5**
- 2.1 Osmosis . . . 5
  - 2.1.1 General assumptions . . . 7
  - 2.1.2 Clay characteristics . . . 7
  - 2.1.3 Clay scales . . . 8
  - 2.1.4 Swelling of clays . . . 9
  - 2.1.5 Diffuse double layer theory . . . 10
  - 2.1.6 Semi-permeability . . . 13
  - 2.1.7 Additional assumptions . . . 14
- 2.2 Coupled processes and applications . . . 14
  - 2.2.1 Chemical osmosis . . . 15
  - 2.2.2 Salt-sieving . . . 16
  - 2.2.3 Electrical effects: definitions . . . 17
  - 2.2.4 Electrical effects: applications . . . 17
- 2.3 Coefficients . . . 18
  - 2.3.1 Coefficient calculation methods . . . 18
  - 2.3.2 The reflection coefficient . . . 23
  - 2.3.3 Electro-osmotic permeability . . . 32
  - 2.3.4 Diffusion coefficient . . . 38
  - 2.3.5 Cation exchange . . . 41
  - 2.3.6 Electrical conductivity . . . 43
- 2.4 Summary . . . 45

3 Equations for chemical and electro-osmosis in soils **47**
- 3.1 Introduction . . . 47
- 3.2 Non-equilibrium thermodynamics . . . 47
  - 3.2.1 Validity of the Onsager relations and Saxen's law . . . 52

3.3 Equations for chemical osmosis . . . 54
3.3.1 Effective diffusivity for a semipermeable membrane . . . 57
3.3.2 Limiting behaviour for σ . . . 57
3.3.3 Concentration dependence of σ . . . 58
3.3.4 Effect of multiple ion species on osmosis . . . 58
3.4 Equations for chemico-electro-osmosis . . . 59
3.5 Mass balances . . . 61
3.6 Summary . . . 62

4 Mathematical analysis 65
4.1 Assumptions . . . 65
4.1.1 Peclet number . . . 65
4.1.2 Gravity . . . 66
4.1.3 Thermo-osmosis . . . 66
4.1.4 Fluid density . . . 67
4.1.5 Timescale of electric relaxation . . . 67
4.2 Equations . . . 68
4.2.1 Balance equations . . . 69
4.2.2 Equations of state . . . 69
4.2.3 Mathematical analysis . . . 70
4.3 Analytical solutions . . . 73
4.3.1 Time scales . . . 75
4.3.2 Limiting values of σ . . . 77
4.4 Applications of analysis . . . 78
4.4.1 Influence of coefficients on osmotic pressure . . . 78
4.4.2 Concentration dependent reflection coefficient . . . 80
4.4.3 Optimal osmotic pressure . . . 84
4.4.4 Tracer . . . 85
4.5 Conclusions . . . 88

5 Comparison with experiments [1] 89
5.1 Introduction . . . 89
5.2 Theory . . . 91
5.3 Analysis . . . 94
5.3.1 Balance equations . . . 94
5.3.2 Equations of state . . . 94
5.3.3 Mathematical analysis . . . 95
5.4 Results . . . 96
5.4.1 Keijzer experiments . . . 96
5.4.2 Neuzil model . . . 103
5.4.3 The Boussinesq limit . . . 107

5.5 Conclusions 108

6 Membrane potential **111**
6.1 Introduction 111
6.2 Derivation of an expression for membrane potential 112
6.3 Membrane potential and chemical osmosis 115
6.4 Membrane potential and diffusion 116
6.5 Experiments 118
6.5.1 Experimental setup 118
6.5.2 Experimental results 120
6.6 Measuring potentials 120
6.7 Membrane potential value 123
6.8 Modelling procedure 126
6.8.1 Equations 126
6.8.2 Model domain 126
6.8.3 Initial and boundary conditions 127
6.9 Modelling results for bentonite: high Δc 127
6.9.1 Pressure development 127
6.9.2 Membrane potential development 128
6.9.3 Concentration development 129
6.9.4 Coefficients 129
6.10 Modelling results for bentonite: low Δc 132
6.11 Results with homo-ionic clay 133
6.12 Conclusions 136

7 Modelling osmosis with METROPOL **139**
7.1 Introduction 139
7.2 The program 140
7.2.1 Routines 140
7.2.2 Numerical method: description 140
7.2.3 Numerical method: drawback 142
7.3 The adapted METROPOL equations 143
7.4 Test cases 147
7.4.1 Simple computational domain 147
7.4.2 Simple composite domain 153
7.4.3 Keijzer domain 153
7.5 Using METROPOL: conclusions 155

Summary **159**

Bibliography **159**

Samenvatting **163**

Glossary **167**

Nomenclature **173**

Curriculum Vitae **187**

189

Chapter 1

Introduction

1.1 Background

The notion of Darcy's Law describing flow of water in a porous medium, the water being driven through the soil from high to low hydraulic head, is of paramount importance in hydrology. Unknown to many however, in clayey soils, Darcy's Law does often not suffice. When instead, or aside from a head difference, variations in the salt concentration in the pore water exist, an additional flow of water may be present, which is caused by a process called osmosis. This phenomenon is known from chemistry and biology and it is sometimes associated with human cells, boats or animated movies. Osmosis in clay originates from the fact that clay can be seen as a semi-permeable membrane. Such a membrane (partly) restricts movement of solutes without hindering movement of solvent. Often, such restrictions are caused by the geometrical properties of a membrane, i.e. solute molecules may be larger than the pores of the membrane. Clay, on the other hand, is an example of a charged membrane: because clay consists of negatively charged platelets, ions passing through the clay are restricted by electrical repulsion. Hence, clay can act as a semi-permeable membrane and, provided the clay is subject to a salt concentration gradient, all conditions are met for osmosis.

This can be mathematically accounted for by extending Darcy's Law with a term depending on the salt concentration gradient and a reflection coefficient, a parameter that expresses the degree of semi-permeability of a membrane. However, it is well known that other physical driving forces may induce water movement as well. Examples are flow due to a temperature gradient and flow due to an electrical potential gradient. Exploiting the analogy with osmosis, these processes are called thermo-osmosis and electro-osmosis respectively. Because these somewhat misleading designations have permeated throughout the literature on coupled effects, 'regular' osmosis, in this study, is called chemical osmosis, whereas the term

osmosis is defined as non-hydraulic water flow in general.

In geohydrology, next to Darcy's Law to characterize groundwater movement, Fick's law is used to model transport of dissolved solutes. Analogous to the extensions of Darcy's Law, terms related to temperature, electrical potential and hydraulic gradients can be added to Fick's law. To complete this description: the same holds for Fourier's law (flow of heat) and Ohm's law (electrical current). Many of these in total 16 effects have been named after the 19-th century scientists who experimentally have shown the existence of these effects: e.g. Seebeck, Soret, Peltier and Dufour. Other phenomena are prosaically called membrane potential or electrophoresis. They were not necessarily discovered in soils as such: few studies on coupled phenomena in soils are known that were performed before 1950. The work of Casagrande [14],[15], dating from 1948 and 1949 respectively, was probably an important catalyst for the application of electrical effects in soils. The same can be said about the work of Hanshaw [43], some 14 years after this, for the advancement of the study on chemical osmosis in the subsurface. Especially in the sixties and the early seventies a multitude of studies on coupled effects was published in the literature [35],[24],[38],[65],[68],[69],[11]. The equations describing coupled effects were, starting in the fifties, usually based on non-equilibrium thermodynamics, on the subject of which a number of relevant books appeared during that time [62],[40],[25]. Finally, microscopic theories to explain electro-osmosis were known from the 19th century [53],[107],[102], but in the 1960s and 1970s, a number of theories were proposed that included chemical effects or provided a general description of coupled effects [29],[38],[11],[43].

What has been lacking in nearly all aforementioned studies is the incorporation of coupled effects in transient models that are able to predict and interpret simultaneous development of pressure, concentration, electrical potential and temperature. Some attempts were made in Mitchell et al. [82] where a one-dimensional model was used to investigate the pore pressure reduction in a clay layer subject to saline boundary conditions at top and bottom of this layer. The authors focused on chemico-osmotic consolidation of the layer and only presented non-dimensionalized and spatially averaged pore pressure and concentration changes in the clay layer. More recently, Soler [108] presented a one-dimensional model to study the role of coupled transport phenomena, including thermal osmosis, in radionuclide transport from a repository of high level nuclear waste in the Opalinus Clay, Switzerland. The model was reduced, however, to a conventional advection-diffusion problem with constant advection velocity, thereby negating the feedback of temporal and spatial changes in the concentration gradients contributing to osmotic transport. Sherwood [106] performed transient flow calculations expressed in terms of pressure and salinity values on either side of a membrane and therefore greatly simplified the full transient flow and transport behaviour within the membrane. In [32], Ghas-

semi and Diek described shale deformation due to chemo-mechanical processes, but their model disregards a process called ultrafiltration and does not properly describe important aspects of the reflection coefficient. Malusis and Shackelford [76] presented a more extensive model that includes multiple ionic species and cation exchange. Unfortunately, Malusis and Shackelford [76] only presented model simulations in which membrane effects were set to zero.

So, few model studies exist on coupled effects in groundwater. This study is most likely the first in which, from an geohydrological point of view, chemical and electrical effects are included in the equations of groundwater flow and solute transport. Hence, we emphasize in the title of this thesis, i.e. 'Chemical and electrical extensions to Darcy's Law', the fact that we employ the extended Darcy's Law to incorporate the aforementioned osmotic effects. However, extensions of Fick's and Ohm's Law are employed as well.

We investigate the mathematical equations that follow from the combination of extended flux equations and the usual conservation equations, in order to simulate transient behaviour of physical variables in real experiments. The buildup of osmotic pressure, possibly corrected for electro-osmosis, follows from these equations, and its timescale is strongly correlated to the timescale of simultaneous diffusion of the solute. The goal is clear: using such a model, one should be able to address questions regarding, for instance, anomalous pressure buildups or salinity profiles in compacted clayey environments (see Section 2.2), especially in coastal areas, or in any area where salt gradients may be expected to be present.

Summarizing, in this study, we address the following research questions:

- How can chemical and electrical effects be introduced in the governing equations for flow of groundwater and transport of solutes, to quantify the influence and magnitude of these processes?

- Is it possible to obtain analytical solutions for equations describing osmotically-induced groundwater flow, and what are the properties of these solutions? Furthermore, what do numerical solutions of similar problems tell us about chemical and electro-osmosis in groundwater?

- The quintessential coefficients in this study are the reflection coefficient and the electro-osmotic permeability. How do different expressions for these coefficients from literature compare and how do the dependencies of these coefficients on e.g. salt concentration influence, for instance, the buildup of osmotic pressure?

1.2 Thesis outline

This work is organized as follows: the current **Chapter 1** is of an introductional nature. In **Chapter 2** we go from general remarks on osmosis, an introduction to clay and so-called diffuse double layer theory, to a review of semi-permeability of clays, the relevant coupled processes and the corresponding coefficients. In **Chapter 3** we show how non-equilibrium thermodynamics provides us with equations that are subsequently specified for the different processes, and which balance equations are relevant for our purposes. In **Chapter 4**, some analytical solutions of this set of equations are presented for artificial but relevant example problems. Some properties of these solutions are investigated along with, for example, the influence on osmotic pressure buildup of the choice of dependence of the reflection coefficient on concentration. The model equations are put to the test in **Chapter 5**: here, two experiments from literature are modelled. It is shown how analytical and numerical methods can be applied to simulate these experimental results. Moreover, limitations of the analytical model are discussed and it is shown under which circumstances we have to rely on numerical modelling to obtain solutions. In **Chapter 6**, we use a similar model, extended with electro-osmosis, to predict the evolution of pressure and concentration distributions with and without electrical effects. Moreover, we use an advanced model to explain experimental results on membrane potentials. In **Chapter 7**, it is shown how a numerical groundwater code called METROPOL is extended with osmosis and some results of numerical modelling with this code are presented. The thesis is completed with a general summary of the study, a glossary of terms related to osmosis and a nomenclature.

Chapter 2

Theory

In hydrology literature, osmosis is usually disregarded because it is supposed to be a second order effect, which is for many circumstances not entirely unjustified. It has, however, been known for decades that specific circumstances may create a soil environment in which osmotic processes may thrive. In this chapter, the role of coupled processes in flow of groundwater and transport of solutes is explained. It contains an extensive literature review and some new results on, for instance, the microscopic derivation of the so-called reflection coefficient and the relationship between the diffusion coefficient and the semi-permeability of clay layers. Most of the processes and coefficients involved in the study of coupled processes in soils are presented, defined and commented on, in greater or lesser extent. The chemical background of the semi-permeable behaviour of clay is explained, some current theories of clay-water interaction are presented and the assumptions used in this study are justified. Finally, a glossary and a nomenclature are given in the appendix of this work.

2.1 Osmosis

If two solutions of different concentration are separated by a membrane that is permeable to the solvent molecules but not to the solute molecules, the solvent will flow from the low to the high concentration side. This is called osmosis: the word originates from the greek word $\omega\sigma\mu\omega\sigma$, meaning *to push*.

Generally speaking, we can say that osmosis refers to non-hydraulically driven water flow [94]. As we usually attribute water flow to pressure differences, when other physical processes are responsible for fluid movement, this is called chemical osmosis (for salt concentration gradients), electro-osmosis (for electrical potential gradients) and thermo-osmosis (for temperature gradients).

Another way to interpret osmosis is as diffusion of solvent molecules. In this

case, the energy of the solvent molecules per unit volume may be considered to be the osmotic pressure. This would imply that water flows due to osmosis from high to low osmotic pressure. There is some discussion about what is considered to be high and low osmotic pressure, as the driving force is not hydraulic. In chemistry literature, for instance, it is customary to say that the pressure needed to stop the osmotic flow is the osmotic pressure.

The osmotic pressure π can be calculated as follows: assume the schematic setup of Figure 2.1. The chemical potential μ for an ideal solution is defined as

$$\mu = f(T) + p\bar{V} + \nu RT \ln(1 - x_m), \tag{2.1}$$

where $f(T)$ is the part of the chemical potential that is only dependent on temperature, p is pressure, $\bar{V}$ molal volume, ν is the dissociation constant, R is the gas constant, T is temperature and x_m is molar fraction of salt. The salt concentration in the fresh water region is assumed to be zero. Subscripts f and s denote fresh and salt water regions respectively. At equilibrium, the thermodynamic potential of the solvent in the two regions must be equal, therefore:

$$\mu_f = \mu_s \tag{2.2}$$

$$f(T) + p_f\bar{V}_f = f(T) + p_s\bar{V}_s + \nu RT \ln(1 - x_m) \tag{2.3}$$

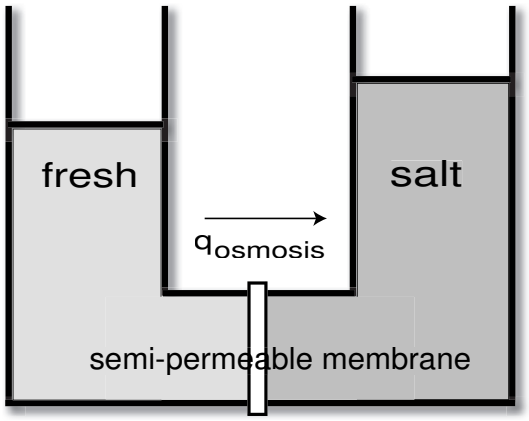

Figure 2.1: *Schematic picture of an osmotic process*

If we assume the fresh water and salt water molal volumes to be roughly equal- i.e. the molal salt volume to be very small, and introduce the solute concentration c, we find

$$p_s - p_f = \frac{-\nu RT}{\bar{V}_f} \ln(1 - x_m) \tag{2.4}$$

$$\pi = p_s - p_f \approx \frac{\nu RT}{\bar{V}_f} x_m = \nu RTc \tag{2.5}$$

This last equation is commonly referred to as van't Hoff's law, after van't Hoff [56], who received the first Nobel prize for chemistry for formulating this law.

2.1.1 General assumptions

Partly following Yeung [124], the default non-equilibrium thermodynamic system we consider, consists of a charged semi-permeable clay membrane, bounded by two well-mixed reservoirs of water with a certain hydraulic pressure, that contain solutes of a certain concentration, and electrodes in the reservoirs that have a certain electrical potential difference. However, as we consider natural soils, the domain may consist entirely of soil, and concentration and electrical potential gradients may extend continuously across the soil.

A membrane is defined as a thin layer, separating two different regions, sometimes permeable to some, but not all, constituents of the regions. Different approaches have been considered for membrane systems [53]. For instance the membrane is regarded as a discontinuity, separating two fluid phases, where driving forces are the differences between chemical potentials of the two phases. Because our research involves the study of osmotic effects in clay liners with a certain extent, we do not *a priori* consider the membranes to be thin. So we speak of soils behaving *as if they were ((semi-)permeable) membranes*. The approach we will follow considers the membrane as a separate, quasi-homogeneous phase of finite thickness.

2.1.2 Clay characteristics

According to Mitchell [80], the term clay refers to either a particle size term, denoting particles smaller than approximately $2\mu m$, or a mineral term denoting a so-called clay mineral. The latter refers to a crystalline particle, a primarily hydrous aluminum silicate consisting of sheets built of silica tetrahedron units. These consist of a silicon ion tetrahedrally coordinated with four oxygen ions (shown in Figure 2.2) and aluminum or magnesium octahedron units, i.e. an aluminum or magnesium ion octahedrally coordinated with six oxygen or hydroxyl ions. Clay classification is based on the arrangement of these sheets: one octahedral and one tetrahedral sheet build a so-called 1:1 platelet; kaolinite is an example of a

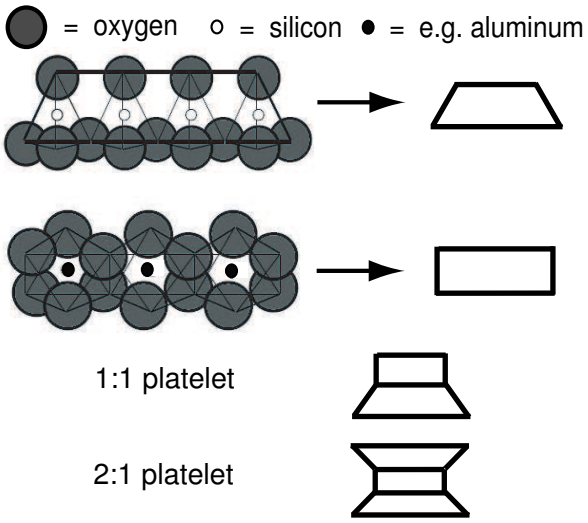

Figure 2.2: *Clay structure [127]*

clay configured this way. When an octahedral sheet exists between two tetrahedral sheets, this is called a 2:1 platelet, an example of which is montmorillonite. Within clay groups, the distinction can be made between minerals of different isomorphous substitution, i.e. the occupation of an octahedral or tetrahedral position by a cation other than the default cation. When this substitution is of a cation of lesser valence, the platelet will become negatively charged, which is ultimately the cause for osmosis.

In Figure 2.2, in the octahedral part, the aluminum ion (valence 3+) could be substituted by, for instance, a magnesium ion (valence 2+). The clays in experiments that are modelled here, are of the bentonite type. According to [37], bentonite is *any natural material composed predominantly of the clay minerals of the smectite group whose properties are controlled by these minerals.* Bentonite comes in two flavours, of which the sodium, or Wyoming bentonite is considered in this study. In Table 2.1, the types and names of clays encountered in this work, are tabulated (from [80]). In this table, $\mathcal{C}$ denotes cation exchange capacity.

2.1.3 Clay scales

It is common to distinguish between different scale descriptions for clays. Usually, a microscopic scale is defined where clay is assumed to consist of platelets that

type of clay	structure	$\mathcal{C}$ (meq/l)	description
illite	$2:1$	$10-40$	$2:1$-stacks connected by potassium
montmorillonite	$2:1$	$80-150$	
smectite	$2:1$	$80-150$	general name for montm.-like clays
kaolinite	$1:1$	$3-15$	
bentonite	$2:1$	$80-150$	mixture of montm. and beidellite
beidellite	$2:1$	$80-150$	type of smectite

Table 2.1: *Some types of clay*

are surrounded by water and ions. Several properties of the clay can be derived by considering the interaction between the clay matrix and the solution. Often, these properties are upscaled to allow for a macroscopic description of the clay by, for instance, homogenization or volume averaging. Some details are presented further on. Usually, in a macroscopic setup, ionic constituents are not considered separately anymore, and parameters such as the reflection coefficient and the permeability are assumed to be properties of the entire clay-solute-water system. An alternative approach is described in [75]: the authors work with mixture theory, considering n overlapping phases (every phase occupying the entire domain). In essence, a clay is assumed to consist of clusters of around 1000 platelets. The clay clusters are termed clay particles.

An interesting approach is the one described in [86]. Three different scales are defined: a micro-scale, where clay platelets and vicinal water exist, a meso-scale, where the model consists of bulk pore water and clay particles, and the macro-scale, consisting of the meso-scale particles and bulk water. Hybrid mixture theory [85] is used to upscale from the micro-to the meso-scale and homogenization to upscale from the meso- scale to the macro-scale.

2.1.4 Swelling of clays

Clay soils are known to undergo rather large volume changes when the internal pressure changes. This may cause significant problems: bore walls of oil drillings may become unstable [75] or buildings may subside due to a non-uniform soil heave. Swelling of clay can be exploited as well, to improve barriers that prevent contaminant transport. Swelling of soils may occur by imposing salt or electrical potential gradients, causing water flow by chemical and electro-osmosis respectively. The extra water pushes the clay platelets apart, causing the clay to swell. This is called chemical [75] or electrical swelling. Another type of swelling occurs when the soil is unsaturated, and swelling is driven by capillary forces. This is called matric swelling.

In this study, we do not consider macroscopic volume changes. This is mainly because our main interest lies in the transport processes in clay soils under a large

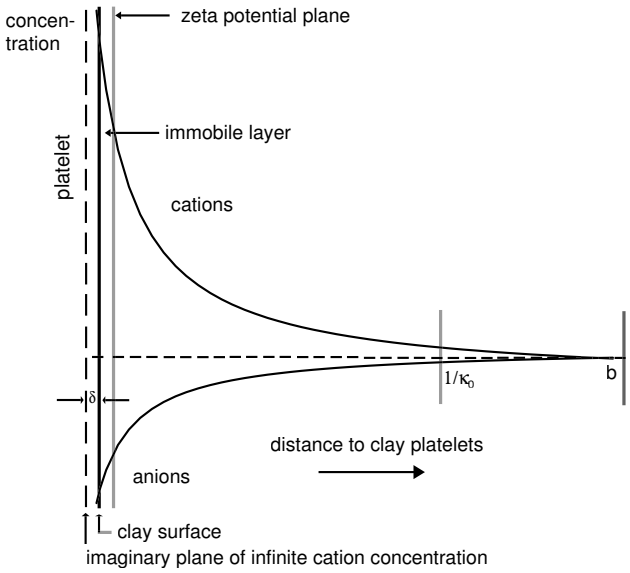

Figure 2.3: *A negatively charged clay platelet attracting a cloud of cations*

overburden pressure, where swelling is assumed to be marginal. However, we do consider the porous medium to be deformable; i.e., we allow for porosity changes.

2.1.5 Diffuse double layer theory

Consider a negatively charged clay platelet and a saturated salt solution. Near the surface of the platelet the concentration of cations is higher, whereas the concentration of anions is lower, as illustrated in Figure 2.3. Cations tend to diffuse to areas of lower concentration in the free solution, but are attracted by the negative electric charge of the clay surface. The anion concentration, however, is low near the surface and increases towards the free solution; this is called negative adsorption. The union of clay surface and distribution of ions near the clay surface is called the diffuse double layer, often abbreviated to DDL. In Figure 2.3 the following symbols are introduced: the thickness of the liquid film on the charged surface b, which is defined to be positioned either at the midplane between two clay platelets (see Figure 2.4) or at the location where the anion and cation concentration become equal (see Figure 2.3). In a number of theories, the distance δ is defined to be the location of an imaginary plane where the concentration of ions reaches infinity. Furthermore, the clay platelet is assumed to attract a small immobile layer of water. The electric potential at the point between the immobile and mobile layer is called the zeta potential ζ, and finally, the parameter κ_0, which is specified later on, is the so-called Debye reciprocal length: the thickness of the

diffuse double layer, although theoretically infinite [91], is usually represented by the parameter $1/\kappa_0$. Sometimes, the term normalized or effective double layer thickness is used for the product $b\kappa_0$.

The structure of the double layer is often described using the Gouy-Chapman theory, although many adjustments have been made. What follows is a brief synopsis, where we follow [115].

The concentration of ions in the double layer is governed by the Boltzmann distribution, assuming a 1:1 electrolyte:

$$\begin{aligned} c_- &= c_-^0 e^{F\Phi/RT}, && (2.6)\\ c_+ &= c_+^0 e^{-F\Phi/RT}, && (2.7)\\ \rho &= F(c_+ - c_-) = -2Fc_0 \sinh(F\Phi/RT), && (2.8) \end{aligned}$$

where ρ is charge density. The concentrations of anions and cations are c_- and c_+ respectively, superscript 0 denotes ionic concentration in the equilibrium solution. In the equilibrium solution, we assume electro-neutrality: $c_-^0 = c_+^0 = c_0$; F is Faraday's constant, R is the gas constant, T is temperature and Φ is electric potential of the ionic charge distribution.

From one of the Maxwell's equations

$$\nabla \cdot \mathbf{E} = \frac{4\pi}{\varepsilon_r}\rho, \tag{2.9}$$

where ε_r is the relative permittivity, and the expression for the electric field $\mathbf{E} = -\nabla\Phi$, follows Poisson's equation

$$\nabla^2\Phi = -\frac{4\pi}{\varepsilon}\rho. \tag{2.10}$$

This leads to a differential equation for Φ:

$$\nabla^2\Phi = \frac{8\pi F c_0}{\varepsilon_r}\sinh(F\Phi/RT), \tag{2.11}$$

for a flat double layer. If x denotes the distance to the clay surface, this equation, in one dimension reads:

$$\frac{d^2\Phi}{dx^2} = \frac{8\pi F c_0}{\varepsilon_r}\sinh(F\Phi/RT). \tag{2.12}$$

This equation is usually written in terms of the dimensionless quantities y, s, ξ:

$$y = F\Phi/RT, \tag{2.13}$$
$$s = F\Phi_0/RT, \tag{2.14}$$
$$\xi = \kappa_0 x, \tag{2.15}$$

where Φ_0 is the potential at the clay surface and

$$\kappa_0 = \sqrt{\frac{8\pi F^2 c_0}{\varepsilon_r RT}}. \tag{2.16}$$

Because c_0 is the equilibrium solution solute concentration, we deduce that the reciprocal thickness of the double layer is dependent on the square root of concentration. Now the equation for the double layer electric potential reduces to

$$\frac{d^2y}{d\xi^2} = \sinh y. \tag{2.17}$$

With the boundary condition $\xi = 0, y = s$, the solution of (2.17) reads:

$$e^{y/2} = \frac{e^{s/2} + 1 + (e^{s/2} - 1)e^{-\xi}}{e^{s/2} + 1 - (e^{s/2} - 1)e^{-\xi}}. \tag{2.18}$$

This formula expresses the relation between the electrical potential in a diffuse double layer and the distance to the clay platelets. It will be used later on, in a slightly different version, to calculate macroscopic coefficients from microscopic properties of the clay-water system.

Often, the so-called Debye-Hückel approximation is used for equation (2.17). It involves linearizing equation (2.17) to get:

$$\frac{d^2y}{d\xi^2} = y. \tag{2.19}$$

This approximation is also used to express activity coefficients in terms of concentrations.

In [9], an extension to these formulas is presented for the case where divalent ions are present as well.

A number of corrections on this theory has been proposed:

- In the Stern model, the Stern layer is introduced to correct the high values of the concentration near the surface. This layer is of finite thickness and extends from the surface; the counter-ions are statistically distributed over this layer in analogy to a Langmuir type derivation of the adsorption isotherm.

- In a different interpretation, the boundary of the Stern layer is usually called the Outer Helmholtz Plane (OHP); between the OHP and the surface, the ions are only partially solvated, outside fully. There is also an Inner Helmholtz Plane (IHP), that indicates the distance from the surface within which the ions are 'unsolvated'

- In the Bolt model [10], the potential energy term in the Boltzmann equation is extended with a polarization energy term, a Coulomb interaction term and a repulsion term

Important for our purposes is what happens when double layers overlap: if one platelet is located at $x = 0$ and the other at $2d$, the center is at d, the electrical potential at this location is Φ_d and u is defined as $u = F\Phi_d/RT$. The following relation then applies:

$$\int_s^u (2\cosh y - 2\cosh u)^{-1/2}\, dy = -\kappa_0 d \tag{2.20}$$

This integral can be easily evaluated in terms of elliptic integrals of the first kind to yield an explicit relation between the midplane potential and the distance between platelets.

2.1.6 Semi-permeability

When the double layers in the clay overlap (as shown in Figure 2.4), which is most likely to happen in compacted samples, the distribution of ions now imposes electrical restrictions on ions meaning to migrate through the clay, provided the double layers do not degenerate because of high bulk concentration. Anions approaching the aqueous film between the platelets are repelled by the electrical charge on the platelets. This is called anion exclusion, Donnan exclusion or negative adsorption [63],[80]. The movement of the cations is restricted as well, as the cations remain near the anions to maintain electro-neutrality. A membrane that exhibits this property, is called semi-permeable or leaky, as it allows water molecules to pass and (partially) restricts ionic movement. A semi-permeable membrane is called ideal when no solute may pass at all, and non-ideal otherwise.

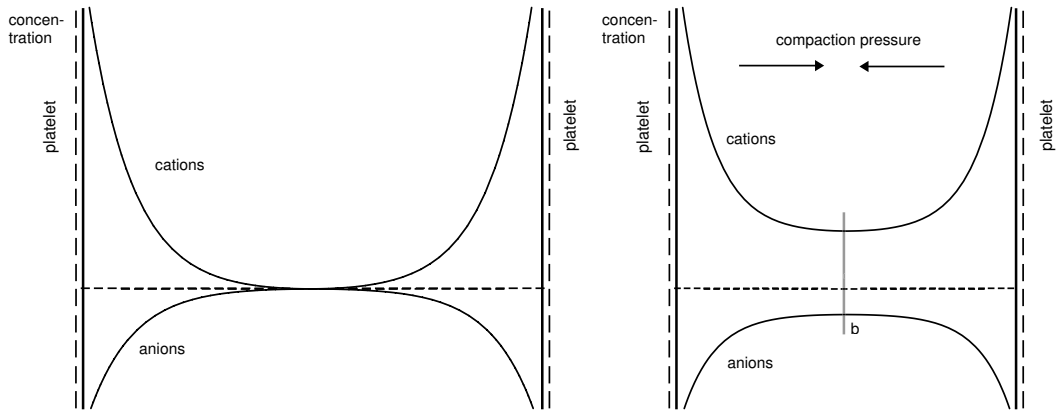

Figure 2.4: *Overlapping double layers impose restrictions when the clay is compacted*

2.1.7 Additional assumptions

In practice, most natural clay soils do not entirely consist of clays. Also, completely different types of clays may be present in a sample. For simplicity we assume the clays to be homogeneous.

In some publications, especially where mixture theory is used [86], the clay setup is modelled using a two-phase description. The pore water and possible absorbed water are assumed to belong to the fluid phase and the matrix and all solute particles are in the solid phase. We distinguish three different phases: the clay matrix, the fluid phase and the dissolved solute. The clay matrix can interact with the solute by adsorption or cation exchange. The solute under consideration is in all cases NaCl, hence many simplifications may be applied that hold for 1:1 electrolytes. In Chapter 3, it is shown how a multitude of solutes influences the equations for chemical osmosis.

Flow of ions through the clay is described using a molecular diffusion coefficient. In Chapter 4, an example problem shows why mechanical dispersion can be neglected. Furthermore, the clay soil is in all cases assumed to be saturated with water.

2.2 Coupled processes and applications

We have seen how microscopic properties of the clay-water system result in the semi-permeable behaviour of clay membranes. In general we have limited information about the structure and composition of a clay, hence it is common to treat it as a 'black box', implying that we attribute certain macroscopic properties to the sample, e.g. the reflection coefficient and the electro-osmotic permeability. In

the next chapter it is shown how, from non-equilibrium thermodynamics certain macroscopic driving forces are related to macroscopic fluxes of solvent, ions and charge by coupling coefficients such as the reflection coefficient. More precisely, it is demonstrated how, for instance, the macroscopic solvent flux $\mathbf{q}$ is related to gradients of pressure p, chemical potential of solute μ_s and electrical potential V as follows:

$$\mathbf{q} = -L_{11}\nabla p - L_{12}\nabla \mu_s - L_{13}\nabla V. \tag{2.21}$$

Here, gravity was disregarded. A motivation for this is given in Section 4.1. The coupling coefficients L_{ij} can now be identified as macroscopic parameters. The coefficient L_{11} is, by analogy to Darcy's law, equal to the ratio of the intrinsic permeability and the viscosity. Chemical osmosis is related to the coefficient L_{12} that depends on the aforementioned reflection coefficient and the coefficient L_{13} describes electro-osmosis via the electro-osmotic permeability. This is discussed in detail in Chapter 3, where a complete overview of the coupled processes in a soil system is listed, including thermal effects that are ignored in this study. Subsequently, we review some implications and applications of some of the coupled processes.

2.2.1 Chemical osmosis

One of the implications of chemical osmosis is the possible decrease of reliability of clay liners used to store toxic or radio-active waste. In Figure 2.5 a simplified setup is shown of such a situation. The situation resembles the simple model of a semi-permeable membrane and a salt concentration gradient, which gives rise to chemical osmosis. When $c_a \neq c_0$, water will flow from low to high concentration by chemical osmosis, which may have implications for the clay liner. The pressure inside the repository may increase to a level at which cracks form, which in turn may lead to leakage. On the other hand, non-charged substances may be advected with the water flowing outside of the repository to contaminate the groundwater.

An example is given in [106]: when an oil well is drilled, drilling fluid may be drawn by osmosis into the clay rocks surrounding the wellbore. This can lead to swelling of the clay and can even lead to complete closure of the wellbore. This can be prevented by increasing the salt content of the drilling fluid.

The occurrence of chemical osmosis may also lead to problems in the storage of sludge. As was already pointed out in [63], harbour sludge may act as a semi-permeable membrane. The main harbour sludge depot in the port of Rotterdam is called *De Slufter*. In the study reported in [63], samples were taken from this site to assess the semi-permeable properties of the sludge. The aforementioned

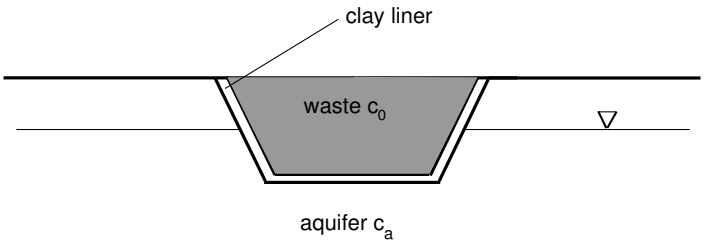

Figure 2.5: *Simple setup of a clay liner and waste*

reflection coefficient was obtained and it was shown how the *Slufter*-site is an excellent example of a situation where osmosis might become a hazard. As the top of the sludge layer is recharged by rain and the bottom is in contact with a salt water aquifer, water is transported into the aquifer by chemical osmosis, and non-charged contaminants such as Polycyclic Aromatic Hydrocarbons (PAH's) can be advected into the groundwater. The formula for the discharge q [m/s] attributed to chemical osmosis is discussed later on but reads:

$$q \sim \nu\sigma RT\frac{k}{\mu}\frac{\Delta c}{L}, \tag{2.22}$$

where $L \approx 20$m is the sludge depot thickness, $\nu = 2$, $R = 8.314$J·mol/K and $T = 293$ K are the dissociation constant, gas constant and temperature respectively, $\Delta c \sim 100$ mol/m^3 is the salt concentration difference across the sludge, $k/\mu \sim 10^{-13}$m^{3}s/kg is the hydraulic mobility and $\sigma \sim 0.03$ is the reflection coefficient. With these values, the discharge is approximately $q \sim 1.2{\cdot}10^{-10}$m/s which amounts to about 2.5 mm/year, which is more than is allowed by Dutch legislation.

Other implications of chemical osmosis are: the occurrence of 'anomalous' hydraulic heads [89], [77] and thrust faulting [45].

2.2.2 Salt-sieving

Salt-sieving, or hyperfiltration is defined as the non-advective solute flux due to a pressure gradient. When water is pushed through a semi-permeable membrane, and ions are electrically restricted, they induce a relative solute flux. In [28], it was shown how salt-sieving was responsible for calcite precipitation, and copper deposits in New Mexico may have been formed by this effect as well [119].

There is a large number of applications and literature on reverse osmosis, which is related to filtration of ions that are restricted by their size. An obvious example is desalination: depending on the size of the pores of the membranes, the corresponding process is called micro-, nano-, or ultrafiltration.

2.2.3 Electrical effects: definitions

In Chapter 3 a table is presented where a number of coupled processes is mentioned. Among those are electrophoresis (solute flow by an electrical potential gradient) and membrane potential (electrical potential caused by a salt concentration gradient). The former is of minor importance in this study while to the latter, Chapter 6 is devoted. Two other processes couple hydraulic and electrical effects: streaming potential is the electrical potential caused by an hydraulic gradient and electro-osmosis is fluid flow caused by a gradient of electrical potential. Electro-osmosis is reviewed in one of the following sections. First, its many applications are listed.

2.2.4 Electrical effects: applications

Using the concept of electro-osmosis, water can be transported by applying an electrical gradient. In low permeability soils, this process is much more efficient compared to water transport by an hydraulic gradient. Consider for example a soil with an intrinsic permeability of $k = 10^{-19}$ m^2, which is a common value for clayey soils [5], and an typical electro-osmotic permeability [80] of $k_e = 5 \cdot 10^{-9}$ m^2/Vs. Then, a potential gradient of 1 mV/m is equally as effective to induce water flow as an hydraulic gradient of 5 m/m. In [125],[15], a number of applications is listed. For instance, undesired seepage along a slope may be counteracted by an electrical gradient to decrease the water content in the soil and enhance the shear strength. Similarly, embankments and dams can be stabilized in this way. Also, electro-osmosis was considered in the investigation of stabilizing the leaning tower of Pisa [125].

In cases where a metal pipe is drilled in the soil or is used to scoop sludge from an underwater depot, electro-osmosis can be used to decrease the friction between metal and soil by creating a thin layer of water that acts as a lubricant [125], [116]. As a matter of fact, it has been proved that the motion of earthworms is actually enhanced by electro-osmosis. During alternate contraction and expansion of its body, an electric potential difference exists between the moving and stationary parts of the worm and soil water will be extracted to the earthworms body surface. The water film then reduces the friction of motion of the worm.

Electro-osmosis is also used for soil treatment purposes: for instance, contaminants can be extracted from a soil sample. In [95] it is shown how this process,

which is sometimes called soil-washing, can remove contaminants such as heavy metals with an efficiency up to 93.5%.

When other methods prove to be infeasible or ineffective, electro-osmosis may be employed to fixate a toxic substance by introducing a reacting agent into the clay by electro-osmosis that degrades the contaminant, changes it into a non-toxic or immobile species or enhance stable sorption on the matrix [95].

Clay liners are used to prevent contaminated waste to get in contact with uncontaminated soil and/or groundwater. Long-term seepage is always a problem in clay liners and electro-osmosis can be used to counteract undesired flow [125]. This is called an electro-kinetic barrier. However, desiccation followed by forming of cracks may jeopardize the function of the clay liner.

Another application involves changing the flow pattern of groundwater where a contaminant plume is present. By electro-osmosis, the groundwater flow can be manipulated [125] to improve control over the extent and evolution of a plume.

Furthermore, one can use electro-osmosis for *in situ* analysis of properties of soils, such as the intrinsic permeability [125].

2.3 Coefficients

2.3.1 Coefficient calculation methods

Obviously, there exists a direct relationship between the microscopic characteristics of a clay and the macroscopic coefficients. Different theories exist on how to go from micro-scale to macro-scale. In all cases, some assumptions are made about the structure of the porous medium. For example, in the first upscaling method under consideration, the porous medium is assumed to be composed of a solid uniformly pierced by capillaries filled with a salt solution. In general, the equations valid locally, are upscaled by for instance, averaging, leading to expressions valid for the porous medium as a whole. The upscaled microscopic coefficients then relate to familiar macroscopic coefficients.

In this section, a selection of examples is shown: first, two simple averaging methods are shown for different assumed geometries of the domain. Second, it is shown how, by homogenization of the microscopic model, very similar coefficients are derived.

Gross Osterle

In [41], the transport coefficients for a semi-permeable membrane are derived using a model consisting of a free solution and a solid consisting of capillary pores of length l and radius a. The hydrodynamic equations extended with electrochemical

forces are stated and subsequently integrated over the capillaries. The resulting equations are written in the form of the equations as governed by non-equilibrium thermodynamics. This yields a relationship between the relevant macroscopic and microscopic parameters.

The concentration c_i of ions in the capillaries was given in Section 2.1.5, i.e.

$$c_i = c_0 e^{-z_i F\psi/RT} \tag{2.23}$$

where F is Faraday's constant, R and T are the gas constant and the temperature respectively, z_i is the valence of the corresponding ion, c_0 is the free solution concentration and ψ is the electrical potential in the capillaries.

We consider gradients of variables along the axis of a capillary (x-direction) and perpendicular to that axis (r-direction). The fluid flowing through the capillaries must obey the following modified Stokes equation:

$$-\nabla\bar{p} - F(c_+ - c_-)\nabla\bar{V} + \mu\nabla^2\mathbf{v} = 0 \tag{2.24}$$

where $\bar{p}$ is the total pressure in a capillary, $\bar{V}$ is the total electrical potential and $\mathbf{v}$ is the fluid velocity along the capillary axis. Using a number of assumptions and the formulas listed in [41], the axial (x) component of the modified Stokes equation is integrated twice with respect to the radius of a capillary. The result is written in the form of integrals times driving forces, yielding:

$$\begin{aligned}
\mathbf{v} &= \left(\frac{a^2 - r^2}{4\mu}\right)\left(-\frac{dp_0}{dx}\right) && (2.25)\\
&+ \frac{1}{\mu}\int_r^a \frac{1}{r_2}\int_0^{r_2}(c_+ + c_-)r_1 dr_1 dr_2 \left(-RT\frac{d\ln c}{dx}\right) && (2.26)\\
&+ \frac{F}{\mu}\int_r^a \frac{1}{r_2}\int_0^{r_2}(c_+ - c_-)r_1 dr_1 dr_2 \left(-\frac{dV}{dx}\right), && (2.27)
\end{aligned}$$

where $p_0 = \bar{p} - (c_+ + c_-)RT$ is called the partial pressure and r_1, r_2 are dummy variables. The total electrical potential $\bar{V}$ is the sum of the global electrical potential V and the local radial potential ψ. The relation between the radial potential and r is obtained by solving the Poisson-Boltzmann equation, as shown, for a Cartesian domain, in Section (2.1.5). The total flux trough the capillaries is now obtained by integrating over the cross-sectional area of the tubes. We can now obtain an expression for e.g. the global water flux through the porous medium following the procedure outlined in [41]

$$q = -L_{11}\frac{dp}{dx} - L_{12}\frac{d\pi}{dx} - L_{13}\frac{dV}{dx}, \tag{2.28}$$

where $p = p_0 + \pi$ is the global hydraulic pressure, $\pi = 2cRT$ is osmotic pressure and L_{ij} are the coupling coefficients. The relevant coupling coefficients are given by

$$L_{11} = \frac{a^2}{8\mu}, \tag{2.29}$$

$$L_{12} = \frac{1}{2a^2\mu}\int_0^a (a^2 - r^2) r \cosh\left(\frac{F\psi}{RT}\right) dr - \frac{a^2}{8\mu}, \tag{2.30}$$

$$L_{13} = -\frac{2\varepsilon_r}{a^2\mu}\int_0^a r(\psi_a - \psi) dr, \tag{2.31}$$

where ψ_a is the electrical potential at the wall of the capillary.

From the analogy to Darcy's law, the intrinsic permeability is shown to be $\frac{a^2}{8}$. As usual [5], the permeability is given by a shape factor times a length parameter squared. The other terms are related to the reflection coefficient and the electro-osmotic permeability: $L_{13} = k_e$ and:

$$\sigma = -\frac{L_{12}}{k/\mu} = 1 - \frac{4}{a^4}\int_0^a (a^2 - r^2) r \cosh\left(\frac{F\psi}{RT}\right) dr. \tag{2.32}$$

These expressions can be obtained in closed form if the double layer formulas relating ψ to r are inserted.

Bolt

In Bolt [9], something similar is done for a geometry that is more applicable to clays: instead of capillaries, rectangular slits are considered. Following the same steps, an intrinsic permeability is derived that reads:

$$k = \frac{nb^2}{3\tau}. \tag{2.33}$$

Here, the porosity n and the tortuosity τ were used to account for the geometrical constraints of the porous medium as a whole. For comparison with the previous

expression (2.29), these parameters should be set to one. Finally, the parameter b is the half-distance between the clay platelets. Obviously, the expression for k is very similar to the one in the cylindrical domain. The other coupling parameters are given by

$$L_{DV} = \frac{n}{\tau b}\int_0^b \left(bx - \frac{x^2}{2}\right)\left(1 - \frac{1}{u}\right) dx, \tag{2.34}$$

$$L_{EV} = -\frac{n\varepsilon_r}{4\pi\tau b\mu}\int_0^b (\zeta - \psi)\left(u - \frac{1}{u}\right) dx \tag{2.35}$$

Here, the subscripts D, V and E denote diffusive, volume and electrical flow respectively. The potential ψ_m is the electrical potential at the clay platelet. The parameter u is the Boltzmann factor, appearing as the exponential in (2.23):

$$c_+ = c_0 e^{-F\Phi/RT} = c_0 u,\ c_- = c_0 e^{F\Phi/RT} = \frac{c_0}{u}. \tag{2.36}$$

For a simple cartesian domain the relation between u and x yields closed-form expressions for the reflection coefficient and the electro-osmotic permeability, as is shown later in this chapter.

Homogenization

In [83], some of the coupling coefficients are derived using an homogenization procedure. This method of upscaling is an alternative to the REV approach where instead of smoothing and averaging of functions, a scale parameter, defined to parameterize the micro-scale equations, is sent to zero [58]. The macroscopic porous medium is represented by a bounded domain with a periodic structure. Two length scales are defined: one associated with the size of a pore l, and one associated with macroscopic size of the porous medium, where heterogeneities can not be distinguished (L). The ratio of these length scales is the perturbation parameter $\varepsilon = l/L$ and hence assumed to very small ($\varepsilon \ll 1$). The microscopic equations, for which $\varepsilon = 1$, are defined on the sub-domains that are the periodic unit cells dividing the total domain. Macroscopic coordinates $\mathbf{x}$ are then related to microscopic coordinates $\mathbf{y}$ by the relation $\mathbf{x} = \varepsilon\mathbf{y}$. Then, the unknowns f^ε are expanded by

$$f^\varepsilon = f^0 + \varepsilon f^1 + \varepsilon^2 f^2 + ... \tag{2.37}$$

Following the method of Matched Asymptotic Expansions, the powers of ε are equated to yield a set of macroscopic equations. These are cleverly rewritten to obtain familiar forms of the coupled equations. An example is Darcy's law, which can readily be derived from upscaling the Navier-Stokes equations [112]. In [83], additional terms regarding chemical and electro-osmosis are derived by including electro-chemical terms in the Navier-Stokes equations. The resulting macroscopic equations allow for different unit cell geometries, leading to different homogenized coefficients. For clay, it is most suitable to choose the geometry mimicking the parallel plates setup of the clay. Skipping all intricacies related to their derivation, we only list here the final expressions for the hydraulic mobility:

$$K_p = \frac{b^2}{3\mu}, \tag{2.38}$$

the chemico-osmotic coefficient:

$$K_c = A \cdot \left\{ \frac{1}{6} + \frac{1}{2\gamma^2} \left(\cosh\gamma - \frac{1}{\gamma} \sinh\gamma \right) \right\}, \tag{2.39}$$

$$\begin{aligned} A &= \frac{\Sigma^2 b^2}{2\mu\varepsilon_r c_0 \sinh^2(\gamma/2)}, & (2.40)\\ \gamma &= \frac{2b}{L_D}, & (2.41)\\ L_D &= \sqrt{\frac{\varepsilon_r RT}{8\pi F^2 c_0}} = \frac{1}{\kappa_0}, & (2.42) \end{aligned}$$

and the electro-osmotic coefficient (for a slit):

$$K_e = \frac{\Sigma L_D}{\mu} \left\{ \frac{2}{\gamma} - \coth\frac{\gamma}{2} \right\}. \tag{2.43}$$

In these equations, L_D is the Debye length, b is the half plane distance, Σ is the surface charge density, ε_r is the relative permittivity. The permeability is equal to the one obtained (in the slit geometry) by Bolt, provided we neglect tortuosity and set $k/\mu = K_p n$ (as $\mathbf{v} \sim -K_p \nabla p$ in [83] and $n\mathbf{v} = \mathbf{q} \sim -k/\mu \nabla p$ in general).

In the following sections, the specific expressions for the reflection coefficient and the electro-osmotic permeability obtained by homogenization are listed.

2.3.2 The reflection coefficient

The reflection coefficient σ is the macroscopic parameter that expresses the degree of semi-permeability of a membrane. As it usually ranges between 0 (passages of all solutes permitted) and 1 (full restriction of passage of solutes), it indicates how strongly the membrane 'reflects' the solute. It is also called osmotic selectivity coefficient, osmotic efficiency [124] or chemico-osmotic efficiency coefficient [76]. The name reflection coefficient, and the symbol σ were introduced by Staverman [110]. The authors of [76] propose to utilize the symbol ω to avoid confusion with the electrical conductivity and the stress. We use the symbol σ for electrical conductivity consequently with a subscript, and as we hardly consider volume change of soils, we don't use the effective stress symbol at all. In [106], the transmission coefficient λ is defined as $\lambda = 1 - \sigma$. Similar to this is the solute permeability (see Chapter 3) ω from [62], which attains a maximum value for $\sigma = 0$ and equals zero for $\sigma = 1$.

The reflection coefficient is usually defined as follows: assume we may write the specific discharge $\mathbf{q}$ as being linearly dependent on an hydraulic pressure gradient ∇p via a coefficient L_D and an osmotic pressure gradient $\nabla \pi$ via L_{DP}, then the reflection coefficient is defined as [72]:

$$\sigma = -\left(\frac{L_D}{L_{DP}}\right). \tag{2.44}$$

The reflection coefficient is dependent on such factors as bulk concentration and porosity. High efficiencies have been experimentally shown and theoretically predicted in clay membranes under high overburden pressure, that exhibit low porosity and are exposed to dilute electrolytes. These properties may be explained by, for instance, diffuse double layer theory. In the next sections, different theories from literature regarding the reflection coefficient are presented and discussed.

Typical values of the reflection coefficient

There is a large amount of experimental studies available with respect to the reflection coefficient in a wide range of clays and experimental conditions. A nice review is given in [63]. Measurements in clay rich materials were taken as early as 1961 [65]. Reflection coefficients were obtained for kaolinites [69], smectites [7] and bentonites [69],[63],[79], in laboratories using direct measurements [68],[63],[67] or reverse osmosis [7],[29], and in field experiments [89],[31]. Experimental values of the reflection coefficient range between 0.00002 [4] and 0.99 [44], while values encountered for reasonably salty bentonite clays under realistic overburden pressures are of the order 0.02 [63],[51].

Simple expressions for σ

Semi-permeability is usually attributed to the electrical restrictions imposed by the membrane, and hence the reflection coefficient is often calculated using the diffuse double layer theory that describes the distribution of ions in the clay. Some authors use size restricting arguments as well, or even exclusively, to obtain an expression for σ. An example of this is given in [66].

The 'default' expression for the reflection coefficient stems from the observation that the degree of exclusion is related to the relative amount of anions in the pores [68]:

$$\sigma = 1 - \frac{c_a}{c_0}, \tag{2.45}$$

where c_a is the local anion concentration in the pores and c_0 is the bulk salt concentration. The anion concentration may be assumed constant [62] or be defined by the Gouy-Chapman model, for instance. The ratio $\frac{c_a}{c_0}$ is actually equal to the Boltzmann factor u for the anion, as

$$c_a = c_0 u = c_0 e^{\frac{F\psi}{RT}}, \tag{2.46}$$

where F is Faraday's constant, ψ is the electric potential in the double layer, and R and T are the gas constant and the temperature respectively. In [90], the electric potential ψ_b in the midplane is substituted in this equation:

$$\sigma = 1 - e^{\frac{F\psi_b}{RT}}. \tag{2.47}$$

The authors of [90] have given an empirical version of this to improve correspondence with their experimental results:

$$\sigma = 1 - e^{\frac{F\psi_b}{RT}\left(1+3e^{-F\psi_b/RT}\right)}. \tag{2.48}$$

Katchalsky and Curran

In Katchalsky and Curran [62], an expression for the reflection coefficient is given:

$$\sigma = 1 - \frac{K f_{sw}}{n(f_{sw} + f_{sm})}, \tag{2.49}$$

where the molar salt volume is neglected. Here, f_{sw} is the friction coefficient between the solute and water, f_{sm} is the friction coefficient between the solute and

the matrix, n is porosity and K is the coefficient describing the distribution of ions on the membrane versus the pore solution. If we equal the latter to the Boltzmann factor u and assume the friction between solute and matrix small compared to friction between solute and water, i.e. $f_{sm} \ll f_{sw}$, then (2.49) reduces to

$$\sigma = 1 - \frac{u}{n}, \tag{2.50}$$

which is the 'default' expression corrected for the porosity.

On the other hand, when substituting equation (12.61) from [62] in (2.49), equation (2.49) is shown to reduce to

$$\sigma = 1 - \frac{cn}{Q_v t_+}, \tag{2.51}$$

where Q_v is excess surface charge and t_+ is the cationic Hittorf transference number. Defining $\alpha = n/(Q_v t_+)$ transforms the latter expression for σ into

$$\sigma = 1 - \alpha c. \tag{2.52}$$

This convenient expression will be used in Chapter 4.

Bresler

In [11], different experimental results are compared with theoretical calculations based on the method of Bolt, which is discussed later on. Bresler numerically calculated values of σ for a number of different concentrations, and in Figure 2.3.2 is it shown how this compares to experimental values.

The graph by Bresler has often been used for prediction of reflection coefficients and hence the fitted line, as shown in the figure, is expressed in terms of $b\sqrt{c_0}$, where b is the water film thickness, i.e. midplane distance:

$$\sigma_{\text{Bresler}} = \frac{1}{2}\left(1 - \operatorname{erf}\left[\frac{0.4(v-7)}{\sqrt{0.9v}}\right]\right), \tag{2.53}$$

where

$$v = b\sqrt{\frac{c_s}{1000 M_s}}, \tag{2.54}$$

where M_s is the solute molar mass.

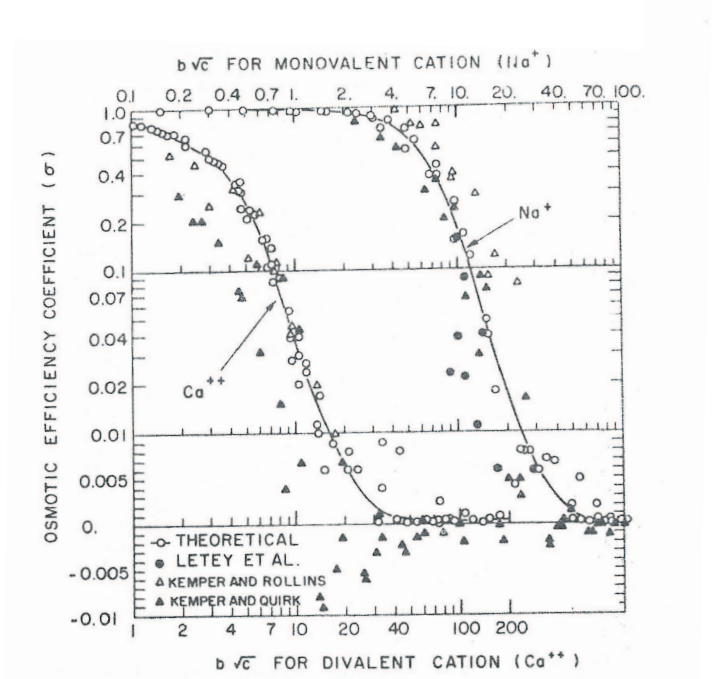

Fig. 1—Osmotic efficiency coefficient (σ) as a function of $b\sqrt{c}$. Here c is the concentration of monovalent anion in normality, and $2b$ is the film thickness in Å. Note that below $\sigma = 0.01$ the log scale of the ordinate has been changed to a linear scale.

Figure 2.6: *Graph by Bresler [11] depicting the dependence of σ on salt concentration*

Fritz and Marine

The reflection coefficient of Fritz and Marine [29] is an extension of the expression of Katchalsky and Curran and is given by

$$\sigma_{fm} = 1 - \frac{K_s(R_w + 1)}{\left[\left(R_w \frac{c_a}{c_c} + 1\right) + R_{wm}\left(R_m \frac{c_a}{c_c} + 1\right)\right]}. \tag{2.55}$$

The distribution coefficient between solute in the membrane $\bar{c}_s$ and solute in the solution c_0 is $K_s = c_a/c_0$, and R_w, R_{wm} and R_m are ratios of friction coefficients.

Bolt

As seen in a previous section, the reflection coefficient can be derived from microscopic theories using equation (2.34):

$$L_{DV} = \frac{n}{\tau b}\int_0^b \left(bx - \frac{x^2}{2}\right)\left(1 - \frac{1}{u}\right) dx. \tag{2.56}$$

If we use the regular Boltzmann factor u, then, for a simple 1:1 electrolyte, we may use the expression for the double layer thickness, derived from the Poisson equation:

$$\kappa_0 x = -\ln\left[\frac{\sqrt{u} - 1}{\sqrt{u} + 1}\right] + \ln\left[\frac{\sqrt{u_s} - 1}{\sqrt{u_s} + 1}\right]. \tag{2.57}$$

This expression may be used in the formula for the reflection coefficient:

$$\sigma = -\frac{L_{DV}}{L_V} = -\frac{\int (bx - x^2/2)\left(1 - \frac{1}{u}\right) dx}{\int (bx - x^2/2) dx}, \tag{2.58}$$

introducing

$$\left(1 - \frac{1}{u}\right) = \frac{4t}{(1+t)^2}, \tag{2.59}$$

$$\kappa_0 x = -\ln(t/t_s,) \tag{2.60}$$

$$\kappa_0 \delta = -\ln(t_s) = y, \tag{2.61}$$

$$\kappa_0 b = -\ln(t_d/t_s) = w, \tag{2.62}$$

graph number	equation	description
1	(2.63)	exact solution; $\kappa_0\delta = 0.45$
2	(2.63)	exact solution; $\kappa_0\delta = 0$
3	(2.67)	approximation for large $\kappa_0 b$
4	Bolt [9] (11.40)	Kemper estimate for σ
5	Bolt [9] (11.39)	approximated integral for σ
6	(2.45)	σ for constant Boltzmann factor
7	Keijzer [63] (1.20)	different version of Bolt (11.39)

Table 2.2: *Graph numbers corresponding to Figure 2.7*

so

$$\begin{aligned}\sigma &= -\frac{\int (d_1 x - x^2/2)(1-1/u)dx}{\int (d_1 x - x^2/2)dx} \\ &= \frac{3}{(\kappa_0 b)^3}\left[\kappa_0 b \int_{t_s}^{t_d} \ln(t/t_s)\frac{4}{(1+t)^2}dt + \frac{1}{2}\int_{t_s}^{t_d}\ln^2(t/t_s)\frac{4}{(1+t)^2}dt\right] \\ &= \frac{3}{(\kappa_0 b)^3}\left[A+B\right], \end{aligned} \tag{2.63}$$

where

$$A = 4\kappa_0 b\left\{\frac{t_d \ln(t_d/t_s)}{1+t_d} + \ln\frac{1+t_s}{1+t_d}\right\}, \tag{2.64}$$

by integration by parts. The same can be applied to

$$B = \frac{2t_d \ln^2(t_d/t_s)}{1+t_d} - 4\left[\mathcal{L}(1+t_d) - \mathcal{L}(1+t_s)\right] - 2\ln(t_d/t_s)\ln(1+t_d), \tag{2.65}$$

where $\mathcal{L}(x)$ is the dilogarithmic function, defined as

$$\mathcal{L}(x) = -\int_1^x \frac{\ln(t)}{t-1}dt = \sum_{k=1}^{\infty}(-1)^k\frac{(x-1)^k}{k^2}. \tag{2.66}$$

In [9], a similar calculation is performed but the result is approximated, probably for the sake of simplicity. Formula (2.63) however, is exact, and in Figure 2.7 we can see how the exact solution compares to the approximate solution given

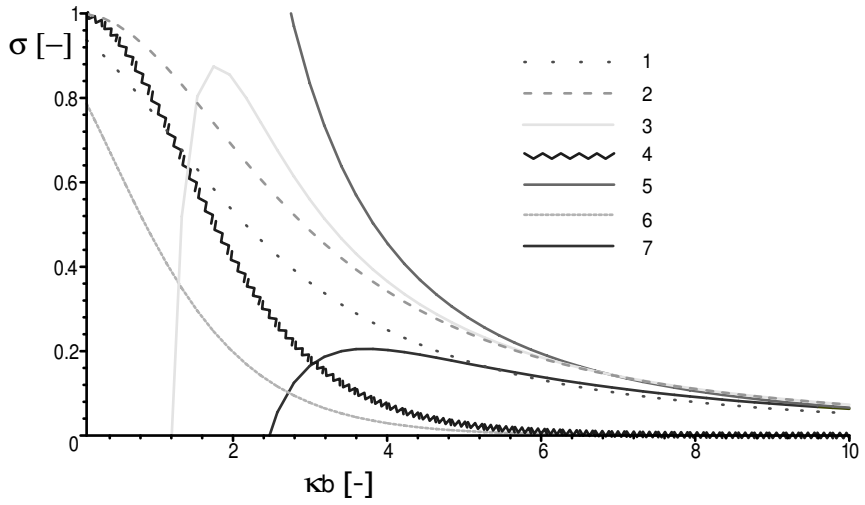

Figure 2.7: *comparison of different expressions for σ*

by Bolt, i.e. the case where the immobile layer is zero, the simple approximation $\sigma = 1 - 1/u$ and the approximation: $t_d = 0$ and $t_s = 1$, yielding:

$$A \approx \kappa_0 b \ln 2, \tag{2.67}$$

$$B \approx -\pi^2/12, \tag{2.68}$$

$$\sigma \approx \frac{12 \ln 2}{(\kappa_0 b)^2} - \frac{\pi^2}{(\kappa_0 b)^3}. \tag{2.69}$$

Homogenization

In Section 2.3.1, we have obtained an expression for the chemico-osmotic coefficient by homogenization. This coefficient relates to the reflection coefficient as:

$$K_c = 2\sigma RT \frac{k}{\mu}. \tag{2.70}$$

Because K_c is, from equation (2.39):

parameter	unit	value
b	$\mathring{A}$	50
R_w	-	1.63
R_{wm}	-	0.1
R_m	-	1.8
n	-	0.5
ρ_s	g/m^3	2.5
M_s	kg/mol	0.06
$\mathcal{C}$	mol/g	0.001
$\lvert\zeta\rvert$	mV	20

Table 2.3: *Parameters used in the graph (2.8)*

$$K_c = A \cdot \left\{ \frac{1}{6} + \frac{1}{2\gamma^2} \left(\cosh\gamma - \frac{1}{\gamma} \sinh\gamma \right) \right\} \tag{2.71}$$

$$A = \frac{\Sigma^2 b^2}{2\mu\varepsilon_r c_0 \sinh^2(\gamma/2)} \tag{2.72}$$

$$\gamma = \frac{2b}{L_D} \tag{2.73}$$

$$L_D = \sqrt{\frac{\varepsilon_r RT}{8\pi F^2 c_0}}, \tag{2.74}$$

the corresponding reflection coefficient is

$$\sigma_{hom} = \frac{3}{2} \left(\frac{F\zeta}{RT} \right)^2 \frac{1}{\cosh^2 \gamma/2} \left\{ \frac{1}{6} + \frac{1}{2\gamma^2} \left(\cosh\gamma - \frac{1}{\gamma} \sinh\gamma \right) \right\}, \tag{2.75}$$

under the assumption of a small diffuse double layer. The validity of this approximation is rather limited, as the expression, as cited from [83] is derived using the Debye-Hückel approximation (see Section 2.1), valid for larger diffuse double layers.

Comparison of expressions

In Figure 2.8, curves obtained from various expressions for the reflection coefficient are compared. Table 2.3 lists the parameters used.

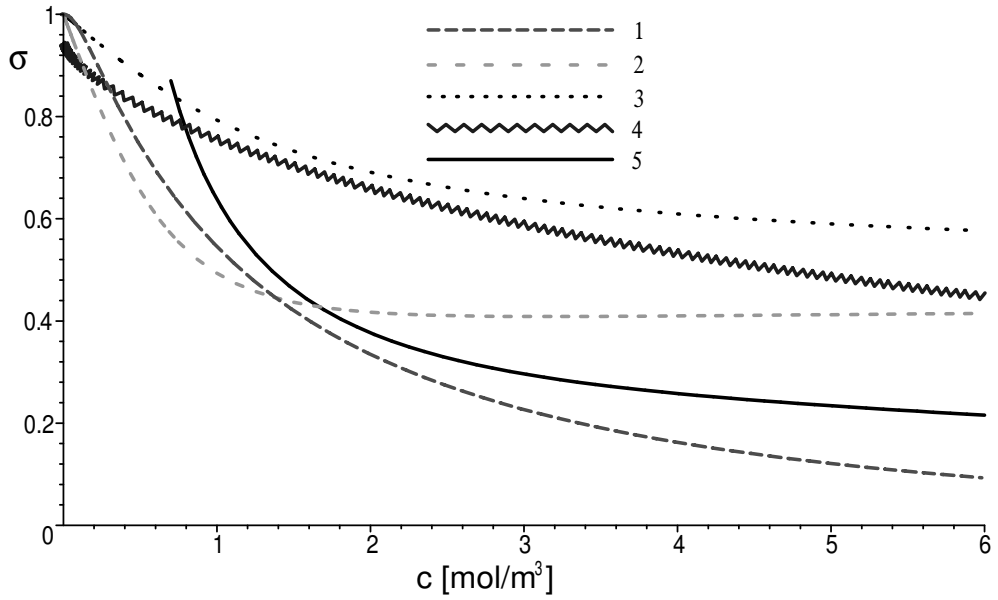

Figure 2.8: *Comparison of different expressions for σ*

graph number	description
1	Bresler (2.53)
2	FMM (2.55)
3	Simple (2.45)
4	Bolt (2.63) exact solution; $\kappa_0\delta = 0.45$
5	Homogenization (2.75)

Table 2.4: *Graph numbers corresponding to Figure 2.8*

Anomalous osmosis, negative values of σ

When a clay sample is subjected to a salt concentration gradient and water flows from high to low concentration instead of the other way around, this is called anomalous, abnormal, or negative osmosis. There are roughly two explanations for this behaviour. When a membrane potential develops due to a concentration gradient, this may induce electro-osmosis that causes a counterflow decreasing the flow by chemical osmosis. This flow may, in certain circumstances, even cancel or reverse the overall flow. In this case, the anomalous osmosis can be easily explained by electrical effects. However, experiments have shown anomalous osmotic behaviour even for electrically shorted systems [42]. In [42],[94] it is argued that the fluid may be dragged along with the ions that move by diffusion, analogous to electro-osmosis. This depends on the effective transport coefficients of the ions relative to the water. Anomalous osmosis may even cause the reflection coefficient to become negative, as is observed in a number of experiments [42],[94].

2.3.3 Electro-osmotic permeability

The coefficient of electro-osmotic permeability k_e is the coefficient coupling an electric potential gradient ∇V linearly to the specific discharge $\mathbf{q}$:

$$\mathbf{q}_{\text{electro-osmosis}} = -k_e \nabla V. \tag{2.76}$$

As a clay sample is subjected to an electrical potential, the excess cations in the clay will drag water molecules toward the low potential side, creating an effective water flow. The counterpart of electro-osmosis is streaming potential, which is usually represented by the following equation:

$$\mathbf{I}_{\text{streaming}} = -\frac{k_e}{\sigma_e} \nabla p, \tag{2.77}$$

where $\mathbf{I}$ is the electrical current and σ_e is the electrical conductivity. Water is pushed through a clay sample, and the distribution of ions is disturbed; the cations are dominant and they will be advected downstream, creating an electrical current.

Several theories exist for the description of these two quite interrelated processes and the determination of the electro-osmotic permeability. Starting with the Helmholtz-Smoluchowski theory, which is most often applied in electro-osmosis problems, we briefly review the Schmid theory, the Spiegler friction model and ion hydration. Furthermore, the expressions of k_e derived using averaging and homogenization techniques are mentioned and compared. This overview is taken from the book of Mitchell [80]

Helmholtz-Smoluchowski

In 1879, Helmholtz [53] published a paper on the theoretical description on electrokinetic phenomena. The result was refined by Smoluchowski [107] in 1914, and the theory became later known as the Helmholtz-Smoluchowski theory.

We consider a single water saturated capillary with the walls carrying negative charge and a immobile cation layer of thickness δ, as shown in Figure 2.9.

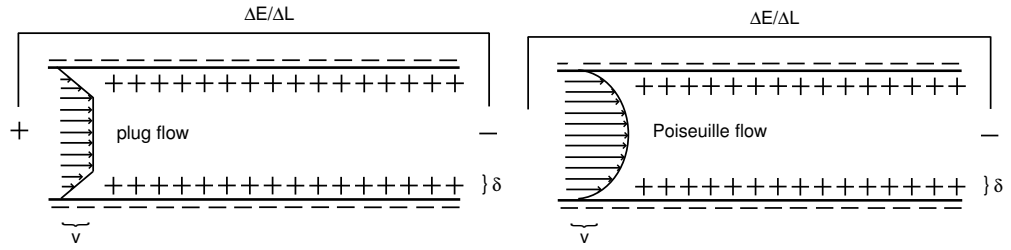

Figure 2.9: *Helmholtz-Smoluchowski and Schmid model for electro-osmosis*

The mobile cations drag the water along with a constant velocity v because of an applied electrical potential gradient ∇V. The Lorentz force F_L due to this gradient is balanced by the viscous part of the force F_V in the Navier-Stokes equation due to the friction between the mobile part and the wall:

$$F_L = F_V, \tag{2.78}$$

$$\Sigma \nabla V = \mu \frac{\mathbf{v}}{\delta}, \tag{2.79}$$

where Σ is the charge density, and μ is the fluid viscosity. If we treat the clay platelet and immobile cation layer system as a parallel plate capacitor and if we assume a uniform electrical field, we then find that the potential difference between the imaginary plates of the capacitor is given by

$$V_{cap} = \frac{\Sigma \delta}{\varepsilon_r}, \tag{2.80}$$

where ε_r is the relative permittivity of the medium between the plates. The potential V_{cap} is commonly referred to in clays as the zeta potential ζ, which denotes in general the potential difference between the no-slip plane and the reference position (mid-plane). To upscale this equation to a bundle of capillaries, one needs only to multiply the equation for the flow rate with the porosity n, leading to an expression for the discharge $\mathbf{q}_{el}$ due to electro-osmosis:

$$\mathbf{q}_{el} = -k_e \nabla V, \tag{2.81}$$

where k_e can now be identified as

$$k_e = \frac{\zeta \varepsilon_r n}{\mu}. \tag{2.82}$$

Note that in some publications (e.g. [52]), the electro-osmotic permeability is defined as the ratio of flow rate and electrical current at zero pressure. This leads to the ratio of 'our' electro-osmotic permeability and the electrical conductivity, which we call the streaming potential coefficient. Obviously, these two definitions have to be distinguished carefully.

Schmid

In the Schmid theory [102], the cations are assumed to be distributed uniformly across the capillary and the velocity profile is described by the Poiseuille equation. This implies for the electro-osmotic permeability:

$$k_e = \frac{A_0 F R^2 n}{8\mu}, \tag{2.83}$$

where A_0 is wall charge concentration per unit fluid volume, R is the capillary (=pore) radius and F is Faraday's constant. An interesting conclusion comes from comparing the Helmholtz-Smoluchowski and the Schmid expression: the latter depends on the pore radius, contrary to the former. In general, the values of k_e fall in the range $k_e \in (0.2, 1) \cdot 10^{-8}$ m^2/Vs [9], which indicates an independence on pore radius, as clay samples of quite different structure were considered, and hydraulic conductivity varies in 6 or 7 orders of magnitude. Also, the Helmholtz-Smoluchowski theory seems to give a better prediction for values of k_e obtained in experiments [80]. These two facts have led to the general application of the Helmholtz-Smoluchowski equation as the 'fundamental' equation for electro-osmosis

Other theories for electro-osmosis

In Mitchell [80], two other theories for electro-osmosis are presented. The first one, called the Spiegler friction model, assumes an ideal semi-permeable membrane, i.e. complete exclusion of anions and a concentration dependence of the coefficient of

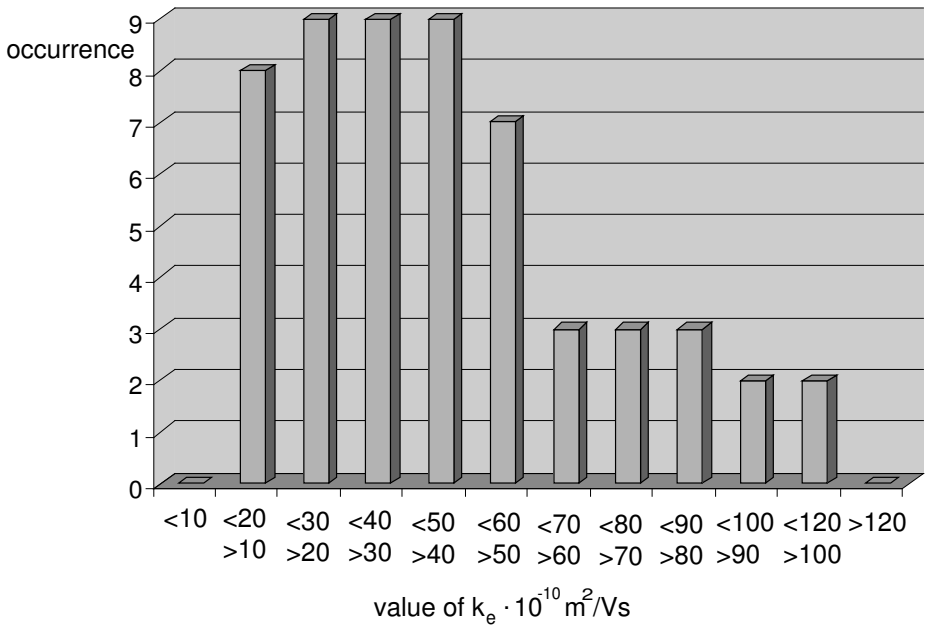

Figure 2.10: *Occurence of electro-osmotic permeability values in the review by [125]*

electro-osmotic permeability. The second theory is called ion hydration; here, hydration water simply moves along with the ions, and the coefficient of electro-osmosis is strongly dependent on the transport numbers of the ions. Both theories have limited applicability in describing electro-osmosis correctly.

Values of k_e

The electro-osmotic permeability has been subject of an enormous amount of experimental studies, which is due to the many applications of electro-osmosis. In [125] and [96] overviews are given of many experimental results, among which those of Casagrande [15], Esrig [24] and Gray and Mitchell [35]. In the thesis of Gray [34], it is shown how many results are either derived using direct measurements on electro-osmosis or indirectly using results of measurements on streaming potential. Throughout the literature, people have found that the experimental values of the electro-osmotic permeability never deviate much from $\sim 3 \cdot 10^{-9}\mathrm{m}^2/\mathrm{Vs}$.

In Figure 2.10 the values of k_e are shown from the collection as obtained by Yeung in [125]. A wide range of experimental circumstances is represented: electro-osmotic permeabilities of very different soils have been obtained, from compacted to loose, from bentonite to silty clay. The ratio between intrinsic permeability and

electro-osmotic permeability differs from 10^{-4} to 10^{5}. In [9] it is argued that this is also an indication that k and k_e are hardly related, as intrinsic permeability is determined by the presence of large pores, whereas the electro-osmotic permeability is only dependent on the mobility of countercharges in the smaller pores, no matter how many large pores may be present. In other words, the electro-osmotic permeability, contrary to the intrinsic permeability, is hardly dependent on compaction or pore structure. This also follows from the Helmholtz-Smoluchowski formula: only the zeta potential could potentially be highly variable. However, experimental values of ζ never deviate much from 30mV.

The electro-osmotic permeability k_e as derived using averaging

In a previous section we have seen that, using the averaging procedure for a slit domain according to Bolt [9], the electro-osmotic permeability can be written as

$$k_e = \frac{n}{\tau} L_{EV}, \tag{2.84}$$

$$L_{EV} = -\frac{\varepsilon_r}{4\pi b\mu} \int_0^b dx \left[(\zeta - \psi) \left(u - \frac{1}{u} \right) \right]. \tag{2.85}$$

For an infinitely extending double layer, in [9] an equation is listed for the relation between ψ and x:

$$\psi = \frac{2RT}{F} \ln \coth \frac{\kappa_0 x}{2}, \tag{2.86}$$

$$\zeta = \psi(x = \delta_m), \tag{2.87}$$

$$\kappa_0 x = -\ln \left[\frac{\sqrt{u} - 1}{\sqrt{u} + 1} \right] + \ln \left[\frac{\sqrt{u_s} - 1}{\sqrt{u_s} + 1} \right], \tag{2.88}$$

where κ_0 is the reciprocal Debye length and u_s is the Boltzmann factor for the zeta potential. Introducing the following definitions:

$$\kappa_0 x = -\ln t/t_s, \tag{2.89}$$

$$\kappa_0 \delta = -\ln t_s = y, \tag{2.90}$$

$$\kappa_0 b = -\ln t_d/t_s = w, \tag{2.91}$$

$$1 - \frac{1}{u} = \frac{4t}{(1+t)^2} \tag{2.92}$$

$$\mathcal{H} = \frac{\varepsilon_r RT}{F\mu}, \tag{2.93}$$

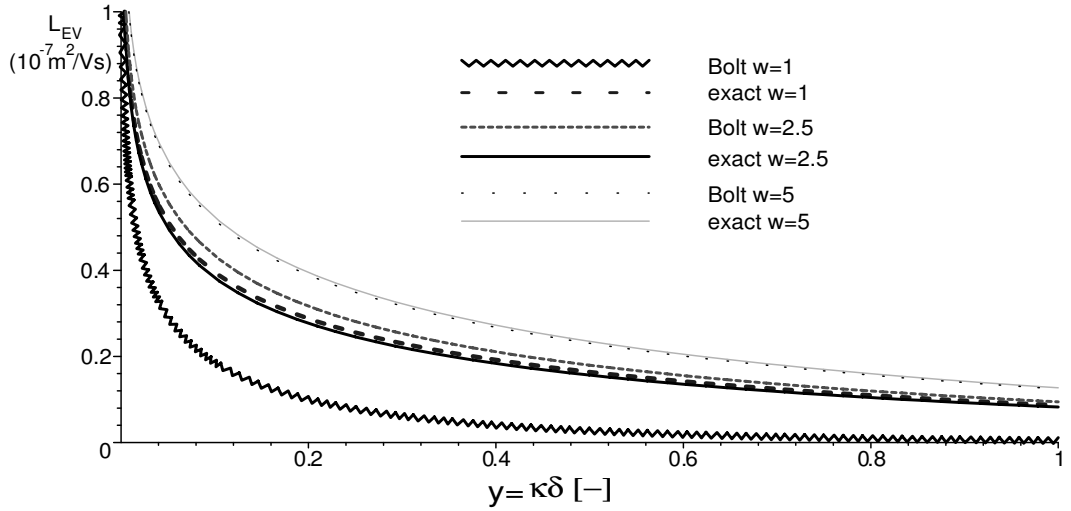

Figure 2.11: *Bolt derivation of k_e: comparison of the exact result (2.94) with the approximation by Bolt*

yields the following exact expression for L_{EV},

$$L_{EV} = \frac{4\mathcal{H}}{w}\int_{t_s}^{t_d} dt \left\{ \ln\left(\frac{t}{t_s}\right) + \ln^2\left(\frac{t}{t_s}\right)\right\}\left(\frac{1+t^2}{(t^2-1)^2}\right), \tag{2.94}$$

$$= \frac{4\mathcal{H}}{w}\left\{ \frac{w-y}{2}\ln\frac{(t_d-1)(t_s+1)}{(t_s-1)(t_d+1)} - \frac{3w^2}{2}\frac{t_d}{1-t_d^2}\right. \tag{2.95}$$

$$-\frac{1}{2}((y-w)\ln(1+t_d) - y\ln(1+t_s)) \tag{2.96}$$

$$\left. -\frac{1}{2}\mathcal{L}(t_d) + \frac{1}{2}\mathcal{L}(t_s) - \frac{1}{2}\mathcal{L}(1+t_d) + \frac{1}{2}\mathcal{L}(1+t_s)\right\}, \tag{2.97}$$

where, as before, $\mathcal{L}(x)$ is the dilogarithmic function (2.66). The particular integral for k_e, as well as for the reflection coefficient σ, is merely approximated in the book of Bolt [9]. As can be seen in Figure 2.11, the result presented in [9] deviates from the exact result.

When we pass to the limits $t_s \to 0, t_d \to 1, y \to 0$, for a small immobile layer and a large double layer, we find

$$L_{EV} = \frac{4\mathcal{H}}{w}\left\{\frac{w}{2}\ln\frac{t_s+1}{1-t_s} - \frac{\pi^2}{4}\right\} \tag{2.98}$$

If we now take $w \to 0$, disregard the tortuosity, i.e. $k_e = nL_{EV}$, and rewrite the argument of the logarithm, then:

$$k_e = 2\mathcal{H}n \ln \frac{1+t_s}{1-t_s} = 2\mathcal{H}n \ln \coth \frac{y}{2}. \tag{2.99}$$

We have seen in equation (2.87) that the zeta potential can be written in terms of y, yielding

$$k_e = 2\frac{\varepsilon_r RT}{F\mu}\frac{F}{2RT}\zeta = \frac{\varepsilon_r \zeta n}{\mu}, \tag{2.100}$$

and hence we find in this limit the Helmholtz-Smoluchowski result.

The electro-osmotic permeability k_e as derived using homogenization

As stated in the section on homogenization the expression derived for the electro-osmotic permeability reads:

$$K_e = \frac{\Sigma L_D}{\mu}\left\{\frac{2}{\gamma} - \coth\frac{\gamma}{2}\right\}. \tag{2.101}$$

For large γ, i.e. small immobile layer, the first term cancels and we find, when introducing the zeta potential ζ, as in [83]

$$\begin{aligned} \zeta &= -\frac{RT}{F}\psi_0 && (2.102)\\ &= -\frac{RT}{F}\frac{\Sigma F L_D}{\varepsilon_r RT}\coth\frac{\gamma}{2} && (2.103)\\ \rightarrow -\Sigma L_D \coth\frac{\gamma}{2} &= \zeta\varepsilon_r, && (2.104) \end{aligned}$$

that the electro-osmotic permeability reduces to

$$k_e = nK_e = \frac{\varepsilon_r \zeta n}{\mu}, \tag{2.105}$$

which, again, is identical to the Helmholtz-Smoluchowski equation.

2.3.4 Diffusion coefficient

The diffusion coefficient D or diffusivity represents the direct coupling of a solute flux $\mathbf{J}_d^s$ to a concentration gradient ∇c. This is expressed by Fick's law:

$$\mathbf{J}_d^s = -D\nabla c. \tag{2.106}$$

The coefficient D as given here may depend on numerous parameters. For diffusion of a 1:1 electrolyte such as NaCl, the free diffusion coefficient D_f is expressed in terms of ionic mobilities u_i as

$$D_f = \frac{2RT}{F}\frac{u_+u_-}{u_+ + u_-}. \tag{2.107}$$

For a porous medium, this expression has to be adapted for the flow paths of the ions going through the pores. A quite general way to do this is to define a formation factor F_0, such that

$$D = \frac{D_f}{F_0}. \tag{2.108}$$

The formation factor exists in different forms (from [5]):

$$F_0 = \frac{1}{n\tau} \text{ Cornell, Katz [19]}, \tag{2.109}$$

$$F_0 = \frac{1}{\sqrt{n\tau}} \text{ Wyllie, Spangler [122]}, \tag{2.110}$$

$$F_0 = C(\tau)n^{-m} \text{ Wyllie, Gardner [121]}, \tag{2.111}$$

$$F_0 = \frac{1}{n\tau^{5/6}} \text{ Winsauer et al [120]}, \tag{2.112}$$

$$F_0 = n^{-m} \text{ Archie [1]}, \tag{2.113}$$

where m is the cementation index, $C(\tau)$ is some function of tortuosity, n is porosity and τ is the tortuosity: using the definition in [5], in one dimension, $\tau = (L/L_e)^2$, where L is the length of the straight line and L_e the length of the tortuous path.

The formation factor is also quite commonly used in the description of the electrical conductivity.

Implicit coupling

An important concept regarding diffusion in semi-permeable media, is implicit coupling. This term is introduced in [76]. It implies that when the membrane is ideal, i.e. completely closed to ions, the diffusion coefficient should vanish as well. Otherwise, according to Fick's law, a solute flux would still be possible.

The precise dependence of the diffusion coefficient on σ, as implied by implicit coupling, has not been established yet. However, the following expression does at least satisfy the criteria for limit values of the reflection coefficient:

$$D(\sigma) = D_0(1-\sigma). \tag{2.114}$$

This relation can actually be derived from the equation for the reflection coefficient as stated by Katchalsky and Curran [62].

Starting from equation (10-56) in [62] for the continuous case:

$$\sigma = 1 - \omega\left[\frac{\bar{V}_s}{k/\mu} + \frac{f_{sw}}{n}\right] = 1 - \omega\cdot g, \tag{2.115}$$

where ω is a solute permeability coefficient introduced in [62] and $g = \bar{V}_s/(k/\mu) + f_{sw}n$ is introduced for convenience. The molar salt volume is $\bar{V}_s$; it is usually assumed to vanish: $\bar{V}_s \approx 0$. The friction coefficient f_{sw} can be written as (using (12-59) and the line after (12-56))

$$f_{sw} = f_{+w} + f_{-w} = \frac{1}{\tau}\left(\frac{1}{u_+} + \frac{1}{u_-}\right). \tag{2.116}$$

In Chapter 3 we will see that we may define, for 1:1 electrolytes

$$D = 2\omega RT. \tag{2.117}$$

Now:

$$\sigma = 1 - \frac{D}{\nu RT}\left[\frac{1}{n\tau}\left(\frac{1}{u_+} + \frac{1}{u_-}\right)\right], \tag{2.118}$$

or

$$\begin{aligned} D &= \frac{2}{g}RT(1-\sigma) && (2.119)\\ &= n\tau\frac{1}{\frac{1}{u_+}+\frac{1}{u_-}}2RT(1-\sigma) && (2.120)\\ &= n\tau\frac{u_+u_-}{u_+ + u_-}2RT(1-\sigma) && (2.121)\\ &= n\tau D_f(1-\sigma), && (2.122) \end{aligned}$$

where we used equation (2.107). If we use the first expression for the formation factor as seen before, we find indeed, using (2.108)

$$D(\sigma) = D(1 - \sigma). \tag{2.123}$$

2.3.5 Cation exchange

The low values of the effective diffusion coefficients observed in experiments can be attributed to both tortuous pathways, i.e. a high formation factor due to high compaction, and retardation due to cation exchange. This is the process where cations in a solute entering a clay soil are exchanged with cations on the clay matrix. This can be interpreted as a kind of sorption. If we assume this sorption to be linear, cation exchange can be described by a retardation parameter $\mathcal{R}$ that retards diffusion: [74]

$$D_r = \frac{D}{\mathcal{R}}, \tag{2.124}$$

where $\mathcal{R} = 1 + \frac{1-n}{n}\rho_s K_d$, ρ_s is the density of solid, D_r is an effective diffusion coefficient corrected for retardation and K_d is a distribution coefficient signifying the relation between the amount of 'adsorbed' cations and bulk concentration. The distribution coefficient may be expressed in terms of the cation exchange capacity $\mathcal{C}$ according to [23]:

$$K_d = \gamma \mathcal{C}, \tag{2.125}$$

where γ is a constant. The cation exchange capacity is defined as the number of exchangeable cations required to balance the charge deficiency of a clay. In [63], [27], the following formula is presented:

$$c_c = c_a + \mathcal{C}\rho_s \frac{1-n}{n}, \tag{2.126}$$

where c_c and c_a are concentration of respectively cations and anions in the double layers.

The cation exchange capacity is usually expressed in units of [meq/g]=[mol$_c$/kg].

In [17] it is shown that adsorption can be considered to be a special case of cation exchange: the equilibrium relationship, i.e. the exchange isotherm, between the

amount of ion on the solid q_i as a function of the concentration of exchangeable ion c_i in solution is:

$$q_i = f(c_0, c_1, ..., c_{n-1}) \text{ cation exchange.} \tag{2.127}$$

So, for ion exchange, the q_i depends on the concentration of all types of cations in solution. Adsorption is basically equivalent; the difference is that cations are not exchanged but 'stick' to the solid: q_i therefore depends only on the concentration of the same cation species in the solution:

$$q_i = f(c_i) \text{ adsorption.} \tag{2.128}$$

The electro-neutrality conditions in the solution and on the solid read, respectively:

$$\sum_i^n c_i = c_0 \text{ solution,} \tag{2.129}$$

$$\sum_i^n q_i = \mathcal{C} \text{ solid,} \tag{2.130}$$

where c_0 denotes the anion concentration in the solution, and $\mathcal{C}$ is the cation exchange capacity, i.e. the number of available exchange sites. This number is effectively the amount of negative charge of the solid, causing the excess of cations in solution.

The chemical reaction corresponding to the process of exchange yields a mass action law (assuming two monovalent cations):

$$K_{ij} = \frac{q_i c_j}{q_j c_i}, \tag{2.131}$$

where K_{ij} are selectivity coefficients. Combining (2.129) and (2.131) yields

$$q_1 = \frac{K_{12} Q_v c_1}{c_0 + (K_{12} - 1)c_1}. \tag{2.132}$$

This equation shows that ion exchange is described by a Langmuir isotherm.

2.3.6 Electrical conductivity

The electrical conductivity σ_e is the parameter that represents the direct coupling between the electrical current $\mathbf{I}$ on an electrical potential gradient ∇V via Ohm's law:

$$\mathbf{I} = -\sigma_e \nabla V. \tag{2.133}$$

For a free 1:1 electrolyte, the electrical conductivity σ_f is defined as

$$\sigma_f = F(u_+ + u_-)a_f, \tag{2.134}$$

where u_i are the ionic mobilities, F is Faraday's constant and a_f is the activity of the fluid. This expression is considered in more detail in Chapter 6. Similar to the diffusion coefficient for instance, the expression for electrical conductivity of a porous medium has to be adapted for the geometrical and electrical restraints. A simple method is to use, again, the formation factor:

$$\sigma_e = \frac{\sigma_f}{F_0}, \tag{2.135}$$

where σ_e is the 'bulk' electrical conductivity of the system composed of the porous medium and the interstitial fluid. We have seen expressions for the formation factor before; σ_e is usually corrected for geometry using Archie's law.

In a number of applications, the influence of the charge on the porous medium is taken into account by a surface diffusion term. In many experiments the following behaviour is found: when σ_e is plotted as a function of σ_f, it increases nonlinearly (upwards convex) and varies linearly afterwards. This may be explained by different tortuosities of the surface and the pores. From [103]: *As σ_f increases, dominant current paths shift from surface to pore...* The previous equation can be adapted for surface effects as follows [118]:

$$\sigma_e = F_0^{-1}(\sigma_f + \sigma_\chi), \tag{2.136}$$

where σ_χ is the conductivity of the exchangeable cations.

An empirical formula for the surface electrical conductivity is given in [118] and reads

$$\sigma_\chi = BQ_v, \tag{2.137}$$

$$Q_v = \rho_s \mathcal{C} \frac{1-n}{n}, \tag{2.138}$$

where Q_v is the excess surface charge density, $\mathcal{C}$ is cation exchange capacity, n is porosity, ρ_s is rock density and B is the mobility of the counter-ions near the surface, which equals, according to an empirical formula [118]:

$$B = (1 - 0.6e^{-\sigma_f/1.3}) \cdot 4.6 \cdot 10^{-8}. \tag{2.139}$$

In [103] it is shown how theoretical arguments lead to a formulation similar to (2.136) and (2.137).

In [98] a generalized version of equation (2.136) is given, which reads:

$$\sigma_e = F_0^{-1}(\sigma_f + f(\sigma_\chi)). \tag{2.140}$$

For low salt concentrations, (only) the cations are affected by the double layers and their dominant paths are located in the grain-water interface, whereas the anions always move in the pore space; at low salt concentrations, their tortuosities are therefore different; at high salt concentrations, the dominant pathways of the cations are located in the pore space as well, and conductivity of cations equals that of anions.

In [98], the function $f(\sigma_\chi)$ is given by

$$f(\sigma_\chi) = t_+ + F_0\xi + \frac{1}{2}(t_+ - \xi)\left(1 - \frac{\xi}{t_+} + \sqrt{\left(1 - \frac{\xi}{t_+}\right)^2 + \frac{4F_0}{t_+}\xi}\right), \tag{2.141}$$

where

$$\xi = \frac{\sigma_\chi}{\sigma_f} \approx \frac{2}{3}\frac{\beta_s}{\sigma_f}\frac{n}{1-n}Q_v. \tag{2.142}$$

The parameter t_+ is the Hittorf transport number for the cation and B is assumed constant in [98]. This formulation implies a particular expression for the surface conductivity for low and intermediate porosities. For high porosity, Sen, in [103] gives the following formula:

$$\xi \approx \frac{3}{2(3-n)}\frac{\beta_s Q_v}{\sigma_f}. \tag{2.143}$$

The model of Groenevelt and Bolt [9] also provides an expression for the electrical conductivity:

$$L_E = \sigma_e = \frac{n}{\tau}\frac{c_f}{w}\left\{2F\Lambda w + Ff(u_s)\left[\frac{8F}{\mu} + 2\Lambda\right]\right\}, \tag{2.144}$$

where $f(u_s) = \sqrt{u_s} - 2 + 1/\sqrt{u_s}$ is a function of $u_s = \coth^2(y/2)$, y is the relative thickness of the immobile layer and w is the relative thickness of the double layer. Tortuosity is τ and the mean mobility of the ions is $\Lambda = (u_+ + u_-)/2$. This expression can be written in the Waxman-Smits [118] formulation as

$$\sigma_e = \frac{1}{F_0}\left(\sigma_f + \sigma_\chi\right), \tag{2.145}$$

where

$$F_0 = \frac{\tau}{n}, \tag{2.146}$$

$$\sigma_f = 2F\Lambda c_f = F(u_+ + u_-)c_f, \tag{2.147}$$

$$\sigma_\chi = \frac{c_f F f(u_s)}{w}\left(\frac{8Fc_f}{\kappa_0^2\mu} + 2\Lambda\right). \tag{2.148}$$

For large double layers (large y) or immobile layers (large w), the surface term vanishes and only the first term remains.

2.4 Summary

In this chapter it was shown which microscopic properties of clay are responsible for the semi-permeability of clayey soils and how this leads to the occurrence of coupled processes in clay such as chemical and electro-osmosis. These processes are described using macroscopic coefficients such as the reflection coefficient and the electro-osmotic permeability and equations describing flow of water and transport of solutes as a result of these coupled processes. An overview of different versions of these coefficients was given and it was shown how they compare and how their description can be improved. In the next chapter, the equations are derived and some of their implications are presented.

Chapter 3

Equations for chemical and electro-osmosis in soils

3.1 Introduction

In order to model osmosis in groundwater, we need to obtain the correct parameters and coefficients, as derived in Chapter 2, and a set of equations, which will be discussed in this part of the study. Macroscopic transport formulations for direct and coupled flow of water and solutes can be derived using approaches based on continuum mechanics [47], homogenization [84], empirical methods and non-equilibrium thermodynamics. In our study, the latter approach [62],[123] is used. The general equations are presented first, after which we list the specific forms of the equations used for modelling chemical osmosis and modelling of combined chemical and electro-osmosis. Finally, known balance laws are listed to complete the general overview of relevant equations.

3.2 Non-equilibrium thermodynamics

When a soil system is subjected to one or more gradients of, for example, salt concentration or electrical potential, it becomes a system out of equilibrium. As classical thermodynamics is only able to describe initial and final states of spontaneous processes, the response to these gradients needs to be formulated using irreversible or non-equilibrium thermodynamics. This theory was developed in the 1940's by Meixner and Prigogine and provides a general framework for the macroscopic description of irreversible processes [124]. An overview of the theory is given by [62], [40], [25]; in this study, we follow the derivation of [124].

In non-equilibrium thermodynamics, all laws of classical thermodynamics are assumed to be valid. To include irreversible processes, the classical theory has to

be extended with the following assumptions:

- local equilibrium: for every instance, the system can be described as if it were in local equilibrium, and the equations from thermodynamics, valid for reversible processes, can then be applied.
- linear phenomenological equations: the fluxes $\mathbf{J}_i$ are linear function of driving forces $\mathbf{X}_j$:

$$\mathbf{J}_i = \sum_j L_{ij} \mathbf{X}_j \tag{3.1}$$

  and the coefficients L_{ij} that relate them are independent of the driving forces; in chapter 4 some non-linear theories are discussed
- Onsager relations: the so-called Onsager theorem is assumed to hold: it states

$$L_{ij} = L_{ji} \tag{3.2}$$

  or: *provided a proper choice is made for the fluxes J_i and driving forces X_j, the matrix of phenomenological coefficients L_{ij} is symmetric.* In a next section, the validity of these equations is discussed

In non-equilibrium thermodynamics, a central role is played by the entropy balance equation:

$$\frac{\partial s}{\partial t} = \sigma_{\text{ent}} - \nabla \cdot \mathbf{J}_s. \tag{3.3}$$

The entropy s of a volume element changes by entropy flowing into the volume element ($\nabla \cdot \mathbf{J}_s$, where $\mathbf{J}_s$ is the entropy flux) and by creation of entropy, specified by the entropy source strength σ_{ent}. For reversible processes, this term vanishes.

The change of entropy S may be derived from the Gibbs equation, which reads

$$TdS = dU + pdV - \sum_{i=1}^{n} \mu_i dn_i, \tag{3.4}$$

where T is temperature, U is internal energy, p is pressure, V is the volume of the system, and μ_i and n_i are chemical potential and number of moles of species

i respectively. In [123] it is shown how, by locally differentiating with respect to time, dividing by the volume and rearranging, this equation can be written as

$$T\frac{\partial s}{\partial t} = \frac{\partial q}{\partial t} - \sum_{i=1}^{n} \mu_i \frac{\partial c_i}{\partial t}. \tag{3.5}$$

Here, the postulate of local equilibrium is applied: although the total system is not in equilibrium, within small mass elements a state of local equilibrium exists [40]. The concentration of species i is c_i and q is the energy per volume unit transported into the volume. The first law of thermodynamics, applied to the volume element v was used: $du = dq - pdv$, where pdv represents the work done on the volume element.

To expand the right hand side of this equation, we have the balances of mass and energy, in the absence of chemical reactions:

$$\frac{\partial c_i}{\partial t} = -\nabla \cdot \mathbf{J}_i \tag{3.6}$$

$$\frac{\partial q}{\partial t} = -\nabla \cdot \mathbf{J}_q, \tag{3.7}$$

where $\mathbf{J}_i$ is mass flux and $\mathbf{J}_q$ is energy flux.

Introducing these and the entropy balance in (3.5)

$$T\left(\sigma_{\text{ent}} - \nabla \cdot \mathbf{J}_s\right) = -\nabla \cdot \mathbf{J}_q + \sum_{i=1}^{n} \mu_i \nabla \cdot \mathbf{J}_i. \tag{3.8}$$

Now, according to [62], under isothermal conditions:

$$T\nabla \cdot \mathbf{J}_s = \nabla \cdot \left(\mathbf{J}_q - \sum_{i=1}^{n} \mu_i \mathbf{J}_i\right), \tag{3.9}$$

so:

$$\Phi = T\sigma_{\text{ent}} = -\sum_{i=1}^{n} \nabla \mu_i \cdot \mathbf{J}_i, \tag{3.10}$$

where we have introduced the dissipation function Φ, which is a measure of dissipation of free energy by irreversible processes [123]. In general this function can be written as the sum of products of fluxes and driving forces

$$\Phi = \sum_{i=1}^{n} \mathbf{J}_i \cdot \mathbf{X}_i. \tag{3.11}$$

Using this procedure the expressions for the fluxes and driving forces are defined.

We may introduce the electrochemical potential $\tilde{\mu}_i$ of species i instead of the chemical potential [62]:

$$\tilde{\mu}_i = \mu_i + z_i F V, \tag{3.12}$$

where z_i is ion valence, F is Faraday's constant and V is electric potential. This total electrochemical potential is given by [124]

$$\tilde{\mu}_i = \mu_i(T) + \bar{V}_i p + \mu_i(c), \tag{3.13}$$

where $\mu_i(T)$ and $\mu_i(c)$ are the temperature and concentration dependent parts of $\tilde{\mu}_i$ respectively and $\bar{V}_i$ is partial volume of species i. In [62] it is shown how (3.10) is also valid for $\tilde{\mu}_i$, and so:

$$\Phi = -\sum_{i=1}^{n} \nabla \tilde{\mu}_i \cdot \mathbf{J}_i \tag{3.14}$$

$$= -\left(\sum_{i=1}^{n} \mathbf{J}_i \bar{V}_i \right) \cdot \nabla p - \sum_{i=1}^{n} \mathbf{J}_i \cdot \nabla \left(\mu_i(c) + z_i F V \right). \tag{3.15}$$

Let's assume we have three species: fluid (f), cation (c) and anion (a). In general, we may apply the Gibbs-Duhem relation [123], that follows directly from comparing the integrated form of the Gibbs equation with the Gibbs equation itself:

$$\sum_{i=f,a,c} c_i \nabla(\mu_i(c) + z_i F V) = 0 \tag{3.16}$$

This equation implies

$$\nabla \mu_f = -\sum_{i=a,c} \frac{c_i}{c_f} \nabla(\mu_i(c) + z_i F V), \tag{3.17}$$

where we use $z_f = 0$ because of the electro-neutrality of the fluid. Now we define the solution flux $\mathbf{q}$

$$\mathbf{q} = \left(\sum_{i=1}^{n} \mathbf{J}_i \bar{V}_i \right). \tag{3.18}$$

Substituting this and the previous result in the dissipation function:

$$\Phi = -\mathbf{q} \cdot \nabla p - \sum_{i=a,c} \left[\left(\mathbf{J}_i - \mathbf{J}_f \frac{c_i}{c_f} \right) \cdot \nabla \left(\mu_i(c) + z_i F V \right) \right]. \tag{3.19}$$

We can assume that the solution is dilute enough to write:

$$\mathbf{q} = \mathbf{J}_f \bar{V}_f + \mathbf{J}_a \bar{V}_a + \mathbf{J}_c \bar{V}_c \approx \mathbf{J}_f \bar{V}_f = \frac{\mathbf{J}_f}{c_f}, \tag{3.20}$$

and we define the ion flux $\mathbf{J}_i^d$ relative to the solution

$$\mathbf{J}_i^d = \mathbf{J}_i - c_i \mathbf{q}. \tag{3.21}$$

This yields

$$\Phi = -\mathbf{q} \cdot \nabla p - \sum_{i=a,c} \mathbf{J}_i^d \cdot \nabla \left(\mu_i + z_i F V \right). \tag{3.22}$$

Now with the electric current density

$$\mathbf{I} = \sum_{i=a,c} \mathbf{J}_i^d z_i F, \tag{3.23}$$

we find

$$\Phi = -\mathbf{q} \cdot \nabla p - \mathbf{J}_a^d \cdot \nabla \mu_a - \mathbf{J}_c^d \cdot \nabla \mu_c - \mathbf{I} \cdot \nabla V. \tag{3.24}$$

Equations (3.11) and (3.24) effectively define the fluxes and driving forces and we may now apply the postulate of linearity of the phenomenological equations:

$$\mathbf{J}_i = \sum_{i=1}^{n} L_{ij}\mathbf{X}_j, \tag{3.25}$$

to get the final form of the flux equations considered in this study:

$$\mathbf{q} = -L'_{11}\nabla p - L'_{12}\nabla\mu_c - L'_{13}\nabla\mu_a - L'_{14}\nabla V, \tag{3.26}$$

$$\mathbf{J}_c^d = -L'_{21}\nabla p - L'_{22}\nabla\mu_c - L'_{23}\nabla\mu_a - L'_{24}\nabla V, \tag{3.27}$$

$$\mathbf{J}_a^d = -L'_{31}\nabla p - L'_{32}\nabla\mu_c - L'_{33}\nabla\mu_a - L'_{34}\nabla V, \tag{3.28}$$

$$\mathbf{I} = -L'_{41}\nabla p - L'_{42}\nabla\mu_c - L'_{43}\nabla\mu_a - L'_{44}\nabla V, \tag{3.29}$$

The prime is written to distinguish the coupling coefficients from the coefficients used in the flux equations in which the flux of salt instead of ions is considered:

$$\mathbf{q} = -L_{11}\nabla p - L_{12}\nabla\mu_s - L_{13}\nabla V, \tag{3.30}$$

$$\mathbf{J}_s^d = -L_{12}\nabla p - L_{22}\nabla\mu_s - L_{23}\nabla V, \tag{3.31}$$

$$\mathbf{I} = -L_{31}\nabla p - L_{32}\nabla\mu_s - L_{33}\nabla V. \tag{3.32}$$

3.2.1 Validity of the Onsager relations and Saxen's law

The Onsager relations read: the matrix of phenomenological coefficients is symmetric, i.e. $L_{ij} = L_{ji}$, as long as the flows and forces appearing in the phenomenological equations are taken in such a way that

$$\sigma = \sum_{i=1}^{n} J_i X_i. \tag{3.33}$$

They are considered by many people to be so fundamental that, in 1968, Lars Onsager was awarded the Nobel Prize for Chemistry for discovering them. There is quite a body of literature on theoretical (statistical) derivations of the Onsager relations [62], [40], [25]. For example, in [40]: '*These reciprocal relations [ ] reflect on the macroscopic level the time reversal invariance of the microscopic equations of motion*'. Moreover, numerous experimental evidence indicates the validity of the relations. Indeed, with many experiments conducted relating to coupled phenomena, the first and foremost goal is to show the equality of coefficients, usually according to Saxen's law [101], which is based on the Onsager relations.

However, some authors question the validity of the Onsager relation. Ghassemi and Diek say in [33]: '...,*whether Onsager's reciprocity theorem is valid or [not] does not need to be verified by experiments*'. They base this on the observation that experimental studies [20] have shown violations of Onsager's symmetry. They refer to Heidug and Wong [50], who state: '*in view of the dispute, it appears that the Onsager relation cannot claim the status of a general statement, even though it may be valid in particular situations*'. They, in turn, refer to the work of Truesdell, who 'denounces' Onsager symmetry based on theoretical grounds, and experimental results that show violations, such as [20] and [78]. Also, Auriault and Strzelecki [2] have shown that Onsager symmetry is only valid if certain pore scale homogeneity conditions are met. On the one hand, one could argue that because the amount of experimental evidence in favour of the relations greatly outweighs the indications against it, the latter experiments should be disregarded. On the other hand, showing that two very similar coefficients are equal is much easier than that proving they are different.

If one considers the flux equations in absence of chemical gradients and in terms of differences in variables, as used by experimenters [80]:

$$q = L_{11}\Delta p + L_{12}\Delta V, \tag{3.34}$$

$$I = L_{21}\Delta p + L_{22}\Delta V, \tag{3.35}$$

a direct consequence of Onsager's law, $L_{12} = L_{21}$ is

$$\frac{L_{12}}{L_{22}} = \frac{L_{21}}{L_{22}} \rightarrow \left(\frac{q}{I}\right)_{\Delta p=0} = -\left(\frac{\Delta V}{\Delta p}\right)_{I=0}. \tag{3.36}$$

This was first experimentally shown by Saxen in 1892, and is therefore known as Saxen's law [101]. Different versions of this law exist, as the equality between cross coefficients can be exploited in other ways by setting other variables to zero.

Brun and Vaula [12] have performed experiments, showing the validity of Saxen's law in a phenolsulfate membrane subject to KCl solutions of different

salinity. Also, the law has been validated in works of Miller, Gray [124], Rutgers and Wijga (in glass capillaries, reported in [71]). Any differences are usually attributed to experimental shortcomings [71]. Many authors, for instance [34] apply Saxen's law to convert electro-osmosis data into streaming potential data.

3.3 Equations for chemical osmosis

The types of interrelated coupled flow that can occur in a soil are given in Table 3.3. This table is based on [80]

	gradient $\mathbf{X}\rightarrow$			
flow $\mathbf{J}\downarrow$	hydraulic	chemical	electrical	temperature
fluid	**hydraulic flow** Darcy's law	chemical osmosis (normal) osmosis	electro-osmosis	thermo-osmosis
solute	ultrafiltration Fick's law	**diffusion**	electrophoresis thermophoresis	Soret effect thermal diffusion
charge	streaming potential	diffusion potential membrane potential	**electrical conduction** Ohm's law	Seebeck effect thermo-electricity
heat	isothermal heat transfer	Dufour effect	Peltier effect	**thermal cond.** Fourier's law

Table 3.1: *Direct and coupled flow phenomena*

On the diagonal are the well-known relations between fluxes and driving forces. The non-diagonal elements correspond to the so-called coupled processes that may be significant under special circumstances, i.e. in the presence of a semi-permeable membrane. In this study, we disregard the gravity term in Darcy's Law. This will be justified in Chapter 4. Moreover, we assume isothermal conditions; as in [123], this is justified because temperature gradients are not likely to be significant in most natural systems. Also, in this section, we restrict ourselves to hydraulic and chemical gradients. We derive equations for a single solute species for reasons of brevity. The formulations can be readily extended for a solute consisting of multiple species following the approach of Malusis and Shackelford [76]. Later on, when we consider electrical effects, we necessarily have to adopt a description with separate ionic species. We acknowledge the fact that Darcy's law is conceptually very different from Fick's law (or Ohm's law, or Fourier's law), but we nevertheless exploit the analogy here. With these assumptions, the basic flux equations in terms of pressure $p\,[\mathrm{Pa}]$ and chemical potential of the solute $\mu_s[\mathrm{kg\,m^2/(mol\,s^2)}]$ are:

$$\mathbf{q} = L_{11}\nabla(-p) + L_{12}\nabla(-\mu_s) \tag{3.37}$$

$$\mathbf{J}_n^d = L_{21}\nabla(-p) + L_{22}\nabla(-\mu_s), \tag{3.38}$$

where $\mathbf{q}$[m/s] is the specific discharge and $\mathbf{J}_n^d$[mol/(m^{2}s)] denotes the diffusive molar flux of solute relative to the solution. Therefore solute molar flux relative to the porous medium is defined as $\mathbf{J}_n = \mathbf{J}_n^d + c_s\mathbf{q}$, where c_s[mol/m^3] is solute concentration. We can write $c_s = \frac{\rho_f \omega}{M_s}$, where ρ_f[kg/m^3] is the fluid density, $\omega[-]$ is the solute mass fraction and M_s[kg/mol] the solute molar mass. The chemical potential of solute can be expanded as

$$\mu_s = \mu_s^0 + \nu RT \ln a_s. \tag{3.39}$$

Here, μ_s^0 is the constant chemical potential for the pure solvent, ν is the dissociation coefficient (a solute dissociates into ν ions), which equals 2 for NaCl. This parameter is often omitted [123],[76],[93], but was correctly taken into account in e.g. [106]. The gas constant is denoted by R[J/(molK)], T[K] is temperature and $a_s[-]$ is the solute activity. Taking the gradient of the chemical potential now yields

$$\nabla \mu_s = \nu RT \frac{1}{a_s} \nabla a_s = \nu RT \frac{\rho_f}{\rho_s} \nabla \omega, \tag{3.40}$$

because $a_s = \gamma\omega\frac{M_f}{M_s}$, where $\gamma[-]$ is the activity coefficient, M_f[kg/mol] is the molar mass of the fluid, and salt mass fraction $\omega[-] = \frac{\rho_s}{\rho_f}$ [8]. Here, ρ_s[kg/m^3] is mass concentration of solute.
As in [62], the reflection coefficient is defined as the ratio of the coupling coefficient relating pressure to specific discharge and the coupling coefficient relating osmotic pressure to specific discharge:

$$\sigma = -\frac{L_{12}}{c_s L_{11}}, \tag{3.41}$$

because the osmotic pressure gradient is $\nabla\pi = c_s \nabla \mu_s$. Employing the analogy with Darcy's law, $L_{11} = k/\mu$ yields

$$L_{12} = -\sigma c_s L_{11} = -\frac{\sigma k \rho_s}{\mu M_s}, \tag{3.42}$$

where $k[m^2]$ is the intrinsic permeability of the porous medium and μ[kg/ms] the dynamic viscosity of the fluid. This implies

$$L_{12}\nabla(-\mu_s) = \frac{\sigma k}{\mu M_s} \nu RT \rho_f \nabla \omega = \lambda \rho_f \nabla \omega, \tag{3.43}$$

where we introduce the chemico-osmotic mobility $\lambda = \frac{\sigma k}{\mu M_s}\nu RT$. This name is chosen because of the analogy with the electro-osmotic permeability, but we acknowledge the fact that it is related to the hydraulic mobility $\frac{k}{\mu}$ rather than the intrinsic permeability k.

Using (3.43) in formula (3.37), the specific discharge becomes

$$\mathbf{q} = -\frac{k}{\mu}\nabla p + \lambda\rho_f\nabla\omega = -\frac{k}{\mu}\left(\nabla p - \sigma\nabla\pi\right). \tag{3.44}$$

The expression for the solute flux can be derived by substituting ∇p from (3.44) into the equation for the solute flux (3.38), yielding

$$\begin{aligned}
\mathbf{J}_n^d &= L_{21}\nabla(-p) + L_{22}\nabla(-\mu_s) \\
&= L_{21}\left(\frac{\mathbf{q}}{L_{11}} + \frac{L_{12}}{L_{11}}\nabla\mu_s\right) - L_{22}\nabla\mu_s \\
&= -\sigma\frac{\rho_f\omega}{M_s}\mathbf{q} + (\sigma\lambda\frac{\rho_f\omega}{M_s} - L_{22}\frac{\nu RT}{\rho_s})\rho_f\nabla\omega,
\end{aligned}$$

because applying Onsager's reciprocity relations yields

$$L_{21} = L_{12} = -\frac{\sigma k\rho_s}{\mu M_s}. \tag{3.45}$$

Analogously to equation (10-23) in Katchalsky and Curran [62], a solute permeability coefficient θ (similar to ω in [62]) is defined:

$$\theta = \frac{L_{22}\frac{\nu RT}{\rho_s} - \sigma\lambda\rho_f\omega/M_s}{\nu RT/M_s} = L_{22}/c_s - \sigma^2 c_s k/\mu. \tag{3.46}$$

If we interpret θ as a kind of solute mobility, or absolute mobility, as in [62], an effective diffusion coefficient $D = \nu\theta RT$ can be inferred, leading to an expression similar to Fick's law. The full equation for solute flux now reads

$$\mathbf{J}_n^d = -\sigma\frac{\rho_f\omega}{M_s}\mathbf{q} - D\frac{\rho_f}{M_s}\nabla\omega, \tag{3.47}$$

or in terms of solute mass flux $\mathbf{J}_s^d = \mathbf{J}_n^d M_s$

$$\mathbf{J}_s^d = -\sigma\rho_f\omega\mathbf{q} - D\rho_f\nabla\omega, \tag{3.48}$$

Writing this equation in terms of gradients yields

$$\mathbf{J}_s^d = \sigma\rho_f\omega\frac{k}{\mu}\nabla p - \sigma\rho_f\omega\lambda\rho_f\nabla\omega - D\rho_f\nabla\omega. \tag{3.49}$$

The first term represents ultrafiltration: when $\nabla\omega = 0$, there is solute flow relative to water because advection of solute is hindered by the membrane. The second term arises because the concentration gradient drives fluid flow by osmosis. Solutes in this flow are reflected by a semi-permeable membrane in the same way as in hydraulically forced ultrafiltration. The third term represents molecular diffusion: equation (3.48) reduces to Fick's law for zero specific discharge.

3.3.1 Effective diffusivity for a semipermeable membrane

As noted above, the effective diffusivity of a semipermeable membrane must be dependent on σ. The existence of such a relationship was recently mentioned by Soler [108] and Malusis and Shackleford [76], but not implemented in their model formulation. The form of the dependency should comply with the following limiting behaviour: D should tend to zero for an ideal membrane and should represent the conventional meaning of diffusivity for media without membrane properties. The simplest relationship that is consistent with these two requirements is

$$D = D_0(1-\sigma), \tag{3.50}$$

where D is a Fickian diffusion coefficient that includes tortuosity. This expressions has been derived from previous theories of Katchalsky and Curran [62] in Chapter 2.

3.3.2 Limiting behaviour for σ

Using $\mathbf{J}_s = \mathbf{J}_n M_s$ as the solute mass flux relative to the porous medium (inserting (3.50)in (3.48)):

$$\mathbf{J}_s = \mathbf{J}_s^d + \rho_f\omega\mathbf{q} = (1-\sigma)\rho_f\omega\mathbf{q} - D_0(1-\sigma)\rho_f\nabla\omega, \tag{3.51}$$

we observe that for $\sigma = 0$, when all membrane properties are absent, this expression reduces to the traditional advection-diffusion flux. For $\sigma = 1$, (3.51) becomes $\mathbf{J}_s = 0$, which accords with the fact that solute transport is completely prohibited in an ideal membrane. Previous studies, e.g. [82], [124], [80], [108], [76], define solute diffusive flux as:

$$\mathbf{J}_n^d = \sigma c_s \frac{k}{\mu} \nabla p - D_0(1-\sigma)\nabla c_s. \tag{3.52}$$

As the total flux is defined as $\mathbf{J}_n = \mathbf{J}_n^d + c\mathbf{q}$, we find

$$\mathbf{J}_n = -(1-\sigma)c_s \frac{k}{\mu} \nabla p + \sigma \frac{k}{\mu} \nu RT \nabla c_s - D_0(1-\sigma)\nabla c_s. \tag{3.53}$$

Here, we used our formulation, and assumed, for simplicity, $\frac{\rho_f}{M_s}\nabla\omega = \nabla c_s$. Hence, for $\sigma = 1$

$$\mathbf{J}_n = \frac{k}{\mu} \nu RT \nabla c_s, \tag{3.54}$$

which is not appropriate, as indicated before.

3.3.3 Concentration dependence of σ

Experimental work shows that the ideality of natural clayey materials is affected by several factors such as cation exchange capacity ($\mathcal{C}$), degree of compaction and solute concentration [63], [29]. Of these factors, the dependence on solute concentration is most amenable for incorporation in the present model. To account for this effect, a number of theoretical formulations of σ in terms of ion concentration, water film thickness and $\mathcal{C}$ were given in Chapter 2.

3.3.4 Effect of multiple ion species on osmosis

We may write the simple Darcy's law extended with chemical osmosis:

$$\mathbf{q} = -\frac{k}{\mu}\nabla p + \lambda \nabla c_s. \tag{3.55}$$

Let's assume $\lambda = \lambda' \nu = \sigma \nu RTk/\mu$ to be constant, then, in the case of NaCl, for instance, the expression can be decomposed as follows:

$$\mathbf{q} = -\frac{k}{\mu}\nabla p + \lambda'(\nabla c_c + \nabla c_a). \tag{3.56}$$

where c_c and c_a are cation and anion concentrations respectively. This result can now be generalized for n ionic species according to Malusis and Shackelford [76]:

$$\mathbf{q} = -\frac{k}{\mu}\nabla p + \lambda' \sum_{i=1}^{n} \nabla c_i. \tag{3.57}$$

3.4 Equations for chemico-electro-osmosis

In Section (3.2) we have derived the full set of equations (3.26-3.28) including electrical gradients and separate ionic fluxes. The time scale of transients of V is very small compared to that of fluid pressure and mass fraction. This is motivated in Chapter 4. Temporal changes in V, therefore, are slave to temporal changes in the other potentials. This behaviour can be approximated by disregarding electrical flow, i.e. $\mathbf{I} = 0$. In that case, (3.29) can be recast into

$$\nabla V = -\frac{L'_{41}}{L'_{44}}\nabla p - \frac{L'_{42}}{L'_{44}}\nabla \mu_c - \frac{L'_{43}}{L'_{44}}\nabla \mu_a. \tag{3.58}$$

Substituting this equation in the flux equations (3.26-3.28) and proceeding as in Section 3.3 one can derive the modified equation for the specific discharge

$$\mathbf{q} = -K^e \nabla p + \Lambda^e_c \rho_f \nabla \omega_c + \Lambda^e_a \rho_f \nabla \omega_a, \tag{3.59}$$

where

$$K^e = \frac{k}{\mu} - \frac{k_e^2}{\sigma_e}, \tag{3.60}$$

$$\Lambda^e_i = \lambda_i + \frac{u_i R T k_e}{\sigma_e M_s} \tag{3.61}$$

are a modified hydraulic mobility and chemico-osmotic mobility respectively. The subscripts $i = c, a$ refer to cations and anions respectively and $\nu_c\omega_c + \nu_a\omega_a = \nu\omega$. We assumed L'_{41} to be equal to the electro-osmotic permeability k_e [m^2/Vs] (as in [124]) and L'_{44} to be equal to the electrical conductivity σ_e [A/Vm] of the porous medium [124]. Also, electrophoresis is represented by the parameters $L'_{24} = u_c c_c$ and $L'_{34} = -u_a c_a$, where u_i [m^2/Vs] denotes ionic mobility. Hence the solute mass fluxes for the cations and the anions are (assuming, as in [124], $L'_{23} = L'_{32} = 0$):

$$\mathbf{J}^d_{cm} = -\Sigma_c c_c \mathbf{q} - D^e_c \rho_f \nabla \omega_c, \tag{3.62}$$

$$\mathbf{J}^d_{am} = -\Sigma_a c_a \mathbf{q} - D^e_a \rho_f \nabla \omega_a, \tag{3.63}$$

where

$$\Sigma_i = -\frac{\Lambda_i^e}{RTK^e}. \tag{3.64}$$

In the case of chemical osmosis, we assumed:

$$L_{22} = D - \sigma^2 c_s^2 \frac{k}{\mu}. \tag{3.65}$$

Now, analogously to this, we write for the cations:

$$L'_{22} = \left(D_c^e - \frac{u_c(u_c - u_a)c_c^2}{\sigma_e} \right) - \frac{(\Lambda_c^e)^2}{K^e} \frac{c_c^2}{(RT)^2} \tag{3.66}$$

Comparing equations (3.65) and (3.66), we see that they are similar, provided we account for the electrical corrections of $D_c^e, k/\mu$ and λ (when writing (3.65) in terms of λ). The anionic diffusion coefficient follows similarly. These expressions will be further specified in chapter 6.

Again, the diffusion coefficients are assumed to be of the form $D_0(1-\sigma)$. It is easy to show how these equations obey desired limiting behaviour for limits of σ and how they reduce to the set of previous derived equations in the absence of electrical effects.

There is some discussion regarding the sign of the corrections for electrical effects in for example the expression for the solvent flux (3.59). In [124], the coefficient L'_{11} is equated to

$$L'_{11} = \frac{k}{\mu} + \frac{L'_{12}L'_{21}}{L'_{22}} = \frac{k}{\mu} + \frac{k_e^2}{\sigma_e}, \tag{3.67}$$

where the correction is of a different sign compared to our formulation (3.60). The difference is explained by noting that we take L'_{11} to be the coefficient that directly relates $\mathbf{q}$ and ∇p, i.e.*a priori* without the electrical effects, whereas Yeung et al [124] consider this not to be the default experimental situation, and therefore attribute L'_{11} to the term with correction.

However, when considering what actually happens in the soil, it becomes clear that the sign of the correction should be as we define it. Take the streaming potential for instance: when a sample is subjected to a negative pressure gradient (left high pressure, right low pressure), water flows in positive direction as governed

by Darcy's law, dragging along excess cations in the direction of low pressure. A positive electrical potential gradient will therefore develop, causing a counter flow of water due to electro-osmosis. The correction for streaming potential necessarily has to be of a different sign than the permeability.

A similar reasoning can be applied to the other terms.

3.5 Mass balances

The macroscopic balance equations, as in [46] for instance, for the water phase read

$$\frac{\partial}{\partial t}(n\rho) + \nabla \cdot (\rho \mathbf{q}) = 0. \tag{3.68}$$

The macroscopic mass balance equation for the solute phase is:

$$\frac{\partial}{\partial t}(n\rho\omega) + \nabla \cdot (\rho\omega \mathbf{q}) + \nabla \cdot \mathbf{J}_i = 0, \tag{3.69}$$

where ω is the mass fraction of solute in the liquid phase.

The process of cation exchange can be introduced in a consistent way [48] if we assume cation exchange to be a similar process as adsorption, with a general isotherm

$$s = s(c), \tag{3.70}$$

where s is the mass of absorbed solute per unit area of solid matrix. The following pore boundary condition holds:

$$\frac{\partial s}{\partial t} = (c\mathbf{v} + \mathbf{j}) \cdot \mathbf{n}|_A \,. \tag{3.71}$$

Not all integrations over the solid-liquid interface disappear when averaging the microscopic equation. The macroscopic adsorption term remains in the macroscopic mass balance:

$$\hat{U} = \frac{1}{V} \int_A (c\mathbf{v} + \mathbf{j}) \cdot dA, \tag{3.72}$$

as

$$\frac{\partial}{\partial t}(n\rho\omega) + \nabla \cdot (\rho\omega\mathbf{q}) + \nabla \cdot \mathbf{J}_i = -\hat{U}. \tag{3.73}$$

In [48] it is shown how $\hat{U}$ can be written as

$$\hat{U} = \frac{\partial(1-n)\rho_s S}{\partial t}, \tag{3.74}$$

where ρ_s is the density of solid matrix, and S is the macroscopic adsorbed mass fraction. The new mass balance now becomes

$$\frac{\partial}{\partial t}(n\rho\omega + (1-n)\rho_s S) + \nabla \cdot (\rho\omega\mathbf{q}) + \nabla \cdot \mathbf{J}_i = 0. \tag{3.75}$$

Writing concentrations instead of mass fractions, assuming constant porosity and solid mass density, and assuming a linear isotherm $S = K_d c$, where K_d is a distribution coefficient, then

$$\alpha\frac{\partial c}{\partial t} + \nabla \cdot (c\mathbf{q}) + \nabla \cdot \mathbf{J}_i = 0, \tag{3.76}$$

where $\alpha = n + (1-n)\rho_s K_d$.

3.6 Summary

We have now made available the full set of equations to model chemical and electro-osmotic effects in groundwater. In Chapter 2, the processes and coefficients were discussed, and in this chapter we introduced the relevant flux and balance equations. In the next chapters, these tools are employed to construct models and to provide analytical and numerical solutions for equations corresponding to these models. In Chapter 4, we start with some simple analytical examples to illustrate what one might expect from modelling of osmosis in groundwater.

Chapter 4

Mathematical analysis

The equations derived previously are employed to build a model which enables us to simulate experimental situations. First, however, we discuss some assumptions and subsequently, we analyze the equations in one dimension. We then show how they can be simplified and how simple analytical solutions can be obtained that illustrate general evolution of concentration and pressure in sample problems of osmosis in groundwater.

4.1 Assumptions

In the next section a justification is given for neglecting mechanical dispersion, gravity, temperature effects, and the transient part of the equations for charge conservation.

4.1.1 Peclet number

The Peclet number expresses the ratio between convective and diffusive transport. For values less than 0.5 [5], dispersion is dominated by molecular diffusion and mechanical dispersion can be disregarded. The Peclet number is given by

$$\mathrm{Pe} = \frac{|q|L}{D_m} \approx \frac{kp_t}{\mu D_m}, \tag{4.1}$$

where L is a typical length scale and p_t is a typical pressure. Molecular diffusion is, for now, given by D_m, although in the rest of this study we use the symbol D. If we, for instance, substitute the parameters applicable for the first experiment in Chapter 6, we find $k/\mu = 2.3 \cdot 10^{-15}\mathrm{m}^2$, $D_m = 2.7 \cdot 10^{-10}\mathrm{m}^2/\mathrm{s}$ and $p_t = 3500$ Pa, and henceforth Pe= 0.03. This is well below the value of 0.5, implying that mechanical dispersion may safely be neglected.

4.1.2 Gravity

In this study, we disregard all gravity effects. In other studies [80], [76] it is shown how the equations for osmosis include gravity as follows:

$$\mathbf{q} = -\frac{k}{\mu}\left(\nabla p - \rho \mathbf{g}\right) + \lambda \nabla c, \tag{4.2}$$

where ρ is fluid density and $\mathbf{g}$ is acceleration of gravity. Because most experiments we model were set up to ensure horizontal water flow, the corresponding calculations are performed on one-dimensional horizontal flow, which excludes gravity as its vector points in the vertical direction. If we do calculate the influence of gravity in the case of vertical flow, we are able to show that gravity effects are very small relative to the pressure gradients that develop. We can present the vertical component of the specific discharge q_z:

$$q_z = -\frac{k}{\mu}\left(\frac{\partial p}{\partial x} - \rho g\right). \tag{4.3}$$

If we consider, for instance, the data from the Keijzer experiment in Chapter 5, and calculate the ratio of the pressure and the gravity term, where L is the membrane thickness,

$$\frac{\Delta p / L}{\rho g}, \tag{4.4}$$

we find that, with $L = 2.3\text{mm}$, $\Delta p \approx 7000\text{Pa}$ and $\rho g = 1 \cdot 10^4 \text{kg}/(\text{ms})^2$, this ratio is 300, implying that gravity may safely be disregarded.

4.1.3 Thermo-osmosis

Temperature effects such as thermal osmosis are disregarded in this work. According to Mitchell [80], thermo-osmosis is described by the following extension of Darcy's law, where k_T is the thermo-osmotic permeability

$$\mathbf{q} = -\frac{k}{\mu}\nabla p - k_T \nabla T. \tag{4.5}$$

Here, chemical and electro-osmosis are neglected. Dividing the hydraulic term by the thermo-osmotic term, at zero specific discharge, implies:

$$-\frac{|\nabla p|}{|\nabla T|} = \frac{k_T}{k/\mu} \equiv \Gamma'. \tag{4.6}$$

In [22], experimental results were given on Γ', for different clays, average temperatures and overburden pressures. For a strongly compacted bentonite of average temperature 25^oC, a value of $\Gamma' = 150$ was found. Considering the formula (4.6), this implies that a head gradient of 2 cm/m is still more effective in transporting water than a temperature gradient of 10^oC/m. As such temperature differences are rarely encountered in soils, we can conclude that thermo-osmosis may be disregarded.

4.1.4 Fluid density

Aside from the pressure dependence we saw earlier, the fluid density depends on the mass fraction ω and temperature T according to:

$$\rho_f = \rho_f^0 e^{-\beta_T(T-T_0)+\gamma\omega}, \tag{4.7}$$

where β_T is the coefficient of thermal expansion and γ is an experimental constant. This coefficient of thermal expansion equals $\beta_T = 5.0 \cdot 10^{-4}$ 1/K [73] and $\gamma = 0.69$ [73]. An increase of ten degrees Kelvin implies an increase of fluid density of 0.5%. Such temperature differences are seldom observed in soils, thus we may safely ignore thermal expansion effects. The typical mass fraction in experiments considered in this study is 0.006. If we take the influence of mass fraction on fluid density into account, the increase of fluid density is 0.4%, which is, again, too small to be of any significance.

4.1.5 Timescale of electric relaxation

In this study, we assume the total electrical current to be zero to ensure overall electro-neutrality, i.e. all contributions to the total electrical current are immediately compensated by other currents. In other words, we assume the timescale of electric relaxation to be very small compared to the diffusion timescale. To motivate this, we consider the one-dimensional charge conservation equation:

$$\frac{\partial Q}{\partial t} + \frac{\partial I}{\partial x} = 0. \tag{4.8}$$

Here, we define: $Q = C_{\text{eff}} V$ and $I = -\sigma_e \frac{\partial V}{\partial x}$, where C_{eff} is effective capacitance of the clay system, given by

$$C_{\text{eff}} = \frac{\varepsilon S}{L}, \tag{4.9}$$

where ε is the electrical permittivity, L is a length scale and S is the area of a sample.

This yields:

$$\frac{nC_{\text{eff}}}{\sigma_e}\frac{\partial V}{\partial t} = \frac{\partial^2 V}{\partial x^2}. \tag{4.10}$$

Non-dimensionalizing, according to $x' = x/L$, $V' = V/V_0$, $t' = t/t_{\text{electric}}$ yields

$$\frac{\partial V'}{\partial t'} = \frac{\partial^2 V'}{\partial x'^2}, \tag{4.11}$$

provided we define

$$t_{\text{electric}} = \frac{nC_{\text{eff}}L^2}{\sigma_e}, \tag{4.12}$$

as the timescale of the problem. For a typical clay sample in this study, e.g. the sample used in the first experiment in Chapter 6, we have: $L = 2.5$ mm, $n = 0.5$, $\sigma_e = 0.1$ S/m, $\varepsilon \approx 5 \cdot 10^{-11}$ F/m [99] and $S = 2 \cdot 10^{-3}$ m^2 [63]. Now, the typical timescale is $t_{\text{electric}} = 2.5 \cdot 10^{-15}$ s.

If we compare this with, for instance, the typical timescale of diffusion, which, in this case is about $t_{\text{diff}} = 4000$ s, we conclude that it is useless to consider the transient behaviour of the electrical potential as such.

4.2 Equations

Summarizing the results of Section 3.3: in the rest of this chapter, we will use the following flux equations:

$$\mathbf{q} = -\frac{k}{\mu}\nabla p + \lambda\rho_f\nabla\omega, \tag{4.13}$$

$$\mathbf{J}_s^d = -\sigma\rho_f\omega\mathbf{q} - D\rho_f\nabla\omega. \tag{4.14}$$

4.2.1 Balance equations

The governing microscopic mass balances are averaged over REV's [46], [73] with the following assumptions: the REV is constant in space and time, there is no mass exchange between the fluid and the porous medium, and no chemical reactions occur, or, in the case of sorption, are accounted for by a bulk diffusivity. This provides us with the following sourceless continuity equations for isothermal liquid and solute transport in a porous medium, where $n[-]$ is porosity:

Fluid mass balance

$$\frac{\partial n\rho_f}{\partial t} + \nabla \cdot (\rho_f \mathbf{q}) = 0. \tag{4.15}$$

Salt mass balance

$$\frac{\partial n\rho_f \omega}{\partial t} + \nabla \cdot (\rho_f \omega \mathbf{q}) + \nabla \cdot \mathbf{J}_s^d = 0. \tag{4.16}$$

4.2.2 Equations of state

Under the assumption that fluid density is solely a function of pressure, i.e. temperature and mass fraction effects on liquid density are disregarded, the equation of state is given by

$$\rho_f = \rho_0 e^{\beta(p-p_0)}. \tag{4.17}$$

Here, β is the compressibility of the liquid, ρ_0 is the reference value for the fluid density when $p = p_0$.

The porosity of the porous medium is assumed to be related to the pressure as follows [73]:

$$n = 1 - (1 - n_0)e^{-\alpha p}, \tag{4.18}$$

where n_0 is a reference porosity, and $\alpha[1/\text{Pa}]$ is the compressibility of the porous medium.

The storage properties of the solid and liquid phase can be represented by a single storage parameter $S_s = n\beta + (1-n)\alpha$, in order to be able to write

$$\frac{\partial n\rho_f}{\partial t} = \rho_f(n\beta + (1-n)\alpha)\frac{\partial p}{\partial t} = \rho_f S_s \frac{\partial p}{\partial t}. \tag{4.19}$$

To get a simple description for the volume change of a soil, we assume this storage parameter to be constant, as well as the dynamic viscosity of the fluid μ, the intrinsic permeability k, and the diffusion coefficient D. Finally, in the next section, the reflection coefficient is also assumed to be constant.

4.2.3 Mathematical analysis

In case of a one-dimensional finite cartesian domain, with $\mathbf{q} = q\hat{\mathbf{x}}$ and $\mathbf{J}_s^d = J_s^d\hat{\mathbf{x}}$, the balance equations reduce to

$$\frac{\partial n\rho_f}{\partial t} + \frac{\partial \rho_f q}{\partial x} = 0, \tag{4.20}$$

and

$$\frac{\partial n\rho_f\omega}{\partial t} + \frac{\partial \rho_f\omega q}{\partial x} + \frac{\partial J_s^d}{\partial x} = 0, \tag{4.21}$$

with

$$q = -\frac{k}{\mu}\frac{\partial p}{\partial x} + \lambda\rho_f\frac{\partial \omega}{\partial x}, \tag{4.22}$$

and

$$J_s^d = -\sigma\rho_f\omega q - D\rho_f\frac{\partial \omega}{\partial x}. \tag{4.23}$$

Using (4.19), (4.17) and (4.22) in (4.20) and (4.19), (4.17) and (4.23) in (4.21) yields

$$nS_s\frac{\partial p}{\partial t} + \frac{\partial q}{\partial x} + \beta q\frac{\partial p}{\partial x} = 0, \tag{4.24}$$

and

$$\begin{aligned} n\frac{\partial \omega}{\partial t} + nS_s\omega\frac{\partial p}{\partial t} &+ (1-\sigma)\frac{\partial \omega q}{\partial x} + \\ (1-\sigma)\beta\omega q\frac{\partial p}{\partial x} &- D\frac{\partial^2\omega}{\partial x^2} - D\beta\frac{\partial \omega}{\partial x}\frac{\partial p}{\partial x} = 0. \end{aligned} \tag{4.25}$$

We introduce dimensionless variables:

$$\rho_f' := \frac{\rho_f}{\rho_0},\ p' := \frac{p-p_0}{p_i-p_0},\ x' := \frac{x}{L},\ t' := t\frac{k}{\mu S_s L^2},\ q' := q\frac{L\mu}{k(p_i-p_0)},$$

where L is a typical length scale and p_i is a typical pressure.

It is convenient to use the molar salt concentration c instead of the salt mass fraction ω. To justify this change of variable, we write, with M_s is solute molar mass,

$$M_s\frac{\partial c}{\partial x} = \frac{\partial \rho_f \omega}{\partial x} = \rho_f\frac{\partial \omega}{\partial x} + \omega\beta\rho_f\frac{\partial p}{\partial x}, \tag{4.26}$$

or, in dimensionless variables:

$$\frac{\partial \rho_f'\omega}{\partial x'} = \rho_f'\frac{\partial \omega}{\partial x'} + \beta(p_i-p_0)\omega\rho_f'\frac{\partial p'}{\partial x'} \tag{4.27}$$

Assuming $\beta(p_i-p_0) \ll 1$, the last term on the righthand side of (4.27) can be disregarded, implying $\rho_f'\frac{\partial \omega}{\partial x'} = \frac{\partial \rho_f'\omega}{\partial x'} = M_s\frac{\partial c'}{\partial x'}$. A dimensionless concentration $c' := \frac{c-c_0}{c_i-c_0}$ is introduced, where c_i and c_0 are respectively an initial and an ambient concentration. Using similar arguments we find $\frac{\partial \rho_f'\omega}{\partial t'} = M_s\frac{\partial c'}{\partial t'}$.
In terms of the concentration, the salt mass balance reads

$$\frac{\partial nc}{\partial t} + (1-\sigma)\frac{\partial (cq)}{\partial x} - D\frac{\partial^2 c}{\partial x^2} = 0. \tag{4.28}$$

Next are the non-dimensionalized mass balance equations. Omitting primes, this yields for the liquid mass and salt concentration respectively:

$$n\frac{\partial p}{\partial t} + \frac{\partial q}{\partial x} + (\beta(p_i-p_0))q\frac{\partial p}{\partial x} = 0. \tag{4.29}$$

$$n\frac{\partial c}{\partial t} + nS_s(p_i-p_0)c\frac{\partial p}{\partial t} + (1-\sigma)S_s(p_i-p_0)\frac{\partial (cq)}{\partial x} - \frac{S_sD\mu}{k}\frac{\partial^2 c}{\partial x^2} = 0, \tag{4.30}$$

Again, assuming $\beta(p_i-p_0) \ll 1$, the liquid mass balance equation can be simplified, yielding

$$\frac{\partial p}{\partial t} + \frac{\partial q}{\partial x} = 0. \tag{4.31}$$

In addition, the third term of the salt mass balance, which can be regarded as an advective term, can be disregarded when $S_s(p_i - p_0) \ll 1$ and when $(1 - \sigma)S_s(p_i - p_0) \ll \frac{S_s D\mu}{k}$, implying $\lambda M_s(c_i - c_0) \ll D$, provided $q_0 = \frac{k(p_i - p_0)}{\mu L} = \frac{\lambda(c_i - c_0)M_s}{L}$. Solute transport is then described by a diffusion equation. The 'osmotic Peclet number' Pe_{os}, which is a measure of the significance of (osmotic) advective transport compared to diffusion, is given by

$$Pe_{os} = \frac{(1 - \sigma)q_0 L}{D} = \frac{(1 - \sigma)\lambda M_s(c_i - c_0)}{D}. \tag{4.32}$$

The non-dimensionalized specific discharge reduces to

$$q = -\frac{\partial p}{\partial x} + \frac{\partial c}{\partial x}, \tag{4.33}$$

when omitting primes.

Inserting (4.33) in (4.29) and (4.30) yields

$$\frac{\partial p}{\partial t} = \frac{\partial^2 p}{\partial x^2} - \frac{\partial^2 c}{\partial x^2}, \tag{4.34}$$

$$\frac{\partial c}{\partial t} = \varepsilon \frac{\partial^2 c}{\partial x^2}. \tag{4.35}$$

The parameter $\varepsilon = \frac{S_s D\mu}{k n_0}$ is a dimensionless constant describing the diffusion of the solute through the membrane on the timescale of the pressure evolution. Since the effect of changes in porosity due to changes in pressure in the liquid phase are small, we approximate n by n_0.

Such a simple set of coupled equations can be solved by introducing a new variable ϕ:

$$\phi := p - \frac{1}{1 - \varepsilon} c, \tag{4.36}$$

leading to an ordinary diffusion equation in terms of ϕ

$$\frac{\partial \phi}{\partial t} = \frac{\partial^2 \phi}{\partial x^2}. \tag{4.37}$$

Solving (4.37) and (4.35), subject to appropriate initial and boundary conditions, yields expressions for the concentration as well as the pressure.

This method can be applied to model experimental situations, as illustrated in the following chapters. However, it will be shown that its applicability is limited to models with small storage parameters.

Next we use this model to derive some analytical solutions for osmosis in groundwater, after we have listed some additional assumptions that are based on the previous equations.

4.3 Analytical solutions

In this section, we present some analytical solutions of osmosis problems. Under the assumptions presented in the previous subsections, the governing dimensionless equations are:

$$\frac{\partial p}{\partial t} = \frac{\partial^2 p}{\partial x^2} - \frac{\partial^2 c}{\partial x^2}, \tag{4.38}$$

$$\frac{\partial c}{\partial t} = \varepsilon \frac{\partial^2 c}{\partial x^2}. \tag{4.39}$$

Consider a infinite clay soil, endowed with a scaled diffusion coefficient ε. The solution of the second equation, subject to the initial condition:

$$c(x, t = 0) = \text{Heaviside}(x), \tag{4.40}$$

reads, in terms of the similarity variable $\eta = x/\sqrt{t}$:

$$c = \frac{1}{2}\text{erfc}\frac{\eta}{2\sqrt{\varepsilon}}. \tag{4.41}$$

Consequently, the pressure equation yields

$$-\frac{\eta}{2}p' = p'' - f(\eta), \tag{4.42}$$

where the primes denote differentiation with respect to η. Note that the function $f(\eta)$ is given by

$$f(\eta) = (\frac{1}{2}\text{erfc}\frac{\eta}{2\sqrt{\varepsilon}})''. \tag{4.43}$$

Defining $w(\eta) \equiv e^{\eta^2/4}p'$, we obtain

$$w'(\eta) = f(\eta)e^{\eta^2/(4)}, \tag{4.44}$$

yielding

$$w = \frac{e^{\frac{\gamma\eta^2}{4}}}{2\varepsilon^{3/2}\gamma\sqrt{\pi}} + A, \tag{4.45}$$

where $\gamma = 1 - \frac{1}{\varepsilon}$ and

$$p = \frac{\text{erf}\frac{\eta}{2\sqrt{\varepsilon}}}{2\varepsilon\gamma} + A\sqrt{\pi}\text{erf}\frac{\eta}{2} + B, \tag{4.46}$$

where A and B are integration constants. Passing to the limit $t \to \infty$, implies $\eta \to 0$, and we obtain $p = 0$, and therefore $B = 0$. Subsequently, in the limit $t \to 0$, implying $\eta \to \infty$ and we obtain $p = 0$, thus $A = -\frac{1}{2\gamma\varepsilon\sqrt{\pi}}$. Then, the pressure equation becomes:

$$p = \frac{1}{2\varepsilon\gamma}\left\{\text{erf}\frac{\eta}{2\sqrt{\varepsilon}} - \text{erf}\frac{\eta}{2}\right\}. \tag{4.47}$$

An alternative way to obtain this result is to introduce a variable $\phi = p + \frac{1}{\varepsilon\gamma}c$ such that

$$\frac{\partial\phi}{\partial t} = \frac{\partial^2\phi}{\partial x^2}. \tag{4.48}$$

The solution of (4.48) subject to the imposed boundary and initial conditions, reads

$$\phi = A\sqrt{\pi}\text{erf}\frac{\eta}{2} + B. \tag{4.49}$$

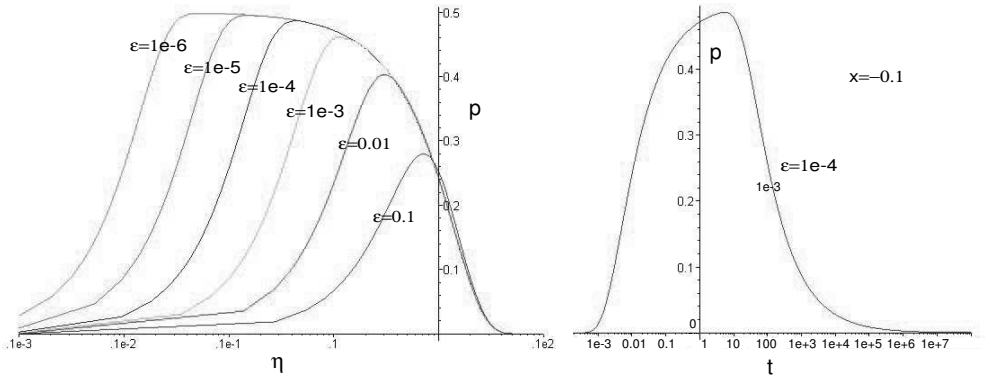

Figure 4.1: *Similarity solutions for the concentration (left) and pressure evolution (right)*

Obviously, the following expression holds:

$$\phi = p + \frac{1}{\varepsilon\gamma}c = p + \frac{1}{2\varepsilon\gamma}\mathrm{erfc}\frac{\eta}{2\sqrt{\varepsilon}} = A\sqrt{\pi}\mathrm{erf}\frac{\eta}{2} + B \tag{4.50}$$

As before, we find $p = 0$ for $\eta \to 0$ and $\eta \to \infty$, so $B = 1/(2\varepsilon\gamma)$ and $A = -1/(2\varepsilon\gamma\sqrt{\pi})$, yielding expression (4.47).

In Figure 4.1, the general pressure solution as a function of the similarity variable η is shown for different values of ε. Also, the evolution of pressure at $x = -0.1$ is shown. In Figure 4.2 the full solutions of the pressure and concentration in time as well as in space are displayed. The pressure evolution is shown for small times, for the purpose of illustration.

In Figure 4.2, the three-dimensional solutions of concentration and pressure are shown for these simple problems. The position axis was shifted and we chose $\varepsilon = 2$. In Figure 4.3 the corresponding time profiles are shown for $x = 0$.

4.3.1 Time scales

In Figure 4.3, the profiles of the pressure and the concentration evolution are depicted to illustrate the different time scales of the problem. From the graphs we observe that, in general, the evolution of the concentration is governed by a single time scale and the evolution of the pressure by two: a fast and a slow time scale. At first, $\frac{dp}{dt} > 0$, and the pressure builds up to a maximum, and subsequently, the pressure declines ($\frac{dp}{dt} < 0$) similarly to the concentration. Let's consider equations (4.38) and (4.39). If we associate t with the fast time scale t_{fast} and introduce the slow time scale $\tau = \varepsilon t$, we are able to observe the following: in fast time, passing

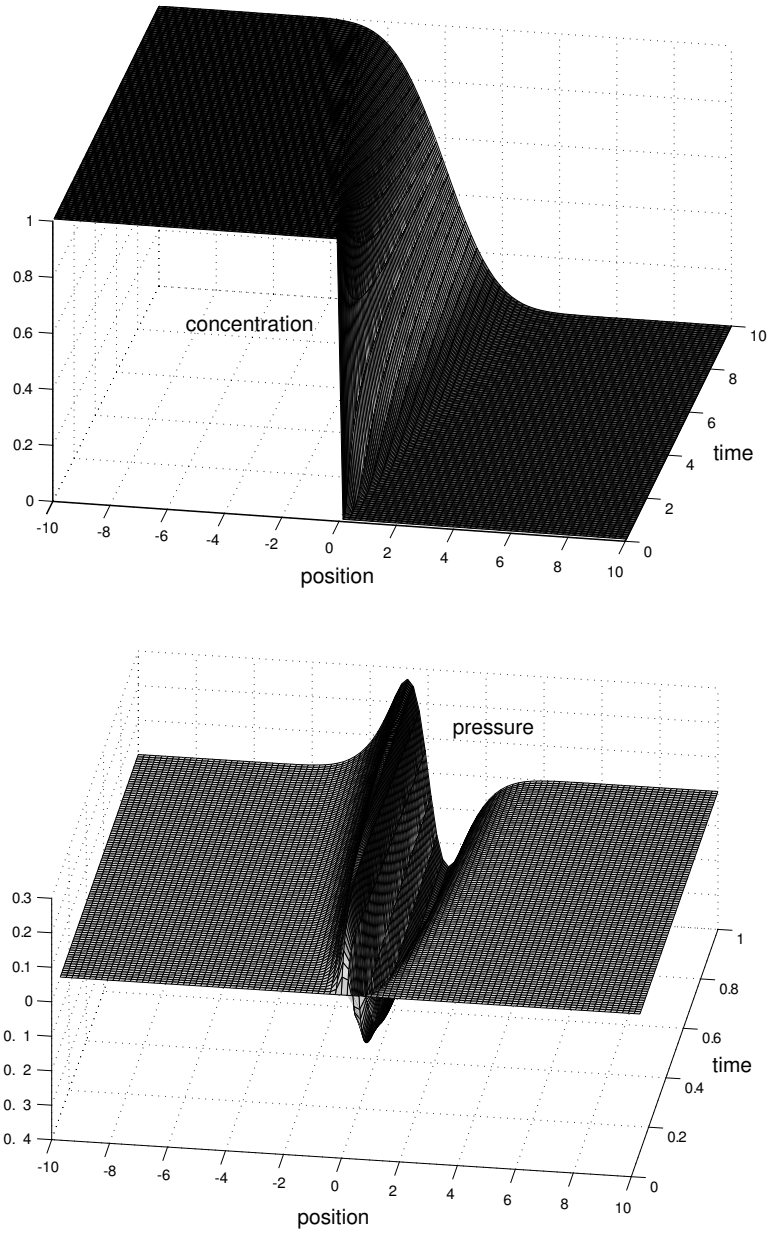

Figure 4.2: *Three-dimensional plots of the concentration (top) and pressure evolution (bottom)*

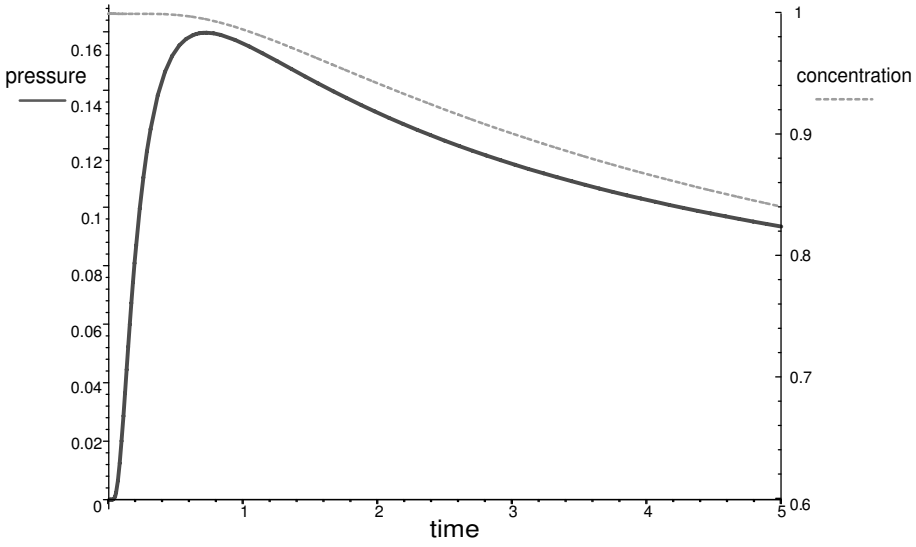

Figure 4.3: *Time evolution of the concentration and the pressure*

to the limit $\varepsilon \to 0$ yields a concentration profile constant in time and a pressure diffusion equation with a source term related to the second order derivative of the Heaviside function. In 'slow' time, the equations change into:

$$\frac{\partial c}{\partial \tau} = \frac{\partial^2 c}{\partial x^2}, \tag{4.51}$$

$$\varepsilon \frac{\partial p}{\partial \tau} = \frac{\partial^2 p}{\partial x^2} - \frac{\partial^2 c}{\partial x^2}, \tag{4.52}$$

implying that, in the limit $\varepsilon \to 0$, the concentration evolution is described by a diffusion equation, and the pressure is in that case linearly related to concentration. This is precisely what is observed in the graphs.

4.3.2 Limiting values of σ

To emphasize the applicability, it can be shown that the model yields the expected pressure profile for limiting values of σ as presented in Katchalsky and Curran [62]. Consider an infinite domain with clay on the negative half plane and a sandy soil on the positive half plane. The clay is initially saturated with a salt solution of concentration $c = c_i$, whereas the sand is saturated with fresh water $c = 0$. The relevant parameters are listed in Table 4.1. Because of chemical osmosis, water will be pushed into the clay. The following equations, which are the dimensioned versions of (4.38) and (4.39), apply:

$$nS_s\frac{\partial p}{\partial t} = \frac{k}{\mu}\frac{\partial^2 p}{\partial x^2} - \lambda M_s\frac{\partial^2 c}{\partial x^2}, \tag{4.53}$$

$$n\frac{\partial c}{\partial t} = D\frac{\partial^2 c}{\partial x^2}, \tag{4.54}$$

where λ is the chemico-osmotic mobility:

$$\lambda = \frac{\sigma k}{\mu M_s}\nu RT. \tag{4.55}$$

When the clay is ideal (i.e. $\sigma = 1$), pressure will build up in the clay up to an asymptotic value. However, when the clay is not entirely restrictive (i.e. $0 < \sigma < 1$), pressure will build up, reach a maximum value, and decline again. This is shown with an (intuitive) picture in e.g. Katchalsky and Curran [62], but using our model the exact solution of the pressure p_1 in the clay leads to a similar graph. The solution then reads

$$p_1 = A_1 \operatorname{erfc}\left(\frac{-x}{2\sqrt{\delta_1 t}}\right) - A_2 \operatorname{erfc}\left(\frac{-x}{2\sqrt{D_1 t}}\right), \tag{4.56}$$

with

$$A_1 = \frac{\lambda c_i \mu}{k_1}\left(1 + \frac{\sqrt{S_{s1}\mu D_1 k_1}}{k_2}\right),\ A_2 = \frac{\lambda c_i}{\left(\frac{k_1}{\mu} - S_{s1}D_1\right)\left(1 + \frac{k_1}{k_2}\right)}, \tag{4.57}$$

where $\delta = \frac{k/\mu}{nS_s}$ and subscripts $1, 2$ refer to the regions clay and sand respectively. Figure 4.4 shows this solution for the pressure at $x = -0.1$m for $0 < \sigma < 1$ and $\sigma = 1$ ($D_1 = 0$). The parameters used are displayed in Table 4.1. Figure 4.4 shows that the model confirms the limiting behaviour for σ.

4.4 Applications of analysis

4.4.1 Influence of coefficients on osmotic pressure

It is rather instructive to see how different coefficients influence the evolution of osmotic pressure. In Figures 4.5 and 4.6 this is shown for the intrinsic permeability, the diffusion coefficient, the reflection coefficient and the specific storativity, where we used equations (4.53) and (4.54). The default case, which is the same in all graphs, corresponds to the pressure profile for $0 < \sigma < 1$ in Figure 4.4.

parameter	clay (region 1)	sand (region 2)
diffusion coefficient D [m^2/s]	10^{-11}	10^{-10}
storativity S_s [1/Pa]	10^{-8}	$4.6 \cdot 10^{-10}$
permeability k [m^2]	10^{-19}	10^{-13}
reflection coefficient σ [-]	0.2	-
porosity n [-]	0.5	1
initial concentration c_i [mol/m^3]	0.1	0

Table 4.1: *Parameters corresponding to Figure 4.4*

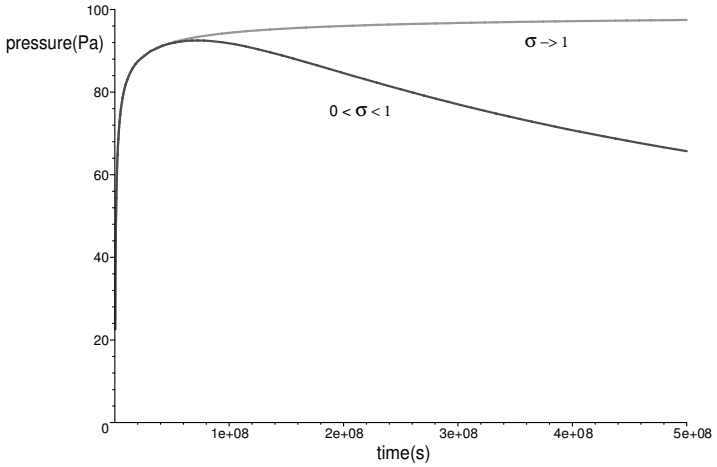

Figure 4.4: *Comparison of pressure evolution for* $\sigma = 1$ *and* $0 < \sigma < 1$

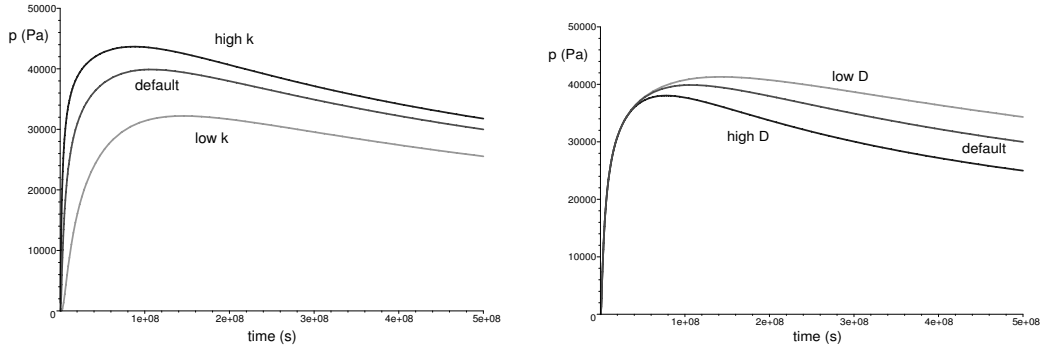

Figure 4.5: *Pressure evolution for varying k and D*

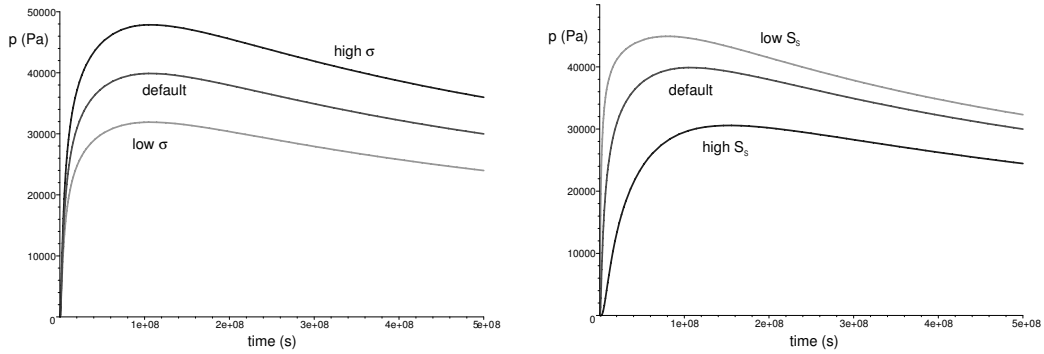

Figure 4.6: *Pressure evolution for varying σ and S*

4.4.2 Concentration dependent reflection coefficient

It is interesting to see how the specific dependence of σ on the concentration affects, for example, the buildup of osmotic pressure in time. Three different dependencies of the reflection coefficient on concentration are assumed. The first one allows for a semi-analytical solution. We first elaborate somewhat on this solution, and subsequently present the graphs corresponding to all three expressions of σ.

Semi-analytical solution of pressure for a simple $\sigma(c)$

First, the analytical method presented in Section 4.3 is used to shed some light on the case of a concentration dependent reflection coefficient. If we assume that σ varies with concentration according to a power law c^n, then the governing equations are

$$\frac{\partial p}{\partial t} = \frac{\partial^2 p}{\partial x^2} - \frac{\partial}{\partial x}\left[c^n \frac{\partial c}{\partial x}\right], \tag{4.58}$$

$$\frac{\partial c}{\partial t} = \varepsilon \frac{\partial^2 c}{\partial x^2}. \tag{4.59}$$

This implies that the pressure equation can be written as

$$\frac{\partial p}{\partial t} = \frac{\partial^2 p}{\partial x^2} - \frac{1}{n+1}\frac{\partial^2 c^{n+1}}{\partial x^2}, \tag{4.60}$$

or, in similarity variable $\eta = x/\sqrt{t}$:

$$-\frac{\eta}{2}p' = p'' - \frac{1}{n+1}(c^{n+1})'', \tag{4.61}$$

where the primes denote differentiating with respect to η.

Proceeding as in Section 4.3, we assume that $c = \frac{1}{2}\mathrm{erfc}\frac{\eta}{2}$ and $g(\eta) = \frac{1}{n+1}(c^{n+1})''$. Defining $z(\eta) = e^{\eta^2/4}p'$ implies

$$z'(\eta) = g(\eta)e^{\eta^2/4}. \tag{4.62}$$

Integration of this equation yields an expression for the pressure, provided we apply boundary and initial conditions.

Of special interest is the simple expression for the reflection coefficient we encountered in Chapter 2:

$$\sigma = 1 - \alpha c, \tag{4.63}$$

where α is a number that varies between 0 and 1. This is the simplest possible expression, proposed by Katchalsky and Curran [62], and Bolt [9] for instance.

Now, the pressure equation is given by

$$\frac{\partial p}{\partial t} = \frac{\partial^2 p}{\partial x^2} - \alpha\frac{\partial}{\partial x}\left[(1-\alpha c)\frac{\partial c}{\partial x}\right], \tag{4.64}$$

If we perform the integration of (4.62), with $g(\eta) = \frac{1}{2}(1-\alpha c)''$, we find:

$$p = \int_0^{\eta} d\eta' \left(e^{-\frac{\eta'^2}{4}} \left[\int_0^{\eta'} d\eta'' \left\{ \frac{(e^{-\frac{\eta^2}{4\varepsilon}})^2}{2\pi\varepsilon} - \frac{\eta'' e^{-\frac{\eta''^2}{4\varepsilon}} \left[1 - \frac{\alpha}{2} \mathrm{erfc} \frac{\eta''}{2\sqrt{\varepsilon}} \right]}{2\sqrt{\pi}\varepsilon^{3/2}} \right\} + C_1 \right] e^{\frac{\eta''^2}{4}} \right) + C_2, \tag{4.65}$$

where C_1 and C_2 are integration constants. This integral has to be evaluated numerically.

Pressure profiles for different expressions of $\sigma(c)$

The first graphs, in Figure 4.7, show the pressure buildup and profiles for $\sigma = 1 - \alpha c$, calculated using the semi-analytical solution of p, for different values of α.

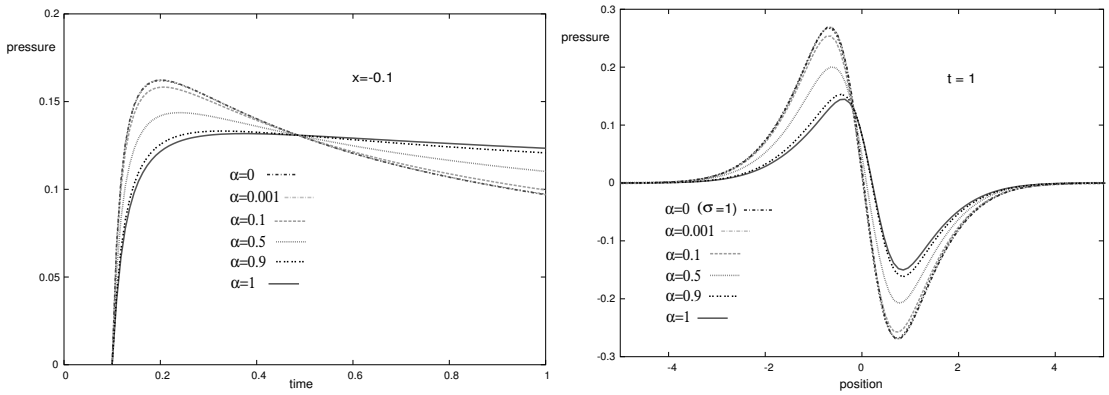

Figure 4.7: *Pressure evolution at $x = -0.1$ and pressure profile at $t = 1$ for varying α when $\sigma = 1 - \alpha c$*

A number of observations can be made from Figure 4.7: as α increases, σ decreases and hence, the osmotic pressures, as expected. It is furthermore interesting to observe that all time profiles pass through a single point in space time and that the 'zero pressure point' in the position graph shifts to the right. This can be explained by noting that due to different initial concentrations in the left and the right part of the domain, as implied by the solution $c = \frac{1}{2}\mathrm{erfc}\frac{\eta}{2}$, the reflection coefficient varies accordingly.

The next formula used to assess the influence of the choice of σ on buildup of osmotic pressure, is the approximate formula (11.39a) in [9] we call the simple Bolt expression, valid for high concentrations. In Chapter 2, it was presented in formula 2.67:

$$\sigma = a\frac{\gamma_4}{c+\gamma_2} - \left(\frac{\gamma_4}{c+\gamma_2}\right)^{\frac{3}{2}}. \tag{4.66}$$

This is a non-dimensionalized expression, where the following definitions were used: $\gamma_4 = \frac{\pi^{4/3}}{(c_h - c_l)\beta b^2}$, $\gamma_2 = \frac{c_l}{c_h - c_l}$, where γ_2 is a normalized concentration, c_h, c_l are the salt concentrations, respectively the high and low one, b is the double layer thickness (of order $100\mathring{A}$) and β and a are constants.

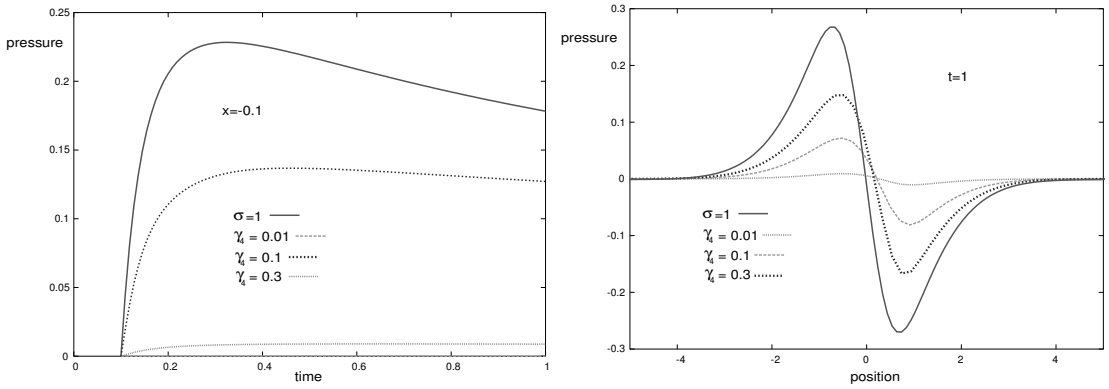

Figure 4.8: *Pressure evolution at $x = -0.1$ and pressure profile at $t = 1$ for varying γ_4 for the simple Bolt description of σ*

In Figure 4.8 it is shown how the dependence of the reflection on the concentration according to the simple Bolt expression affects pressure profiles.

The third equation for σ is the full expression defined in the form of an integral, for which the solution is

$$\sigma = \frac{3}{(\kappa_0 d_l)^3}\left[A + B\right], \tag{4.67}$$

where

$$A = 4\kappa_0 d_l \left\{\frac{t_d \ln(t_d/t_s)}{1+t_d} + \ln\frac{1+t_s}{1+t_d}\right\}, \tag{4.68}$$

and

$$B = \frac{2t_d \ln^2(t_d/t_s)}{1+t_d} - 2\left[L(1+t_d) - L(1+t_s)\right] - 2\ln(t_d/t_s)\ln(1+t_d), \tag{4.69}$$

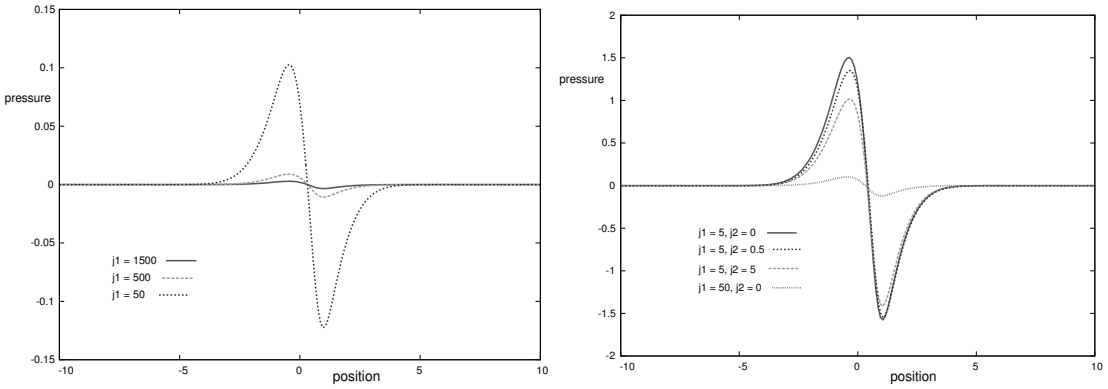

Figure 4.9: *Pressure evolution at $x = -0.1$ for the full Bolt description with varying relative thickness j_1 of the immobile layer and relative thickness j_2 of the diffuse double layer*

where $\mathcal{L}(x)$ is the dilogarithmic function, defined according to formula 2.66.

In Figure 4.9 it is shown how the dependence of the reflection on the concentration according to the full Bolt formula affects pressure profiles. Furthermore, the influence of varying the relative thickness j_1 of the immobile layer versus the influence of varying the relative thickness j_2 of the diffuse double layer is shown.

4.4.3 Optimal osmotic pressure

The osmotic pressure increases linearly with the concentration (difference) when the reflection coefficient is constant. However, when a concentration dependence of σ is accounted for, this behaviour changes drastically, as the reflection coefficient decreases for increasing concentration. Depending on the relation between σ and c, there must be, in some cases, a maximum osmotic pressure corresponding to an 'optimal concentration value'. Let's assume a simple, but realistic expression for the osmotic pressure:

$$\pi = \sigma(c)\nu RTc. \tag{4.70}$$

It is interesting to plot the osmotic pressure for different formulations of $\sigma(c)$: the simple expression and the two 'Bolt expressions' from Section 4.4.2 and the Bresler expression for σ as seen in Chapter 2 in formula 2.53. Assuming $\nu = 2, R = 8.314\text{Jmol/K}$ and $T = 298\text{K}$, the result is displayed in Figure 4.10. Indeed, most expressions for the reflection coefficient yield an optimal pressure. Only the simple Bolt expression implies a monotonically increasing pressure as a function of concentration, analogous to the case of a constant reflection coefficient. This again

shows the relevance of the concentration dependence of the reflection coefficient. We expect the osmotic pressure to be optimal for a particular concentration, as the double layer break down at higher concentrations. Models for σ, such as the simple Bolt expression, that do not obey the physics in this respect, can therefore be disregarded.

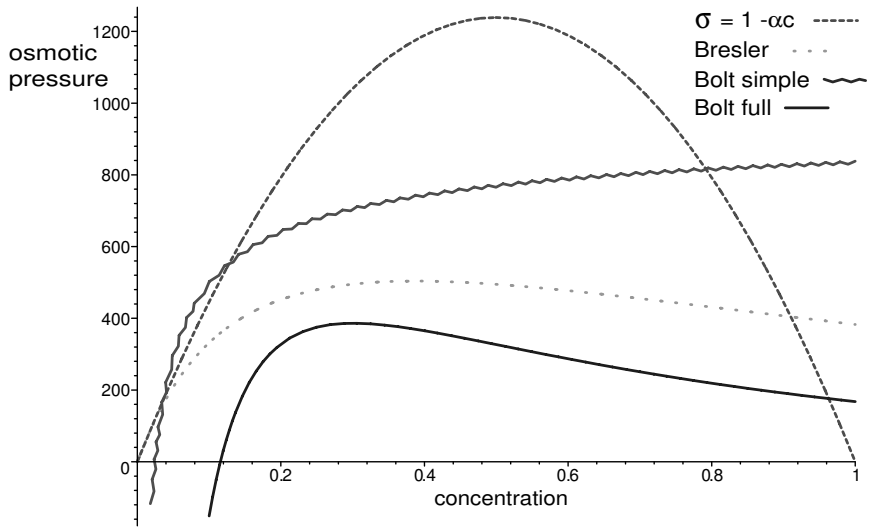

Figure 4.10: *Comparison of osmotic pressure profiles as a function of concentration for different expressions of the reflection coefficient.*

4.4.4 Tracer

Next we consider the following problem. A tracer is released in a domain that consists of clay saturated initially with a salt concentration c_1 in the negative half plane, and salt water with concentration c_0 in the positive half plane. In the water region, the tracer is allowed to diffuse freely, whereas in the clay, not only is diffusion hampered by the porous medium, also an advective flux caused by chemical osmosis will influence the spreading of the tracer in the clay.

At $t = 0$, the tracer is injected at $x = 0$. The concentration is B and the diffusivity of the tracer is D_B. Now, the simple advection-diffusion equation for the tracer is formulated as

$$\frac{\partial B}{\partial t} = \frac{\partial Bq}{\partial x} + D_B \frac{\partial^2 B}{\partial x^2}, \tag{4.71}$$

$$t = 0, B = M\delta(x). \tag{4.72}$$

where chemical osmosis is responsible for the advection velocity q.

Introducing the non-dimensional variables

$$\tilde{B} := \frac{B}{M},\ \tilde{x} = \frac{x}{L},\ \tilde{q} = q\frac{L}{\lambda c_0},\ \tilde{t} = \frac{t}{t_1} = \frac{t\lambda c_0}{L^2},\ \zeta := \frac{D_B}{\lambda c_0}, \tag{4.73}$$

yields, after dropping tildes

$$\frac{\partial \tilde{B}}{\partial \tilde{t}} = \frac{\partial \tilde{B}\tilde{q}}{\partial \tilde{x}} + \zeta \frac{\partial^2 \tilde{B}}{\partial \tilde{x}^2}. \tag{4.74}$$

The tracer concentration was normalized according to the initial tracer concentration and other variables were defined as in Section 4.2.

The diffusion of salt and pressure buildup by chemical osmosis are described by equations (4.38) and (4.39). We assume the same nondimensionalized solutions for the pressure and concentration: $c = \frac{1}{2}\mathrm{erfc}\frac{\eta}{2}, p = \frac{1}{2\gamma\varepsilon}(\mathrm{erf}\frac{\eta}{2\sqrt{\varepsilon}} - \mathrm{erf}\frac{\eta}{2})$ with the similarity variable $\eta = \frac{\tilde{x}}{\sqrt{\tilde{t}}}$.

Next we make the similarity transformations $\tilde{B}(\tilde{x},\tilde{t}) = \phi(\eta)/\sqrt{\tilde{t}}$ and $\tilde{q}(\tilde{x},\tilde{t}) = g(\eta)/\sqrt{\tilde{t}}$. As the non-dimensionalized specific discharge is $\tilde{q}(\tilde{x},\tilde{t}) = \frac{\partial}{\partial \tilde{x}}(c-p)$, this implies $g(\eta) = (c-p)'$, where $()'$ denotes differentiation with respect to η. Consequently, the tracer diffusion equation becomes

$$-\frac{1}{2}(\phi\eta)' = (\phi g(\eta))' + \zeta\phi'', \tag{4.75}$$

Integration of (4.75) yields

$$-\frac{1}{2}\phi\eta = \phi g(\eta) + \zeta\phi' + A, \tag{4.76}$$

where the integration constant A vanishes, when applying appropriate boundary conditions, i.e.:

$$\phi(-\infty) = \phi(+\infty) = 0. \tag{4.77}$$

Therefore:

$$\zeta\frac{d\phi}{d\eta} + \phi\left(g(\eta) + \frac{\eta}{2}\right) = 0. \tag{4.78}$$

This yields:

$$\phi = C_1 e^{-\frac{\eta^2}{4\zeta} - \frac{1}{\zeta}\int g(\eta)d\eta}, \tag{4.79}$$

where C_1 is another integration constant. As we have found $g(\eta) = (c-p)'$, equation (4.79) becomes

$$\phi = C_1 e^{-\frac{\eta^2}{4\zeta} - \frac{1}{\zeta}(c-p)}. \tag{4.80}$$

The integration constant can be found by noting that the mass M of tracer is conserved, implying

$$M = \int_{-\infty}^{\infty} \tilde{B}(\tilde{x})d\tilde{x} = \int_{-\infty}^{\infty} \phi(\eta)d\eta. \tag{4.81}$$

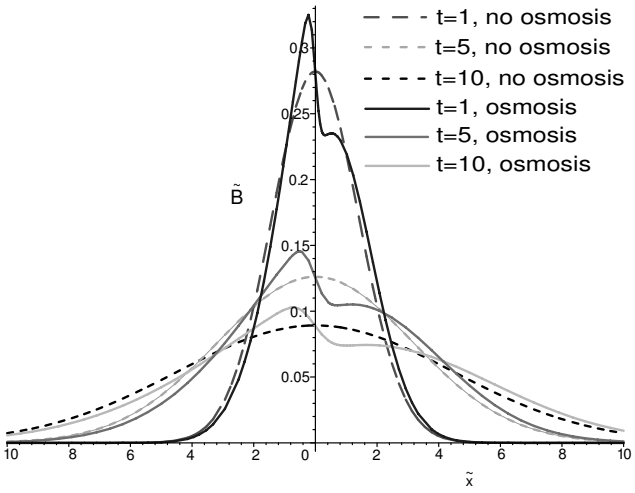

Figure 4.11: *Tracer concentration profiles for different times and with and without osmosis*

Unfortunately, the resulting integral can not be solved using analytical techniques. We can, however, obtain a numerical estimate. We assume $\zeta = 1, \varepsilon = 0.1, M = 1$. Conservation of mass yields

$$1 = C_1 \int_{-\infty}^{\infty} e^{-\frac{\eta^2}{4} - (c-p)}d\eta, \tag{4.82}$$

or

$$C_1 = 0.45. \tag{4.83}$$

Using $\tilde{B} = \phi/\sqrt{\tilde{t}}$, we finally obtain

$$\tilde{B} = \frac{0.45}{\sqrt{\tilde{t}}}\, e^{-\frac{\eta^2}{4} - \frac{1}{2}(c-p)}. \tag{4.84}$$

The profile of the tracer concentration is now displayed in Figure 4.11. The effect of chemical osmosis is obvious in the redistribution of the tracer profile. This implies that osmosis can be responsible for unexpected displacement of contaminants.

4.5 Conclusions

We have seen how from the information derived from Chapters 2 and 3, we can build a mathematical model in which the expected simultaneous buildup and decline of pressure and the evolution of concentration can be simulated. In the next chapter, we will see how this model holds in reality: results of experiments from literature are compared with modelling results. The emphasis is on the range of applicability of the model. In which circumstances can we use simple closed form analytical solutions and when must we resort to numerical solutions?

Chapter 5

Comparison with experiments [1]

5.1 Introduction

It has been known since the 19th century that low-permeable sediments may exhibit membrane behaviour. From the 1960's to the present, extensive evidence has been gained that clay can restrict solute transport relative to the flow of water (e.g., [4], [29], [126], [93], [63], [89], [16]). This property of clay gives rise to chemical osmosis (fluid flow in response to a chemical gradient) and ultrafiltration (solute sieving driven by an hydraulic gradient). They are called coupled flow phenomena to distinguish them from direct flow phenomena such as fluid flow due to an hydraulic gradient. These phenomena may be significant in contaminant transport through natural and artificial barriers [107] and they have been suggested to play a role in the generation of high overpressures in aquifers [89].

Chemical osmosis and ultrafiltration are most pronounced for 'ideal' membranes that totally inhibit passage of solute. However, natural clays typically only partially restrict solute passage: the degree to which membranes are permeable to solute is expressed by the dimensionless 'reflection coefficient' σ [110], [68] that ranges from 0 for non-membranes to 1 for ideal membranes.

The origin of the membrane properties of clays and shales is mostly attributed to the so-called diffusive double layers associated with clay platelets [80], [91]. The double layers are formed by 'clouds' of cations that are in electrostatic equilibrium with the negatively charged clay platelets. Especially when compacted, the water film between the platelets is completely dominated by the overlapping double layers and imposes electrical restrictions that are responsible for the membrane behaviour.

[1] This is a modified transcription of the paper **S. Bader**, H. Kooi 2005 *Modelling of solute and water transport in semi-permeable clay membranes: comparison with experiments* Advances in Water Resources **28** 203-214

Macroscopic transport formulations for direct and coupled flow of water and solutes can be derived using approaches based on continuum mechanics, homogenization [84], empirical methods and non-equilibrium thermodynamics. In our study, the latter approach [62],[123] is used. Previous studies have mainly developed equations to infer membrane efficiencies from laboratory experiments that have been conducted under conditions of steady flow [16] or no flow [63]. Also, pressure and concentration measurements have been performed in reservoirs adjacent to the membrane. These two conditions implied that modelling was usually restricted to discontinuous formulations describing steady state behaviour (see also [92]). Consequently, inferred values of σ are averaged values that integrate across the finite membrane thickness.

Only in a few studies, continuum models of transport through semipermeable membranes have been developed to study transient behaviour. In [82], Mitchell et al. used a one-dimensional model to investigate the pore pressure reduction in a clay layer subjected to saline boundary conditions at top and bottom. The authors focused on chemico-osmotic consolidation of the layer and only presented non-dimensionalized and spatially averaged pore pressure and concentration changes in the clay layer. In a similar study, Greenberg et al. [36] simulated settlement due to consolidation of a confining layer in the Oxnard basin, California, following seawater intrusion into a contiguous aquifer. More recently, Soler [108] used a one-dimensional model to study the role of coupled transport phenomena, including thermal osmosis, in radionuclide transport from a repository of high level nuclear waste in the Opalinus Clay, Switzerland. The model was reduced, however, to a conventional advection-diffusion equation with a constant advection velocity, thereby negating the feedback of temporal and spatial changes in the concentration gradients on osmotic transport. Sherwood [106] performed transient flow calculations expressed in terms of pressure and salinity values on either side of a membrane and therefore greatly simplified the full transient flow and transport behaviour within the membrane. In [32], Ghassemi and Diek described shale deformation due to chemo-mechanical processes, but their model disregards ultrafiltration and does not properly describe limiting behaviour of the reflection coefficient. Malusis and Shackelford [76] presented a more extensive model that includes multiple ionic species and cation-exchange. In their model the phenomenological coefficients are expressed in terms of conventional and measurable porous media parameters as derived by Yeung [123] and Yeung and Mitchell [124]. Unfortunately, Malusis and Shackelford [76] only presented model simulations in which membrane effects were set to zero. None of the above models account for the strong dependence of σ on the local concentration as described by Bresler [11].

The above discussion shows that a lot of progress still can be made both in the development of continuum models of coupled flows and in their application. Such

models are needed not only to exploit the information that resides in measurement of transient conditions in laboratory experiments, which are currently ignored, but also to make realistic predictions of the temporal and spatial development in natural or engineered groundwater systems. We recently presented a model of chemically and hydraulically coupled flow that overcomes most of the above-mentioned limitations and, to our knowledge, modelled for the first time transient data obtained from a laboratory experiment on chemical osmosis [30]. In [70] it was shown that the model further replicates the general behaviour observed in laboratory ultrafiltration experiments on semipermeable membranes.

In this study, a continuum model for chemico-osmotic transport in groundwater is formulated. The derived flux equations are inserted in the mass balance equations for coupled groundwater and solute transport. Next, the model is simplified and analytical solutions are presented of problems corresponding to two experiments from literature. In both cases, extra simplifying assumptions are made compared to the full models to show the applicability of the model. In one experiment [63], to which we will refer as "experiment A", the evolution of pressure and salinity was measured in a bentonite clay membrane subjected to a salt concentration gradient. The experimental setup was such that a uniform flow was present and a one-dimensional version of the governing equations can be used. In the second experiment under consideration [89], a borehole, drilled in a clay soil, was filled with an NaCl solution to induce flow of water from the clay into the borehole. Consequently, we will refer to this experiment as "experiment B". The model consists of the cylindrical borehole and the clay in the surrounding annulus. Numerical studies of both experiments have been documented [30],[70]. It will be shown that under certain conditions, the equations can be simplified in such a way that approximate solutions can be found that match adequately the full numerical as well as the experimental results. For experiment A this is straightforward. However, for experiment B, we demonstrate the limitations of this approximation.

5.2 Theory

As was discussed in Chapter 3, the equations presented here are based on non-equilibrium thermodynamics. As classical thermodynamics only describes initial and final states, transport processes such as diffusion of a solute in a soil need to be analyzed using non-equilibrium thermodynamics. We assume the validity of the laws of classical thermodynamics [40],[124], as well as the postulates of local equilibrium and linearity of the phenomenological equations.

Starting with the linear phenomenological equations relating driving forces $\mathbf{X}_j$ to fluxes $\mathbf{J}_i$

$$\mathbf{J}_i = \sum_{j=1}^{n} L_{ij}\mathbf{X}_j, \tag{5.1}$$

where L_{ij} are the coupling coefficients that relate flows of type i to gradients of type j. In soil processes, the relevant driving forces are gradients in pressure, concentration, electrical potential and temperature. We restrict ourselves to hydraulic and chemical gradients. With these assumptions, the basic flux equations in terms of pressure p [Pa] and chemical potential of the solute μ_s[kg/(ms^2)] are:

$$\mathbf{q} = L_{11}\nabla(-p) + L_{12}\nabla(-\mu_s) \tag{5.2}$$

$$\mathbf{J}_n^d = L_{21}\nabla(-p) + L_{22}\nabla(-\mu_s), \tag{5.3}$$

where the specific discharge is $\mathbf{q}$[m/s] and $\mathbf{J}_n^d$[mol/(m^{2}s)] denotes the diffusive molar flux of solute relative to the solution. Therefore solute molar flux relative to the porous medium is defined as $\mathbf{J}_n = \mathbf{J}_n^d + c_s\mathbf{q}$, where c_s[mol/m^3] is solute concentration. We can write $c_s = \frac{\rho_f\omega_s}{M_s}$, where ρ_f[kg/m^3] is the fluid density, ω_s[$-$] is the solute mass fraction and M_s[kg/mol] the solute molar mass. The gradient of the chemical potential now yields

$$\nabla\mu_s = \nu RT\frac{1}{a_s}\nabla a_s = \nu RT\frac{\rho_f}{\rho_s}\nabla\omega, \tag{5.4}$$

because the solute activity $a_s = \gamma\omega\frac{M_f}{M_s}$, where γ[$-$] is the activity coefficient, M_f[kg/mol] is the molar mass of the fluid, and salt mass fraction ω[$-$] $= \frac{\rho_s}{\rho_f}$ [8]. Here, ρ_s[kg/m^3] is density of solute, ν is the dissociation coefficient, the gas constant is denoted by R[J/(molK)], and T[K] is temperature.

As in [62], the reflection coefficient is defined as the ratio of the coupling coefficient relating pressure to specific discharge and the coupling coefficient relating osmotic pressure to specific discharge:

$$\sigma = -\frac{L_{12}}{c_s L_{11}}, \tag{5.5}$$

because the osmotic pressure gradient is $\nabla\pi = c_s\nabla\mu_s$. Employing the analogy with Darcy's law, $L_{11} = k/\mu$ yields

$$L_{12} = -\sigma c_s L_{11} = -\frac{\sigma k \rho_s}{\mu M_s} = \lambda \rho_f \nabla \omega, \tag{5.6}$$

where $k[m^2]$ is the intrinsic permeability of the porous medium, μ[kg/ms] the dynamic viscosity of the fluid and

$$\lambda = \frac{\sigma k}{\mu M_s} \nu RT. \tag{5.7}$$

The specific discharge now becomes

$$\mathbf{q} = -\frac{k}{\mu} \nabla p + \lambda \rho_f \nabla \omega. \tag{5.8}$$

The expression for the solute flux can be derived by substituting ∇p from (5.8) into the equation for the solute flux (5.3), yielding

$$\begin{aligned} \mathbf{J}_n^d &= L_{21} \nabla(-p) + L_{22} \nabla(-\mu_s) \\ &= -\sigma \frac{\rho_f \omega}{M_s} \mathbf{q} + (\sigma \lambda \frac{\rho_f \omega}{M_s} - L_{22} \frac{\nu RT}{\rho_s}) \rho_f \nabla \omega, \end{aligned}$$

because applying Onsager's reciprocity relations yields

$$L_{21} = L_{12} = -\frac{\sigma k \rho_s}{\mu M_s}. \tag{5.9}$$

Analogously to equation (10-23) in Katchalsky and Curran [62], a solute permeability coefficient θ (similar to ω in [62]) is defined:

$$\theta = \frac{L_{22} \frac{\nu RT}{\rho_s} - \sigma \lambda \rho_f \omega / M_s}{\nu RT / M_s} = L_{22}/c_s - \sigma^2 c_s k / \mu. \tag{5.10}$$

As in [62], we infer an effective diffusion coefficient $D = \nu \theta RT$, leading to an expression similar to Fick's law. The full equation for solute flux now reads

$$\mathbf{J}_n^d = -\sigma \frac{\rho_f \omega}{M_s} \mathbf{q} - D \frac{\rho_f}{M_s} \nabla \omega, \tag{5.11}$$

or in terms of solute mass flux $\mathbf{J}_s^d = \mathbf{J}_n^d M_s$

$$\mathbf{J}_s^d = -\sigma \rho_f \omega \mathbf{q} - D \rho_f \nabla \omega, \tag{5.12}$$

5.3 Analysis

5.3.1 Balance equations

The following balance equations are used, where $n[-]$ is porosity:

Fluid mass balance

$$\frac{\partial n\rho_f}{\partial t} + \nabla \cdot (\rho_f \mathbf{q}) = 0. \tag{5.13}$$

Salt mass balance

$$\frac{\partial n\rho_f \omega}{\partial t} + \nabla \cdot (\rho_f \omega \mathbf{q}) + \nabla \cdot \mathbf{J}_s^d = 0. \tag{5.14}$$

5.3.2 Equations of state

Under the assumption that fluid density is solely a function of pressure, i.e. temperature and mass fraction effects on liquid density are disregarded, the equation of state is given by

$$\rho_f = \rho_0 e^{\beta(p-p_0)}. \tag{5.15}$$

Here, $\beta[1/\text{Pa}]$ is the compressibility of the liquid, $\rho_0[\text{kg/m}^3]$ is the value for the fluid density when $p = p_0$, where p_0 is a reference pressure.

The porosity is related to the pressure as follows [73]:

$$n = 1 - (1 - n_0)e^{-\alpha p}, \tag{5.16}$$

where n_0 is a reference porosity, and $\alpha[1/\text{Pa}]$ the compressibility of the porous medium.

The storage properties of the solid and liquid phase can be represented by a single storage parameter $S_s = n\beta + (1 - n)\alpha$, in order to be able to write

$$\frac{\partial n\rho_f}{\partial t} = \rho_f(n\beta + (1 - n)\alpha)\frac{\partial p}{\partial t} = \rho_f S_s \frac{\partial p}{\partial t}. \tag{5.17}$$

To get a simple description for the volume change of a soil, we assume this storage parameter constant, as well as the dynamic viscosity of the fluid μ, intrinsic permeability k, and the diffusion coefficient D. Finally, in the next section, the reflection coefficient is also assumed to be constant.

5.3.3 Mathematical analysis

In case of a one-dimensional finite cartesian domain, with $\mathbf{q} = q\hat{\mathbf{x}}$ and $\mathbf{J}_s^d = J_s^d\hat{\mathbf{x}}$, the balance equations reduce to

$$\frac{\partial n\rho_f}{\partial t} + \frac{\partial \rho_f q}{\partial x} = 0, \tag{5.18}$$

$$\frac{\partial n\rho_f\omega}{\partial t} + \frac{\partial \rho_f\omega q}{\partial x} + \frac{\partial J_s^d}{\partial x} = 0, \tag{5.19}$$

with

$$q = -\frac{k}{\mu}\frac{\partial p}{\partial x} + \lambda\rho_f\frac{\partial \omega}{\partial x}, \tag{5.20}$$

$$J_s^d = -\sigma\rho_f\omega q - D\rho_f\frac{\partial \omega}{\partial x}. \tag{5.21}$$

In Chapter 4, it was shown by dimensional analysis that, provided relative storage parameters are small, the non-dimensional versions of these equations reduce to

$$\frac{\partial p}{\partial t} = \frac{\partial^2 p}{\partial x^2} - \frac{\partial^2 c}{\partial x^2}, \tag{5.22}$$

$$\frac{\partial c}{\partial t} = \varepsilon\frac{\partial^2 c}{\partial x^2}, \tag{5.23}$$

where the parameter $\varepsilon = \frac{S_s D\mu}{kn_0}$ is a dimensionless constant describing the diffusion of solute through the membrane on the timescale of pressure evolution. Since the effect of changes in porosity due to changes in pressure in the liquid phase are small, we approximate n by n_0.

Such a simple set of coupled equations may be solved by introducing a parameter ϕ:

$$\phi := p - \frac{1}{1-\varepsilon}c, \tag{5.24}$$

leading to

$$\frac{\partial \phi}{\partial t} = \frac{\partial^2 \phi}{\partial x^2}. \tag{5.25}$$

Solving (5.25) and (5.23), subject to appropriate initial and boundary conditions, yields expressions for the concentration as well as the pressure.

This method can be applied to model experimental situations, as illustrated in the following sections. It will be shown that it's applicability is limited to models with small storage parameters.

5.4 Modelling experiments: analytical and numerical results

In this section, a laboratory experiment (A) by Keijzer [63] is modelled, as well as a field experiment (B) conducted by Neuzil [89]. In both models the assumptions of sections 2.2 and 2.3 are imposed.

5.4.1 Keijzer experiments

Experimental setup

In [64],[63] Keijzer reports an experiment to investigate the semi-permeable behaviour of naturally occurring clayey materials. He subjected a sample of commercially available bentonite clay to a salt concentration gradient and used a flexible wall permeameter to measure differential pressure and concentration development over the clay membrane in order to show osmotic behaviour and to assess the value of the reflection coefficient. His results showed a buildup of pressure at one side of the membrane followed by a eventual decrease. The experimental set-up consists of a clay sample confined by two porous stones such that a uniform flow of a salt solution through the clay can be induced. They separate the clay from a (closed) reservoir with high salt concentration solution and an (open) reservoir containing the low salt concentration solution. In Figure 5.1, the set-up is shown schematically. We divide the modelling domain I into three parts, two containing the porous stones, and one representing the clay membrane. We will define I as the interval $[-L, b]$, where the origin is imposed at the intersection of the left porous stone and the membrane and the point a is located at the intersection between the right porous stone and the membrane. Furthermore $a, b, L > 0$. All subscripts will refer to the three regions as shown in Figure 5.1. Also in Figure 5.1, the values of the model parameters are given.

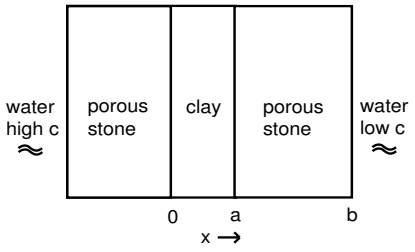

parameter	value in clay	value in porous stone
c_i (mol/l)	0.1	0.1 (l), 0.01 (r)
$n(-)$	0.5	0.56
k (m^2)	$1.2 \cdot 10^{-19}$	$1 \cdot 10^{-13}$
$D(m^2/s)$	$2.6 \cdot 10^{-13}$	$1.2 \cdot 10^{-10}$
$T(^oC)$	25	25
$S_s(1/Pa)$	$1 \cdot 10^{-8}$	$3.4 \cdot 10^{-6}$
$\sigma(-)$	0.019	0
length (mm)	$a = 2.3$	$b - a = 7.2$

Figure 5.1: *Modelling domain Keijzer experiment and relevant parameters*

Most of them are taken from [63]. The pressure data from this experiment were fitted according to a least squares method and the unknown diffusion coefficient and storage parameter were chosen based on this best fit to the data. The storage coefficient in the porous stones is assumed to be higher than in the clay to account for the potentially much larger storage capacity of the porous stones due to their expansion/contraction upon pressure increase/decrease [87]. The diffusion coefficient in the clay is quite low, as it is in the work of Sherwood [106] and Keijzer [63], because of the compactness of the clay and retardation due to cation exchange. To be able to simplify the equations, we assume that $\beta(p_i - p_0)$ and $S_s(p_i - p_0) \ll 1$ and $\lambda M_s(c_i - c_0) \ll D(1 - \sigma)$. This implies that equations (5.22), (5.23) can be employed. The last assumption is not justified based on the values of the parameters in Figure 5.1. However, on the timescale of pressure evolution, diffusion and advection through the clay are rather small; their relative behaviour is then, especially for small times, of minor importance.

Solution

We use the solution method described in Chapter 3. For this specific model, we use the following set of equations:

$$n_i S_s \frac{\partial p_i}{\partial t} = \frac{k_i}{\mu} \frac{\partial^2 p_i}{\partial x^2} - \lambda_i M_s \frac{\partial^2 c_i}{\partial x^2}, \tag{5.26}$$

$$n_i \frac{\partial c}{\partial t} = D_i \frac{\partial^2 c_i}{\partial x^2}, \tag{5.27}$$

where the index $i = 1, 2, 3$ designates respectively the porous stone at the left side in Figure 5.1, the clay membrane, and the porous stone at the right side in Figure 5.1. These regions will be referred to as regions $1, 2$ and 3 respectively.

To solve this set of equations, a new variable ϕ_i is introduced:

$$\phi_i(x,t) = \frac{k_i}{\mu} p_i(x,t) - \frac{\lambda_i M_s}{1-\varepsilon_i} c_i(x,t), \tag{5.28}$$

which leads to:

$$\frac{\partial \phi_i}{\partial t} = d_i \frac{\partial^2 \phi_i}{\partial x^2} \tag{5.29}$$

where $d_i = \frac{k_i}{\mu n_{0i} S_{s\,i}}$. As before, the porosity is assumed to be constant.

Initially, the left porous stone, as well as the clay membrane are saturated with the salt solution, implying the initial conditions:

$$p(x,0) = 0 \,\text{for}\, x \in I, \tag{5.30}$$

and

$$c(x,0) = \begin{cases} c_i \text{ for } x \in (-L,a) \\ c_0 \text{ for } x \in (a,b) \end{cases} \tag{5.31}$$

The boundary conditions are

$$x = -L : \begin{cases} \frac{\partial c_1}{\partial x} = 0 \\ \frac{\partial p_1}{\partial x} = 0 \end{cases} \qquad x = b : \begin{cases} \frac{\partial c_3}{\partial x} = 0 \\ p_3 = 0 \end{cases} \tag{5.32}$$

We assume continuous flux, pressure and concentration at the interfaces between the clay and the porous stones.
The transformed initial and boundary conditions are

$$\phi_1(x,0) = 0,\ \phi_2(x,0) = c_0,\ \phi_3(x,0) = 0, \tag{5.33}$$

$$x = -L : \frac{\partial \phi_1}{\partial x} = 0, \qquad x = b : \frac{\partial \phi_3}{\partial x} = 0. \tag{5.34}$$

To obtain the boundary conditions for the interface between the porous stones and the clay, we impose continuity of the volume flux q:

$$x = 0 :\ q_1 = q_2,\ x = a :\ q_2 = q_3, \tag{5.35}$$

implying

$$x = 0 : \ \frac{\partial \phi_1}{\partial x} = \frac{\partial \phi_2}{\partial x} + \frac{\varepsilon \lambda M_s}{1-\varepsilon} \frac{\partial c_2}{\partial x}, \ x = a : \ \frac{\partial \phi_3}{\partial x} = \frac{\partial \phi_2}{\partial x} + \frac{\varepsilon \lambda M_s}{1-\varepsilon} \frac{\partial c_2}{\partial x} \tag{5.36}$$

and

$$\phi_1 = \frac{k_1}{\mu} p_1 = \frac{k_1}{\mu} p_2 = \frac{k_1}{k_2} (\phi_2 + \frac{\lambda M_s}{1-\varepsilon} c_2) \, \text{at} \, x = 0, \tag{5.37}$$

$$\phi_3 = \frac{k_3}{\mu} p_3 = \frac{k_3}{\mu} p_2 = \frac{k_3}{k_2} (\phi_2 + \frac{\lambda M_s}{1-\varepsilon} c_2) \, \text{at} \, x = a. \tag{5.38}$$

Using all boundary, interface and initial conditions, we can solve (5.28) and (5.27) using Laplace transformation techniques for finite regions, see for example [13]. A Matlab routine [57] is used to solve the inverse Laplace transform problem.

In Figure 5.2, the evolution of mass fraction and pressure at the intersection of the membrane and the left porous stone is shown. It clearly shows an increase and subsequent decline of pressure due to osmosis and diffusion respectively. In Figure 5.3, the mass fraction and pressure profiles over the membrane are given, at different time levels. Mass fraction is plotted because it is the original independent variable in the model.

Numerical solution

Using the scripted finite element builder and numerical solver FlexPDE [26], the full equations (5.13) and (5.14) were modelled numerically. Details about this work can be found in [70]. Figure 5.4 shows the comparison of these numerical solutions with the results of the analytical modelling. The agreement is excellent, which justify the imposed simplifying assumptions.

Figure 5.5 shows the comparison of the modelling solutions for the pressure evolution at the interface between the left porous stone and the clay, with the results of the experiment conducted by Keijzer [63]. Unfortunately, valid mass fraction data for this experiment were not available, so the storage parameter as well as the diffusion coefficient were adapted to fit the data. Nevertheless, the pressure evolution can be simulated rather well. In [30], some additional details can be found.

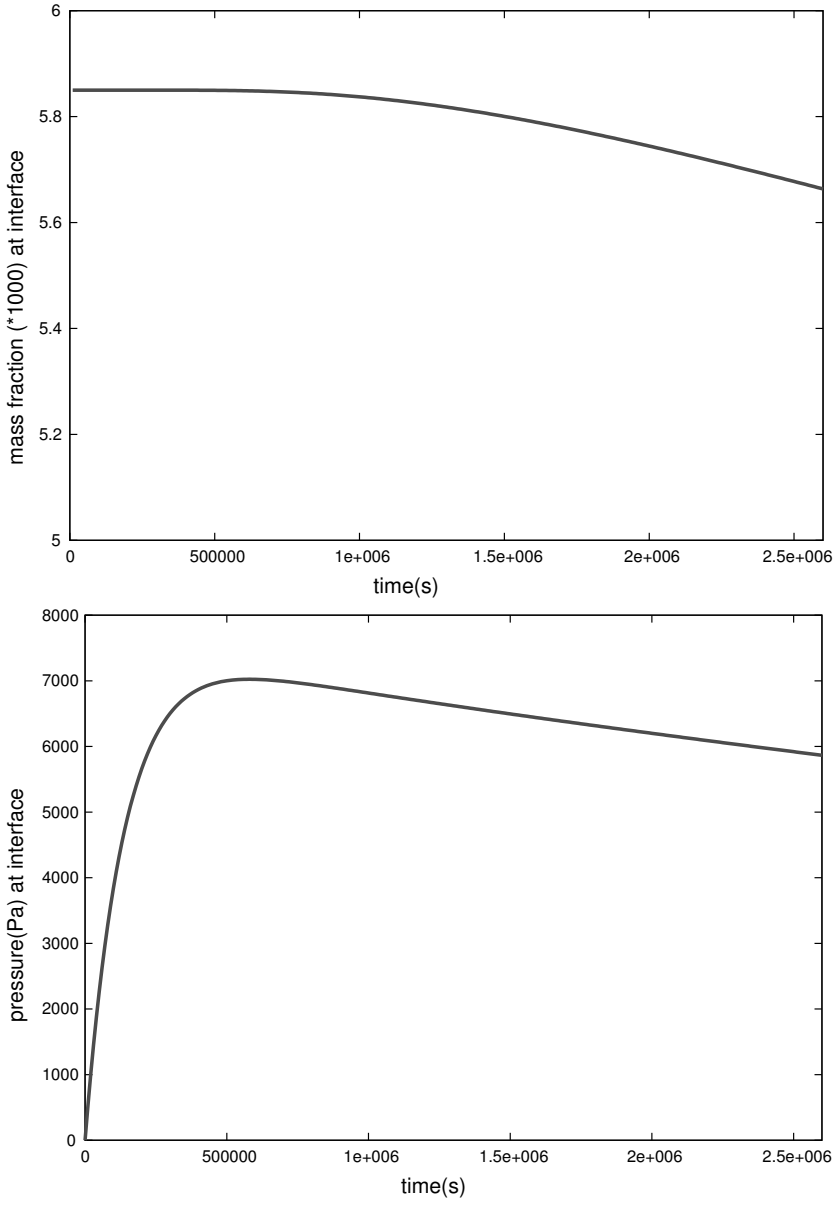

Figure 5.2: Evolution of mass fraction (above) and pressure (below) at the interface of the clay and a porous stone ($x = 0$)

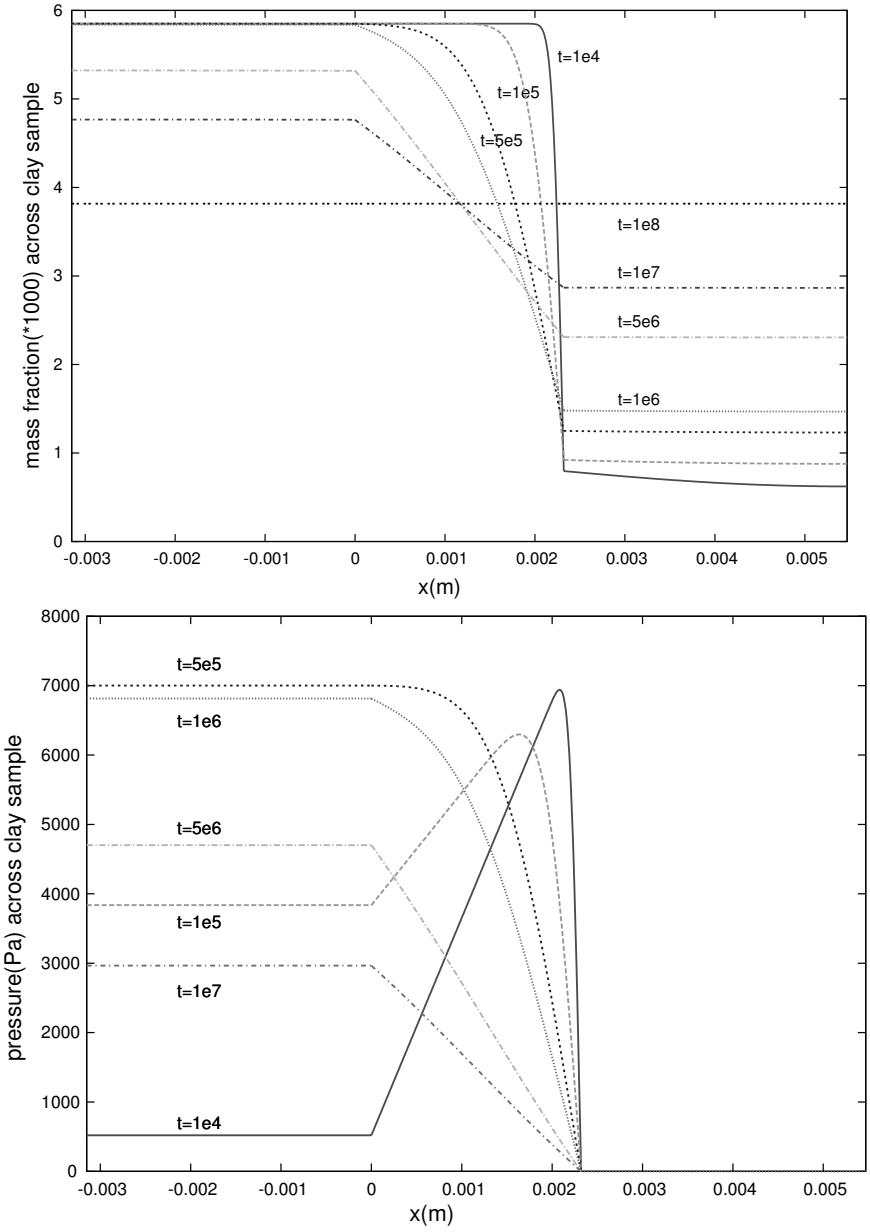

Figure 5.3: Mass fraction (above) and pressure (below) across the clay sample

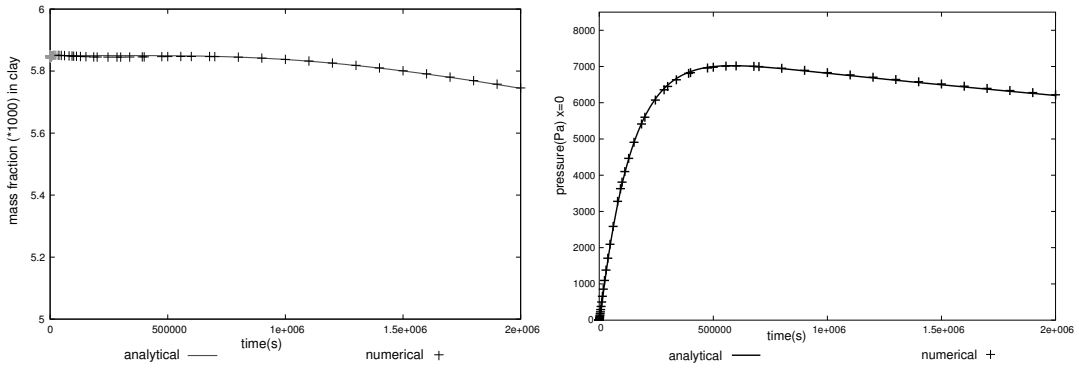

Figure 5.4: Comparison of analytical solution with the solution of the complete numerical model for mass fraction (left) and pressure (right); Keijzer experiment

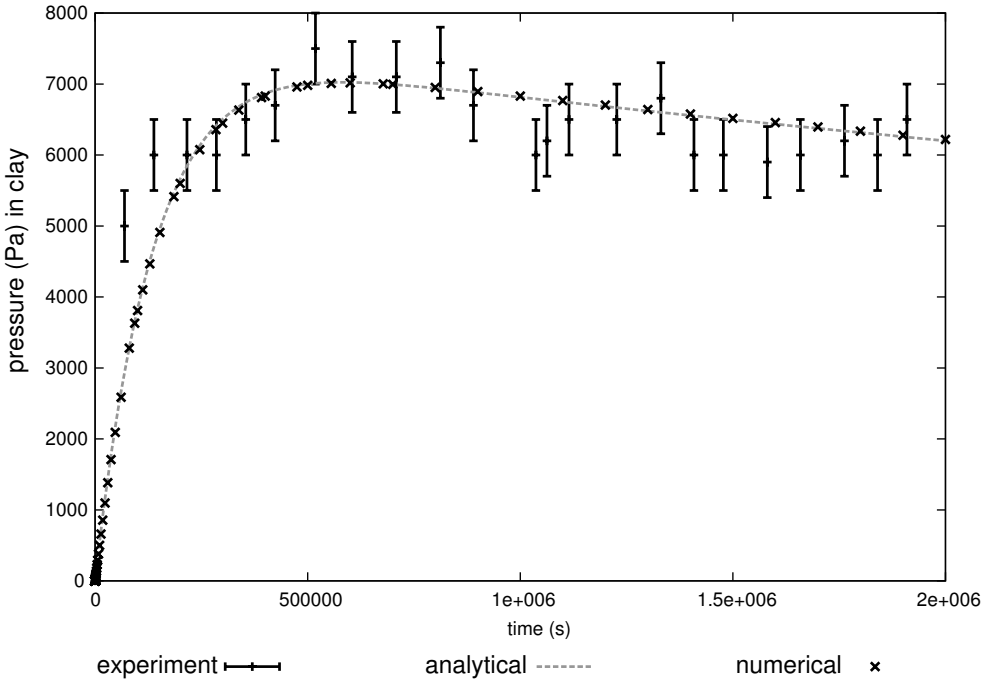

Figure 5.5: Comparison of model solution with experimental results (Keijzer experiment)

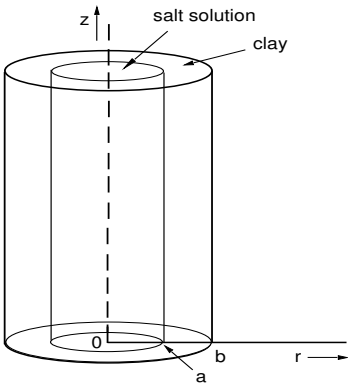

parameter	value in clay	value in borehole
c_i (mol/l)	0.0085	0.085
$n(-)$	0.3	1
$k(m^2)$	$2.6 \cdot 10^{-19}$	$1 \cdot 10^{-13}$
$D(m^2/s)$	$9 \cdot 10^{-12}$	$1 \cdot 10^{-9}$
$T(^oC)$	25	25
$S_s(1/Pa)$	$5.5 \cdot 10^{-9}$	$5 \cdot 10^{-4}$
$\lambda(m^5/\text{kg s})$	$1.9 \cdot 10^{-12}$	0
$\sigma(-)$	0.089	0

Figure 5.6: *Setup and parameters Neuzil model*

5.4.2 Neuzil model

Model setup

In [89], Neuzil reported the results of an experiment that conclusively showed the existence of osmotic pressures in a particular field situation. During this experiment, a number of boreholes were drilled, and filled with saline water. For nine years, the water elevation and salt concentration in the boreholes were measured. The results indicated a diffusive decrease in salinity and a rise in water elevation in the boreholes until a balance was reached, which signalled the end of his experiments.

The experiments of Neuzil have recently been modelled numerically [31]. It is shown that the balance of hydraulic pressure and osmotic pressure is followed by a decline of pressure, as in the experiment of Keijzer. In the current work, a number of simplifications are made to illustrate the analytical method used. This section illustrates the limitations of the simplifying assumptions used.

In a saturated, mainly smectite-illite clay shale, four boreholes were drilled and slotted casings with radii of 3 cm were placed in the boreholes. Two of the casings were filled with water with ten times the solute concentration compared to the shale water and the other two were filled with shale water and deionized water for reference purposes. In the model (see Figure 5.6), the experimental setup is assumed to consist of two concentric cylinders, the inner one with a radius a of 3 cm.

Because the experiment was performed using a number of boreholes, 15 meter apart, the radius of the outer annulus was taken to be 15 m. The inner cylinder is filled with saline water with an initial concentration c_i; the outer annulus consists of clay soil. We assume radial symmetry and no significant flow in the vertical direction, so one-dimensional radial coordinates are adopted.

Equations

The same balance equations (5.13)-(5.14) as before hold, but now in radial coordinates. Following the same procedure as in the previous model, we substitute the momentum balance equations and equations of state in the mass balances, and apply the approximations $\beta(p_i - p_0), S_s(p_i - p_0) \ll 1, \lambda M_s(c_i - c_0) \ll D$. This yields:

$$n\beta\frac{\partial p}{\partial t} = \frac{k}{\mu}\frac{1}{r}\frac{\partial}{\partial r}\left(r\frac{\partial p}{\partial r}\right) - \frac{\lambda M_s}{r}\frac{\partial}{\partial r}\left(r\frac{\partial c}{\partial r}\right), \tag{5.39}$$

$$n\frac{\partial c}{\partial t} = \frac{D}{r}\frac{\partial}{\partial r}\left(r\frac{\partial c}{\partial r}\right). \tag{5.40}$$

Initially, the borehole is filled with saline water with a concentration c_i; the ambient concentration in the aquifer is denoted by c_∞, so the initial conditions are

$$c(x,0) = \begin{cases} c_i \text{ for } r \in [0,a) \\ c_\infty \text{ for } r \in [a,\infty) \end{cases} \tag{5.41}$$

$$p(x,0) = 0 \text{ for } r \in [0,\infty) \tag{5.42}$$

The boundary conditions at the radius b of the outer cylinder are

$$c(b,t) = c_\infty,\ p(b,t) = 0. \tag{5.43}$$

The equation for liquid density in the borehole has to be adapted according to

$$\rho_f = \rho_0\frac{z_i}{z_h}\left(1 + \frac{p}{\rho_0 z_h g}\right) \tag{5.44}$$

with g the acceleration of gravity, z_i the water level in the standpipe and z_h the height of the cylinder. For zero pressure, this expression simulates the situation of a liquid concentrated in the region $z < z_h$ with an apparent density $\rho_0^* = \rho_0\frac{z_i}{z_h}$. The extra storage capacity is expressed by a larger storage parameter in the inner cylinder.

As in the previous model, we introduce a new variable ψ, such that

$$\psi_i(r,t) = \frac{k_i}{\mu}p_i(r,t) - \frac{\lambda_i M_s}{1-\varepsilon_i}c_i(r,t). \tag{5.45}$$

Using this definition we can recast (5.39) and (5.40):

$$\frac{\partial \psi_i}{\partial t} = \frac{d_i}{r}\frac{\partial}{\partial r}\left(r\frac{\partial \psi}{\partial r}\right), \tag{5.46}$$

where $d_i = k_i/\mu n_{0i}\beta_i$. The subscript $i = 1$ refers to the inner cylinder, and $i = 2$ to the outer region.

The initial condition for ψ is

$$r \in [0, a) : \psi(r, 0) = 0, \qquad r \in [a, \infty) : \psi(r, 0) = -\frac{\lambda M_s}{1-\varepsilon} c_\infty, \tag{5.47}$$

and we can derive the following interface conditions at $r = a$:

$$\psi_1(a, t) = \frac{k_1}{k_2}(\psi_2(a, t) + \frac{\lambda M_s}{1-\varepsilon} c_2(a, t)), \tag{5.48}$$

$$\frac{\partial \psi_1(a, t)}{\partial r} = \frac{\partial \psi_2(a, t)}{\partial r} + \frac{\varepsilon \lambda M_s}{1-\varepsilon}\frac{\partial c_2(a, t)}{\partial r}. \tag{5.49}$$

Also,

$$\psi(b, t) = -\frac{\lambda M_s}{1-\varepsilon} c_\infty. \tag{5.50}$$

Solution

The solutions of the diffusion equations (5.40) and (5.46) for the composite cylindrical region can be derived using Laplace transformations [13] and are displayed in Figure 5.7. The same type of pressure and mass fraction evolution is found compared to the first experiment; however, the pressure drop after flow equilibrium is steeper due to a larger diffusion coefficient. is a dummy variable and

Figure 5.7 also shows a comparison of the results obtained with the analytical and the numerical model. Numerical and analytical results differ considerably. This clearly shows the limitations of the simplifying assumptions: the storage parameters $\beta(p_i - p_0), S_s(p_i - p_0)$ are of order one, therefore the pressure and mass fraction development can not be described by the simple model.

Solution for infinite outer cylinder radius

As said before, the experiment is also modelled for the situation that the cylindrical domain is infinite. This yields the following exact solutions for the concentration:

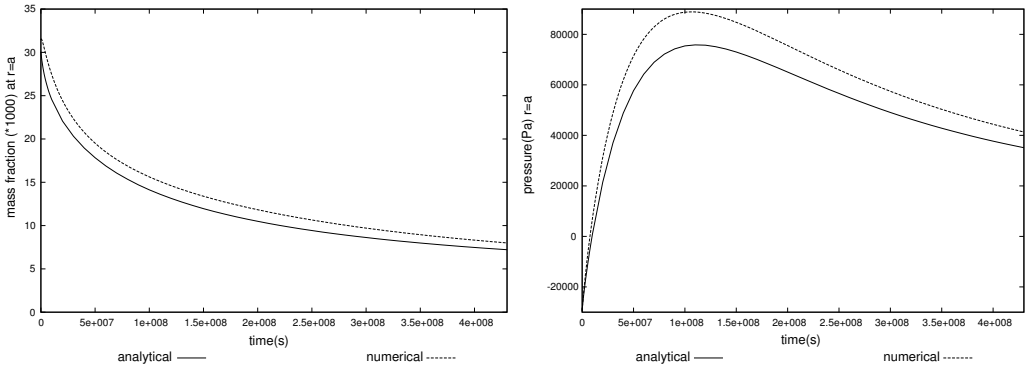

Figure 5.7: Evolution of pressure and mass fraction at $r = a$; comparison of analytical and numerical results

$$c_1 = \frac{4(c_i - c_\infty)D_1 D_2^2}{\pi^2 a} \int_0^\infty e^{-D_1 u^2 t} \Delta_1(u, r) du, \tag{5.51}$$

$$c_2 = \frac{2(c_i - c_\infty)D_1 \sqrt{D_2}}{\pi} \int_0^\infty e^{-D_1 u^2 t} \Delta_2(u, r) du, \tag{5.52}$$

where

$$\Delta_1 = \frac{J_0(ur)J_1(ua)}{u^2(f^2(u) + g^2(u))}, \tag{5.53}$$

$$\Delta_2 = \frac{J_1(ua)(J_0(\nu ur)f(u) - Y_0(\nu ur)g(u))}{u(f^2(u) + g^2(u))}, \tag{5.54}$$

where $\nu = \sqrt{D1/D2}$, u is a dummy variable and

$$f = D_1\sqrt{D_2}J_1(au)J_0(\nu au) - D_2\sqrt{D_1}J_0(au)J_1(\nu au), \tag{5.55}$$

$$g = D_1\sqrt{D_2}J_1(au)Y_0(\nu au) - D_2\sqrt{D_1}J_0(au)Y_1(\nu au), \tag{5.56}$$

where J_0, J_1, Y_0 and Y_1 are Bessel functions. The solutions for pressure are similar.

Figure 5.8 shows the comparison between the numerical and analytical case for the infinite domain case. It shows a similar discrepancy due to the excess storage capacity of the inner cylinder.

Figure 5.9 shows the comparison between the pressure for the finite and infinite b setups. The concentration profiles are identical, whereas the Figure shows that pressure varies considerably.

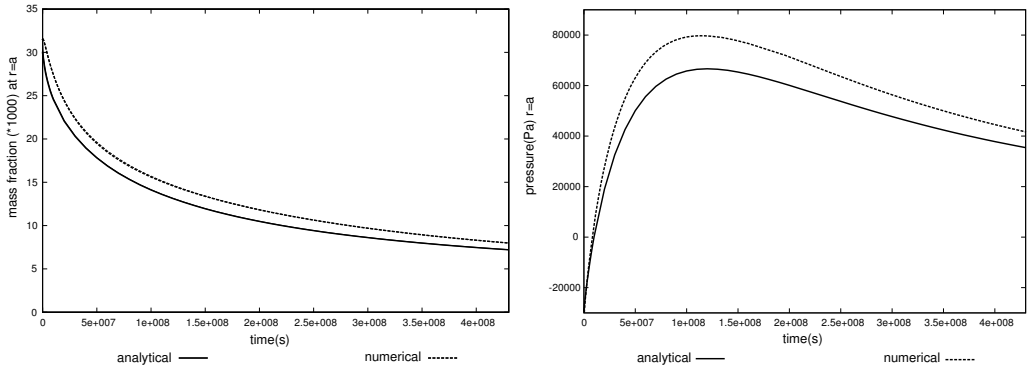

Figure 5.8: Comparison of pressure and mass fraction at $r = a$; infinite domain case

5.4.3 The Boussinesq limit

In this paper, we did not neglect the compressibility of the fluid. To show that this is justified for a rigid clay, we redefine the fluid density and introduce the parameter δ:

$$u = \frac{\rho_f - \rho_0}{\rho_{\max} - \rho_0} = \frac{\rho_f/\rho_0 - 1}{\delta}, \quad \delta = \frac{\rho_{\max} - \rho_0}{\rho_0} \tag{5.57}$$

Here, u is the scaled fluid density, and $\rho_{\max}$ and ρ_0 denote the maximum and minimum values of the fluid density, respectively. The parameter δ specifies the relative variation of the liquid density.

Substitution of (5.57) yields for the fluid mass balance (5.13):

$$\delta(n\frac{\partial u}{\partial t} + \nabla \cdot (u\mathbf{q})) + \nabla \cdot \mathbf{q} = 0. \tag{5.58}$$

The limit $\delta \to 0$, which is known as the Boussinesq limit for incompressible fluids, yields $\nabla \cdot \mathbf{q} = 0$. If we consider a simple one-dimensional cartesian domain, imposing the Boussinesq approximation yields:

$$\frac{\partial q}{\partial x} = -\frac{k}{\mu}\frac{\partial^2 p}{\partial x^2} + \lambda M_s \frac{\partial^2 c}{\partial x^2} = 0 \tag{5.59}$$

$$\to c - \frac{kp}{\mu\lambda M_s} = Ax + B, \tag{5.60}$$

where A, B are integration constants. Here, we neglect the dependence of porosity on pressure. Boundary conditions from the Keijzer experiment yield $A = 0$,

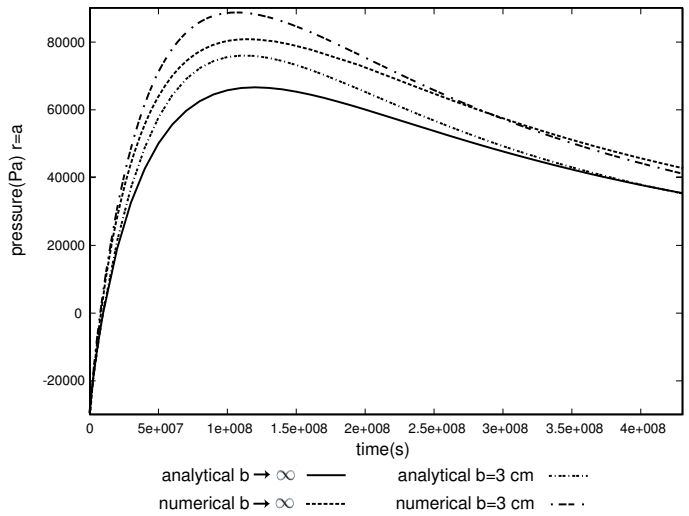

Figure 5.9: Pressure at $r = a$; comparison for finite and infinite b

implying that pressure is linearly related to salt concentration. However, we have seen that the experimental results and the outcome of the numerical modelling show that the pressure increases in time, and eventually will decrease, whereas the concentration is a monotonically decreasing function in time. In Figure 5.10, we observe the discrepancy between the results for pressure evolution with the compressibility turned 'on' and 'off'. Therefore, the Boussinesq limit necessarily does not hold here, also, it clearly shows that the excess water due to osmosis, is stored in the porous medium.

5.5 Conclusions

To illustrate the influence of osmosis on groundwater flow and transport of dissolved particles in clay soils, a model was developed that describes these processes in various situations. This paper shows that the derived model may be simplified as to provide analytical solutions for one-dimensional problems of chemical osmosis in clay membranes. Although there are limitations to the applicability of this approximation, it can be applied for a range of experiments, especially when conditions are comparable with those in the Keijzer experiment. This study also illustrates the importance of the compressibility coefficients in chemically induced groundwater flow situations. Low values of these coefficients imply that the problem can be reduced to a set of diffusion-type equations. However, fully neglecting the compressibilities, i.e. applying the Boussinesq limit, may lead to non-physical situations.

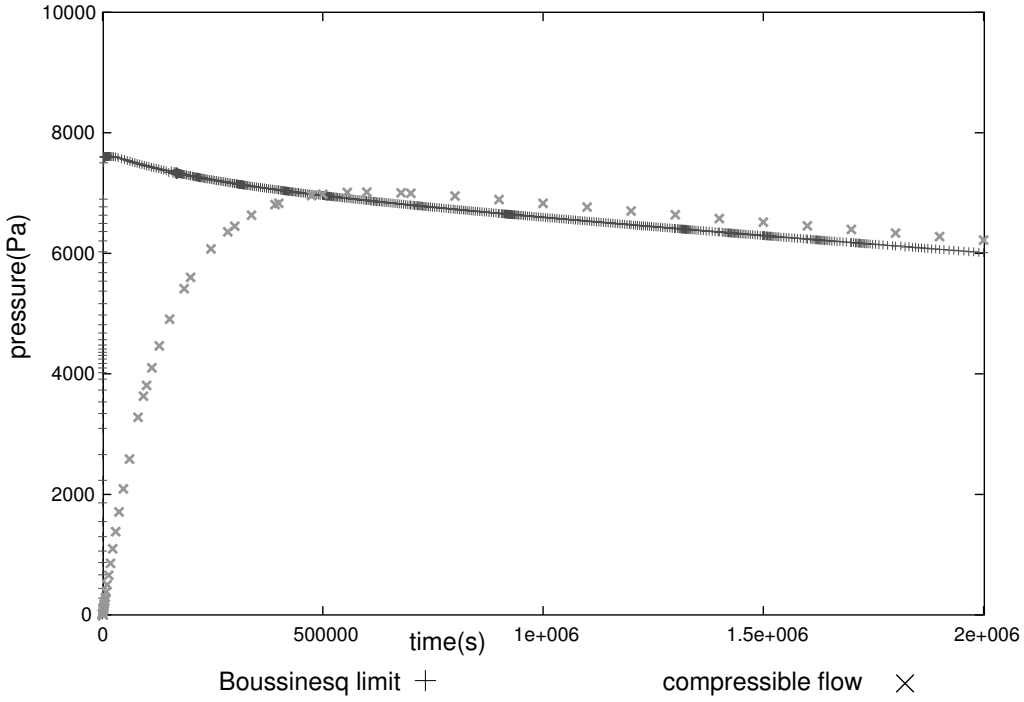

Figure 5.10: Liquid compressibility 'on' and 'off'

The problem of modelling groundwater flow in clay soils becomes increasingly interesting when phenomena such as electro-osmosis and streaming potential are included. Or, as in [76], reactive transport and ion exchange. The mechanisms of swelling and consolidation caused by chemical and electro-osmosis deserve thorough treatment as well. This study will therefore in due course be expanded to include some, or even all of these processes.

Chapter 6

Membrane potential

6.1 Introduction

The membrane potential is the electrical potential difference that compensates the separation of charge due to different velocities of cations and anions in a free electrolyte solution or in a porous medium (partly) saturated with an electrolyte solution. In Chapter 2 it was discussed briefly. In this Chapter, we consider this process in more detail. Different terminologies for this effect are *en vogue*. For example, in [9], Bolt states that a potential difference caused by the restrictive behaviour of the membrane on the ionic mobilities is called the membrane potential whereas the sum effect of liquid and membrane on the ions is called the diffusion potential. In [52] however, the membrane potential is the sum of the so-called concentration potential (the potential difference in a porous medium between two solutions) and the Donnan potential (between the solution and the membrane).

We follow the approach of Revil [98], where membrane potential is the sum effect, and the part caused by the membrane is called the exclusion potential. Schematically, the 'Bolt' and 'Revil' definitions are given by:

$$\begin{aligned} \text{Bolt [9]:} \qquad & V_{\text{membrane}} + V_{\text{liquid}} = V_{\text{diffusion}}, \\ \text{Revil [98]:} \qquad & V_{\text{exclusion}} + V_{\text{liquid}} = V_{\text{membrane}}. \end{aligned}$$

Although the 'Bolt' [9] approach may appear to be somewhat more logical, in most papers, the term membrane potential specifies the sum effect.

We apply the combined set of equations for chemico-electro-osmosis to assess the influence of membrane potential on chemical osmotic flow. A number of experiments were performed quite similarly to those reported in Chapter 5. Details on these experiments can be found in [51]. In a laboratory, a clay sample was subjected to a salt concentration gradient and pressure and concentration were

simultaneously measured. However, the clay was equipped with electrodes to measure the electrical potential as well, and an experimental method was found to short-circuit the clay, in order to turn on and off the electrical effects.

In this chapter, first an expression for membrane potential is derived and it is shown how this influences the equations for chemical osmosis and diffusion. Then, an *exposé* is given of the experiments performed and it is shown how measured potentials compare to theoretical potentials. The measured membrane potential is then shown to be in accordance with the value obtained by applying the theory of Revil [98]. Then, it is shown how experiments and equations alike show the electro-osmotic counterflow caused by membrane potential, and how short-circuiting the setup removes the electrical effects.

6.2 Derivation of an expression for membrane potential

In Chapter 3 we briefly discussed the membrane potential with respect to the equations for electro-chemical osmosis. In this chapter, we derive a somewhat more thorough expression for the membrane potential in this chapter. In general, we start with a microscopic description the processes in a free solution, and then apply certain assumptions to present the description of the processes in a porous medium/pore water system. Throughout, we may use the term membrane potential where it should actually read membrane potential gradient or membrane potential difference. This because of the fact that in literature it is quite common to omit these terms.

We start with the electrical current density $\mathbf{I}$, which is expressed as

$$\mathbf{I} = \sum_{i=+,-} \mathbf{j}_i^d z_i F, \tag{6.1}$$

where $\mathbf{j}_i^d$ are the ionic fluxes in a free solution, z_i are the ionic valences and F is Faraday's constant. For diffusion of separate ions, assuming an ideal solution, we write (see [98], [123])

$$\mathbf{j}_i^d = -\frac{u_i c_i}{F} \nabla \mu_i, \tag{6.2}$$

$$\mu_i = \mu_i^0 + RT \ln c_i + z_i F V. \tag{6.3}$$

where u_i is ionic mobility and μ_i^0 is a reference chemical potential such that $\nabla\mu_i^0 = 0$. Substituting (6.3) in (6.2) yields

$$\mathbf{j}_i^d = -\frac{u_i RT}{F}\nabla c_i - u_i c_i z_i \nabla V. \tag{6.4}$$

For the electrical current density in a 1:1 electrolyte this implies

$$\mathbf{I} = -(u_+ - u_-)RT\nabla c_f - (u_+ + u_-)c_f F\nabla V. \tag{6.5}$$

When electro-neutrality is enforced, the concentrations of anions and cations equal the salt concentration c_f: $c_f = c_+ = c_-$, as are the ionic fluxes: $\mathbf{j}_s^d = \mathbf{j}_+^d = \mathbf{j}_-^d$. We define $u = u_+ - u_-$ as the effective solute mobility and $\sigma_f = (u_+ + u_-)Fc_f$ as the electrical conductivity of the electrolyte, such that (6.5) may be written as:

$$\mathbf{I} = -uRT\nabla c_f - \sigma_f \nabla V. \tag{6.6}$$

If we assume the mobility and the electrical conductivity to be constant, we obtain a simple expression to quantify membrane potential:

$$\mathbf{I} = 0 \rightarrow \nabla V = -\frac{uRT}{\sigma_f}\nabla c_f. \tag{6.7}$$

This expression is often found in literature [123], [76] to describe the membrane potential. The mobility and the electrical conductivity are simply substituted by macroscopic counterparts that are assumed to be constant. However, especially for larger salt concentration gradients, the concentration dependence of the electrical conductivity becomes increasingly significant, as can be seen in Figure 6.1. In this figure, we compared the membrane potential for a concentration dependent σ_f (exact) and for a constant σ_f. The value of σ_f was chosen, in accordance with the mean of the outside concentrations. We assumed a low concentration of $c_{\text{low}} = 0.01$ M and defined the parameter α to be the ratio of high and low concentrations: $\alpha = c_{\text{high}}/c_{\text{low}}$.

For solutions, such as NaCl, it is known that a Cl^- ion moves faster than a Na^+ ion, or: $u_- > u_+$, hence $u < 0$ and the potential gradient is of the same sign as the salt concentration gradient. However, when for example in a clay, the movement of anions is more restricted than the movement of cations, viz. in the case of anion exclusion, the mobility of cations is higher than the mobility of anions and the potential gradient and the salt concentration gradient have different

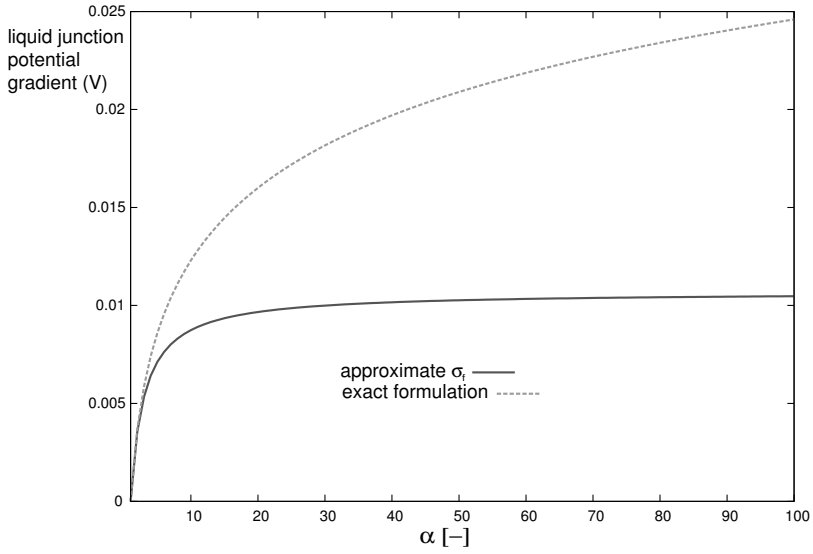

Figure 6.1: Comparison of different expressions for the liquid junction potential gradient

signs. We may follow the approach of [98] and adopt the expression for electrical conductivity; then:

$$\nabla V = -\frac{(u_+ - u_-)RT}{(u_+ + u_-)Fc_f}\nabla c_f = -\frac{RT}{F}(t_+ - t_-)\nabla \ln c_f, \tag{6.8}$$

where t_i are Hittorf transport numbers that specify relative mobility of the ionic constituents:

$$t_i = \frac{u_i}{\sum_{i=+,-} u_i}. \tag{6.9}$$

For a porous medium it is shown in [98] that these equations are valid if we substitute for σ_f, u_i, t_i macroscopic parameters. In [98] it is shown that, for the previous expression for the potential this amounts to:

$$\nabla V = -\frac{RT}{F}(T_+ - T_-)\nabla \ln c_f \tag{6.10}$$

$$T_i = \frac{\sigma_i}{\sigma_f}, \tag{6.11}$$

where σ_i is the contribution of an ion to the bulk electrical conductivity $\sigma_e = \sigma_+ + \sigma_-$ and T_i are the macroscopic Hittorf numbers. This expression can be decomposed in a liquid junction potential and a exclusion potential, respectively:

$$\nabla V = -\frac{RT}{F}(t_+ - t_-)\nabla \ln c_f - \frac{2RT}{F}(T_+ - t_+)\nabla \ln c_f. \tag{6.12}$$

In [98] it is shown qualitatively how in the absence of a porous medium, the macroscopic parameter T_i reduces to t_i.

Alternatively, we may consider the presence of the porous medium to be only accounted for by the formation factor (as in [5]), i.e.

$$\sigma_e = \frac{\sigma_f}{F_0}. \tag{6.13}$$

To avoid confusion, the formation factor is denoted by F_0:

$$\nabla V = -\frac{RT}{F}F_0(2t_+ - 1)\nabla \ln c_f. \tag{6.14}$$

6.3 Membrane potential and chemical osmosis

In Chapter 3 we saw the simple variant of the Darcy flux, corrected for streaming and membrane potential. Here we repeat this relationship, but consider a dependence on a salt concentration gradient instead of the mass fractions of the separate ions.

$$\mathbf{q} = -K^e\nabla p + \Lambda^e \nabla c_f, \tag{6.15}$$

where

$$\Lambda^e = \lambda + \frac{(u_+ - u_-)RTk_e}{\sigma_e}. \tag{6.16}$$

On the other hand, if we insert the expression for the membrane potential we just derived, i.e. equation (6.10), in

$$\mathbf{q} = -\frac{k}{\mu}\nabla p + \lambda \nabla c_f - k_e \nabla V, \tag{6.17}$$

we obtain

$$\mathbf{q}_{nsc} = -\left[\frac{k}{\mu} - \frac{k_e^2}{\sigma_e}\right]\nabla p + \left[\lambda + k_e\frac{RT}{F}(T_+ - T_-)\frac{1}{c_f}\right]\nabla c_f. \tag{6.18}$$

The electric conductivity in the streaming potential is not expanded because this term is quite small and will therefore be neglected later on. The transition from the expression with electrical effects to the one without is formally done by short-circuiting. In the experiments, the system is short-circuited to eliminate any electrical potentials. The flux equations therefore come in two flavours: short-circuited (**sc**) (or shorted), i.e. without electrical effects, and non-short-circuited (**nsc**) (or non-shorted), i.e. with electrical effects. The short-circuited Darcy flux is simply given by

$$\mathbf{q}_{sc} = -\frac{k}{\mu}\nabla p + \lambda\nabla c_f, \tag{6.19}$$

i.e. $\nabla V = 0$ in equation (6.17).

6.4 Membrane potential and diffusion

The simple expressions for the ion fluxes discussed in Chapter 3 are expanded as follows. First, the free solution expression is derived:

$$\begin{aligned}
\mathbf{j}_+^d &= -\left[\mathcal{D}_+ - \frac{u_+(u_+ - u_-)c_f RT}{\sigma_e}\right]\nabla c_f \\
&= -\left[\mathcal{D}_+ - \frac{u_+(u_+ - u_-)c_f RT}{F(u_+ + u_-)c_f}\right]\nabla c_f \\
&= -\mathcal{D}_+\left[1 - \frac{u_+ - u_-}{(u_+ + u_-)}\right]\nabla c_f \\
&= -2t_-\mathcal{D}_+\nabla c_f
\end{aligned} \tag{6.20}$$

Contrary to Chapter 3, we write $\mathbf{j}_s^d$ instead of $\mathbf{J}_s^d$ to stress that we first consider microscopic formulations, and subsequently introduce the upscaled expressons. Assuming $\mathbf{j}_s^d = \mathbf{j}_+^d = \mathbf{j}_-^d = -D_f\nabla c_f$, where D_f is the solute diffusivity in a free solution, we find

$$D_f = 2t_-\mathcal{D}_+ = 2t_+\mathcal{D}_- \tag{6.21}$$

Unfortunately, this equation cannot be 'simply' upscaled by substituting for the macroscopic Hittorf numbers, because we already used the expression for the free solution electrical conductivity. In our description, we do not really have macroscopic values of the diffusion coefficients and the mobilities, but we do have macroscopic values of the Hittorf transport numbers and the corresponding electrical conductivities. It is therefore convenient to write the equations in terms of the latter parameters.

The following method is applied, where the arrow denotes upscaling to the porous medium and the bars denote macroscopic quantities. Note that we do not put bars on the electrical conductivities as they are not defined before separately for cations and anions.

$$\mathcal{D}_+ \rightarrow \bar{D}_+ = \frac{\bar{u}_+ RT}{F} = \frac{\sigma_+ RT}{F^2 c_+} \tag{6.22}$$

The cation flux in the porous medium then becomes

$$\begin{aligned} \mathbf{J}_+^d &= -\bar{D}_+ \nabla c_f - \bar{u}_+ c_f \nabla V \\ &= -\left[\bar{D}_+ - \frac{\bar{u}_+ RT(T_+ - T_-)}{F}\right] \nabla c_f \\ &= -2T_- \bar{D}_+ \nabla c_f. \end{aligned} \tag{6.23}$$

This last term can be written in terms of the electrolyte diffusivity D_f:

$$\begin{aligned} 2T_- \bar{D}_+ &= \frac{2T_- \sigma_+ RT}{F(Fc_f)} \\ &= \frac{2T_- T_+ \sigma_e RT(u_+ + u_-)}{F\sigma_f} \\ &= \frac{T_+ T_- \sigma_e}{t_+ t_- \sigma_f} D_f \\ &= \frac{T_+}{t_+} \frac{D_f}{F_0}. \end{aligned} \tag{6.24}$$

The last step was obtained by using the definition $T_-\sigma_e = \sigma_- = \sigma_f t_-/F_0$.
The macroscopic diffusivity obviously reduces to the electrolyte diffusivity in the absence of a porous medium, i.e. $\gamma = T_+/t_+ \rightarrow 1$ as well as geometrical constraints, i.e. $F_0 \rightarrow 1$. The salt flux is equal to the cation flux in the non-shorted case: $\mathbf{J}_s^d = \mathbf{J}_+^d = \mathbf{J}_-^d$; hence:

$$(\mathbf{J}_s^d)_{nsc} = -\frac{D_f}{F_0}\gamma\nabla c_f. \tag{6.25}$$

When we consider the short-circuited situation, we disregard all electrical contributions. The result is the following: the anionic and cationic diffusion coefficients, concentrations and fluxes are no longer equal. This implies that a successful experimental shortcut separates the charges in the solution. The liquid-junction potential, generated by this separation of charges, is immediately compensated by the potential generated by the virtual shortcut. In the experiments, the Ag|AgCl electrodes only measure the amount of anions in the solution, so instead of the salt flux we have to use the expression for the anion flux to interpret the results of the experiments. Accordingly, the electrolyte anion flux is given by

$$(\mathbf{J}_-^d)_{sc} = -\bar{D}_-\nabla c_-. \tag{6.26}$$

As the electrical conduction of anions is assumed not to be influenced by the charge of the porous medium, but only by its geometry, we find

$$\sigma_- = F\bar{u}_- c_- = \frac{Fu_- c_-}{F_0}, \tag{6.27}$$

and therefore

$$(\mathbf{J}_-^d)_{sc} = -\bar{D}_-\nabla c_- = -\frac{\mathcal{D}_-}{F_0}\nabla c_-. \tag{6.28}$$

6.5 Experiments

In [51], a number of experiments is described in which it is investigated how the membrane potential influences the buildup of osmotic pressure. We show here the results of experiments on bentonite clay, for an initial concentration difference of $0.01 - 0.1$M NaCl and $0.01 - 0.05$M NaCl for natural, hetero-ionic clay and a $\Delta c = 0.01 - 0.1$M NaCl-experiment for homo-ionic clay. In Table 6.1 it is shown how the different experiments are classified.

6.5.1 Experimental setup

The experiment was quite similar compared to the experiment reported by Keijzer [63]. A clay sample was subjected to a salt concentration gradient, but here, the

sample was prepared with electrodes to measure electrical potentials in the clay. To contain the clay, a rigid-wall permeameter was used, consisting of plastics for electrical insulation, with an inner diameter of 50 mm. Within this mould, the clay sample that is situated between two porous stones and nylon filters has the same dimensions as in the flexible-wall permeameter previously used. In addition, it is advantageous that the clay sample can be saturated in-situ before the experiment is started such that distortion of the clay membrane is minimal. Compaction of the clay during the experiment is ensured by putting a mechanical load on the piston of the sample mould. Via the porous stones, the clay is in contact with two fluid reservoirs that are equipped with double junction Ag|AgCl reference electrodes and Cl-sensitive electrodes to measure the electrical potential and the Cl-concentration, and with a calibrated standpipe to quantify the water flow. To prevent concentration polarization and to homogenize the solutions, the reservoirs are continuously circulated with a peristaltic pump. The setup is shown in Figure 6.2.

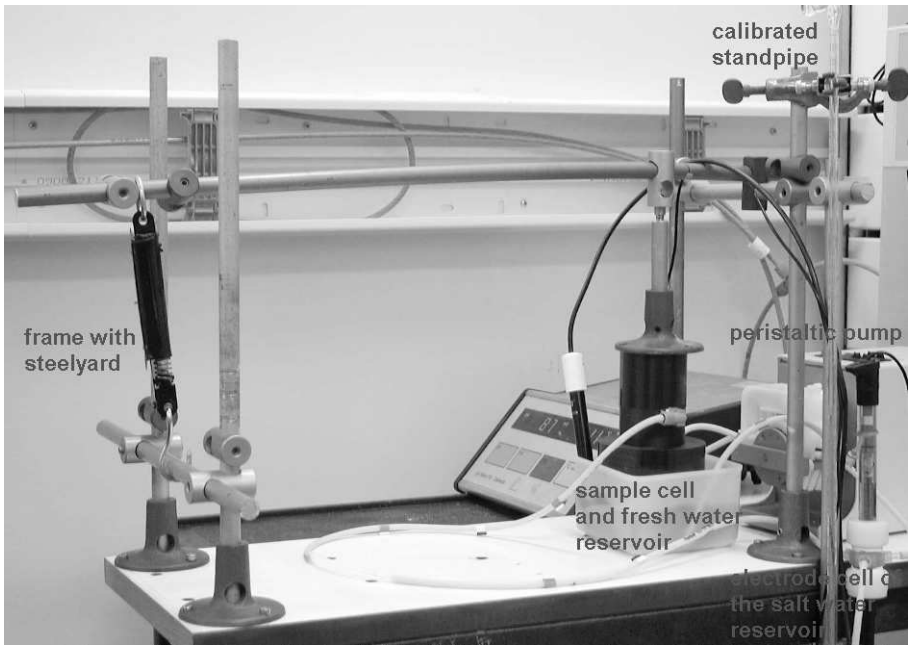

Figure 6.2: Photograph of the experimental setup

To gain insight in the effect of the potential build-up on the water flow across the clay sample, it should be possible to eliminate this potential by short-circuiting the electrodes. However, physical shortening is not viable because conducting current through the reference electrodes produces unpredictable additional potentials. Therefore, an instrument was designed, here referred to as 'virtual shortcut', which

designation	homo-ionic	concentration difference (NaCl)	type of clay	shorted?
be_1nsc	no	0.1-0.01 M	bentonite	no
be_1sc	no	0.1-0.01 M	bentonite	yes
be_{05}nsc	no	0.05-0.01 M	bentonite	no
be_{05}sc	no	0.05-0.01 M	bentonite	yes
2be_1nsc	yes	0.1-0.01 M	bentonite	no
2be_1sc	yes	0.1-0.01 M	bentonite	yes

Table 6.1: Designation of experiments

brings the potential across the sample to zero with a negative feedback current. The virtual shortcut measures the potential with the Ag|AgCl electrodes and applies a corresponding current by a feedback amplifier on noble metal electrodes, which are also inserted in the two fluid reservoirs.

6.5.2 Experimental results

In all experiments, the following occurred: the applied concentration difference induced a membrane potential that built up more or less instantaneously, and then declined, mainly because of diffusion of salt into the clay. The membrane potential, as calculated in the next section, refers to the initial potential difference. Also, because of the salt concentration difference, chemical osmosis induced a water flow through the clay from low to high salt concentration, inducing a relatively slow (due to storativity) buildup of pressure. As before, the pressure declines after reaching a maximum, also because of diffusion of solute through the clay. Two experiments were performed for each case, with different but similar clays. We assume these clays to be identical. Every experiment was performed with and without shortcut. Without shortcut, which is actually the default situation for clays, an electrical potential is present throughout the clay: a sum of membrane and streaming potential. This potential induces electro-osmotic flow, as well as electrophoresis. Or, in particular: a concentration gradient shifts the excess of cations, thereby creating a potential that induces electro-osmotic flow which counteracts flow of water due to chemical osmosis.

6.6 Measuring potentials

Membrane potentials cannot be measured directly [52]. Usually, the total Electromotive Force (EMF) of a system is measured, as displayed in Figure 6.3. The EMF is evaluated as the sum of the electrode potentials, the Donnan potentials and the

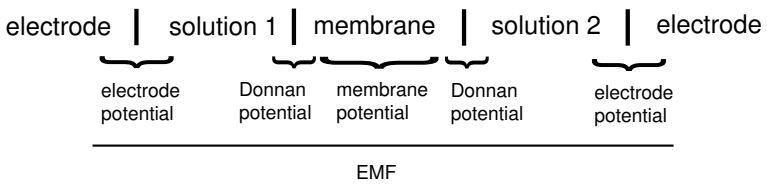

Figure 6.3: Overview of electrical potentials

membrane potential. The electrode potential is the electric potential difference between the electrode and the solution. The electrode potential E_{el} is defined as

$$E_{el} = E_0 + \frac{RT}{F} \ln a_i, \tag{6.29}$$

where E_0 is the standard electrode potential and a_i is the activity of ion i in the solution, to which the electrode is reversible. When calculating the EMF of the system, the two E_0's cancel out. The potential between two phases in contact is called the phase-boundary potential. When a solution is brought in contact with a membrane this is called the Donnan potential. In a negatively charged membrane, the concentration of cations is larger than the concentration of anions, and the concentration of cations is larger in the membrane than in the solution. The cations want to diffuse out of the membrane, but this is prevented by the Donnan potential to attain electro-neutrality. The Donnan potential is defined by

$$E_{\text{Don}} = -\frac{RT}{F} \ln \frac{\bar{a}_i}{a_i}, \tag{6.30}$$

where $\bar{a}_i$ is the activity of ion i in the membrane. As the membrane potential is related to the activities of the ions in the membranes, the formula for the Donnan potential 'translates' the values for the activities in the membranes to the values of the activities in the solutions. As in [52], we get, for a 1:1 electrolyte and a cation-exchanger

$$\begin{aligned} E_{mem} &= E_{\text{diff}} + E^1_{\text{Don}} - E^2_{\text{Don}} \\ &= -\frac{RT}{F}\left[\ln \frac{\bar{a}_{2+}}{\bar{a}_{1+}} + 2\int \bar{t}_- d\ln \bar{a}_f + \ln \frac{\bar{a}_{1+}}{a_{1+}} - \ln \frac{\bar{a}_{2+}}{a_{2+}}\right] \\ &= -\frac{RT}{F}\left[\ln \frac{a_2}{a_1} + 2\int \bar{t}_- d\ln a_f\right] \\ &= \frac{RT}{F}\left[\ln \frac{a_2}{a_1} - 2\int \bar{t}_+ d\ln a_f\right]. \end{aligned} \tag{6.31}$$

Sub- and- superscripts $1, 2$ refer to different sides of the sample and a_f is salt activity in the free solution. In the last lines the definition $\bar{t}_+ = 1 - \bar{t}_-$ was used and it was assumed that the activity of the salt is equal to the activity of the ions. Introducing the notation of [98] for the macroscopic transference number, i.e. T_+ instead of $\bar{t}_+$, where L is the membrane thickness:

$$E_{mem} = -\frac{RT}{F}\int (2T_+ - 1) d\ln a_f. \tag{6.32}$$

When we assume $T_+(L) = T_{2+}$ and $T_+(0) = T_{1+}$ to be constant, we find

$$\begin{aligned} E_{mem} &= -\frac{RT}{F}\left\{(2T_{2+} - 1)\ln a_2 - (2T_{1+} - 1)\ln a_1\right\} &(6.33)\\ &= -\frac{RT}{F}\ln\frac{a_1}{a_2} + \frac{2RT}{F}\left(T_{1+}\ln a_1 - T_{2+}\ln a_2\right). &(6.34)\end{aligned}$$

The total EMF now consists of the electrode potential and the membrane potentials; as in [98], we write:

$$\begin{aligned} E_{tot} &= E_{el1} + E_{mem} + E_{el2} = E_{mem} - \frac{RT}{F}\ln\frac{a_2}{a_1} &(6.35)\\ &= \frac{2RT}{F}\left(T_{1+}\ln a_1 - T_{2+}\ln a_2\right). &(6.36)\end{aligned}$$

Now, in [98], an expression is derived for T_+:

$$\frac{1}{T_+} = 1 + \frac{1 - t_+}{F_0\xi + \frac{1}{2}(t_+ - \xi)\left(1 - \frac{\xi}{t_+} + \sqrt{\left[1 - \frac{\xi}{t+}\right]^2 + \frac{4F_0\xi}{t_+}}\right)}. \tag{6.37}$$

The microscopic Hittorf number for Na^+ is $t_+ = 0.38$. The parameter ξ is defined as the ratio of surface conductivity and fluid conductivity:

$$\xi = \frac{\sigma_\chi}{\sigma_f}. \tag{6.38}$$

As seen in Chapter 2, the surface conductivity in [98] is defined as

$$\sigma_\chi = \frac{2}{3}\frac{n}{1-n}\beta_s Q_v, \tag{6.39}$$

where Q_v is the excess of charge, $n[-]$ is porosity and β_s is a surface ionic conductivity. This definition however, is based on the assumption of low porosity, whereas we deal with high porosity. The approximation for high porosity [103] is

$$\sigma_\chi = \frac{3\beta_s Q_v}{2(3-n)}. \tag{6.40}$$

The excess of charge is calculated using

$$Q_v = \rho_s \frac{1-n}{n} F \cdot \mathcal{C}, \tag{6.41}$$

where ρ_s is the rock density and $\mathcal{C}$ is the cation exchange capacity, expressed in terms of $\mathrm{mol}_c/\mathrm{kg} \sim \mathrm{meq/g}$.

6.7 Membrane potential value

As an example, we review the results of experiment $\mathbf{be_1sc}$ (see Table 6.1) in detail. Here, the overburden pressure applied was 1 bar and the applied concentration difference was roughly $0.1 - 0.01$ M. In the experiment the initial concentrations were measured: $c_1 = 12.2$ mol·m^{-3}, $c_2 = 105$ mol·m^{-3} which implies $a_1 = 11.6$ mol·m^{-3}, $a_2 = 94.1$ mol·m^{-3} by Debye-Hückel theory. The total potential is now

$$E_{tot} = \frac{2RT}{F}\left(T_{1+}\ln 11.6 - T_{2+}\ln 94.1\right). \tag{6.42}$$

The corresponding theoretical liquid-junction potential E_{lp} in the absence of a membrane would be:

$$E_{lp} = \frac{2RTt_+}{F}\left(\ln 11.6 - \ln 94.1\right) = -41\mathrm{mV}. \tag{6.43}$$

The excess of charge, calculated from (6.41), is $Q_v = 3.4 \cdot 10^7$ C/m^3. The mobility of the counterions in the diffuse double layer is, according to [98], equal to $\beta_s = 0.51 \cdot 10^{-8}$ m^2/Vs. This literature value is based on experiments on montmorillonite. With these values of the parameters, the surface conductivity becomes $\sigma_\chi = 0.118$ S/m.

Another parameter considered is the formation factor F_0. It is customary to relate this parameter to the porosity via Archie's law [1]:

parameter	exp 1: 0.1-0.01 M	exp 2: 0.05-0.01 M
low concentration [mol/m^3]	12.2	13.77
high concentration [mol/m^3]	105	55
low activity [mol/m^3]	11.6	13.1
high activity [mol/m^3]	94.1	50.4
cation exchange capacity $\mathcal{C}$ [cmol$_c$/kg]	53	53
porosity n [-]	0.80	0.80
temperature T [K]	298	298
rock density ρ_s [kg/m^3]	2650 [63]	2650
excess of charge Q_v [C·m^3]	$3.4 \cdot 10^7$	$3.4 \cdot 10^7$
surface conductivity [S/m]	0.118	0.118
membrane potential: measured [mV]	-32	-23
membrane potential: calculated [mV]	-34	-23

Table 6.2: Some *a priori*, measured and calculated parameters

$$F_0 = n^{-m}, \tag{6.44}$$

where m is the so-called cementation exponent, usually assumed to be 2. If we assume constant porosity and formation factor, we get $F_0 = 1.56$.

Using all these values and definitions, the macroscopic Hittorf numbers depend only on the concentrations in the reservoirs. Using formula (6.37), we find: $T_{1+} = 0.54$, $T_{2+} = 0.44$, and consequently:

$$E_{tot} = -34mV \tag{6.45}$$

As the experimental result is $E_{tot} = -32 \pm 3$ mV, we have quite a satisfactory agreement between the experimental results and our theoretical value.

Now, the actual membrane potential is

$$E_{mem} = E_{tot} - \frac{RT}{F} \ln \frac{a_1}{a_2} = -32mV + 55mV = +23\text{mV} \tag{6.46}$$

Hence, the actual membrane potential is positive, i.e. of the same sign as the concentration gradient. This is in accordance with flow data of non-shortcircuited tests and short-circuited tests, that strongly indicate a counterflow of water hindering chemical osmotic transport.

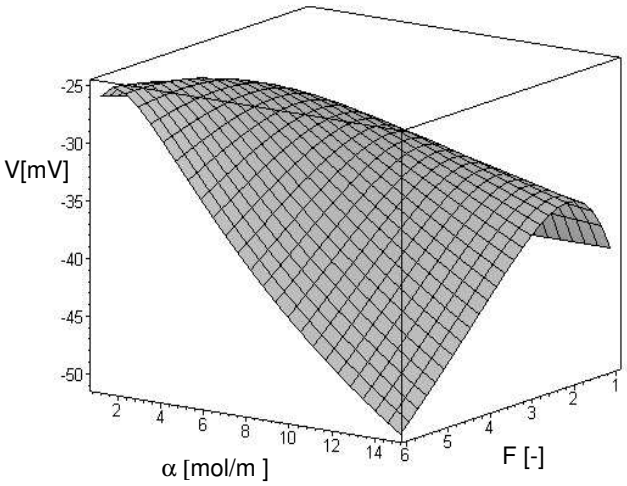

Figure 6.4: Membrane potential values for varying α and F_0

This result is, however, not in accordance with the interpretation as given in [98]. Here, a theoretical range is given for the membrane potential, which amounts for the current experiment to $E_{tot} \in [-110, -41]$, where $E_{tot} = -41$mV corresponds to the case of 'pure' liquid junction potential and $E_{tot} = -110$mV to a 'strong' influence of the membrane on the potential. However, in Figure 6.4, it is shown how the membrane potential, using the values of the activities from the experiment considered in this study, depends on the formation factor and on the parameter $\alpha = \xi \cdot a_f$.

This figure shows that, in the range of α and F_0 that we consider, the membrane potential stays clearly above the -41 mV value. Only for rather large values of F_0 and α, the membrane potential is smaller than -41 mV, as predicted in [98]. Apparently, the interpretation of membrane potential in this respect has to be adapted. Most likely, the large difference in transference numbers for the fresh and salt sides causes this 'anomaly' in the membrane potential. Or, the influence of cation exchange may be different than as proposed in [98].

6.8 Modelling procedure

6.8.1 Equations

The simultaneous evolution of pressure, membrane potential and concentration was modelled using equations from Chapter 3. The model equations, assuming incompressible fluid, no chemical reactions, no temperature effects, and low Peclet number, are (see [3]:

fluid mass balance

$$\frac{\partial n}{\partial t} + \nabla \cdot \mathbf{q} = 0. \tag{6.47}$$

salt mass balance

$$\frac{\partial n c_f}{\partial t} + \nabla \cdot (c_f \mathbf{q}) + \nabla \cdot \mathbf{J}_s^d = 0. \tag{6.48}$$

flux equations

$$\mathbf{q}_{nsc} = -\left[\frac{k}{\mu} - \frac{k_e^2}{\sigma_e}\right] \nabla p + \left[\lambda + k_e RT(T_+ - T_-)\frac{1}{c_f}\right] \nabla c_f \tag{6.49}$$

$$\mathbf{q}_{sc} = -\frac{k}{\mu}\nabla p + \lambda \nabla c_f \tag{6.50}$$

$$(\mathbf{J}_s^d)_{nsc} = -\frac{D_f}{F_0}\gamma \nabla c_f \tag{6.51}$$

$$(\mathbf{J}_-^d)_{sc} = -\frac{\mathcal{D}_-}{F_0}\nabla c_- \tag{6.52}$$

constitutive equation

$$n = 1 - (1 - n_0)e^{-S_s p}, \tag{6.53}$$

where n_0 is a reference porosity, and $S_s[1/\text{Pa}]$ is the compressibility of the porous medium.

6.8.2 Model domain

In Figure 6.5 the general modelling domain for all membrane potential experiments is presented. The parameters not specified are given in the tables corresponding to the respective experiments.

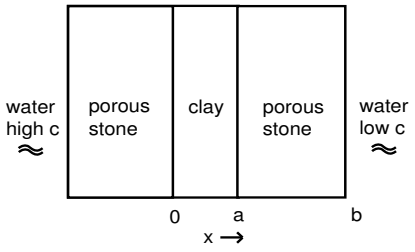

parameter	value in clay	value in porous stone
$n(-)$	0.5	n
$k(\mathrm{m}^2)$	$2.34 \cdot 10^{-18}$	$1 \cdot 10^{-13}$
$D(\mathrm{m}^2/\mathrm{s})$	D	$1.5 \cdot 10^{-9}$
$\alpha(1/\mathrm{Pa})$	$1 \cdot 10^{-9}$	$4.6 \cdot 10^{-10}$
$\sigma(-)$	σ	0
length (mm)	$a = 2.9$	$b - a = 7.2$

Figure 6.5: *Modelling domain membrane potential experiment and relevant parameters*

6.8.3 Initial and boundary conditions

Initially, the pressure and electrical potential are zero in the whole domain, and the concentration is c_0 (high value) in the porous stone at the left-handside and c_a (low value) in the clay and the porous stone at the right-handside.

The following boundary conditions apply:

$$\frac{\partial p}{\partial x} = 0, \frac{\partial c}{\partial x} = 0, \quad \text{at } x = -L \tag{6.54}$$

$$p = 0, \frac{\partial c}{\partial x} = 0, \quad \text{at } x = b \tag{6.55}$$

We imposed $p \equiv 0$ in the left-handside reservoir, because the pressure in this reservoir is atmospheric. The solutions in the reservoir are well stirred, such that the measured concentrations should correspond to the concentrations at the interface between the reservoirs and the porous stones.

6.9 Modelling results for bentonite: high $\triangle c$

6.9.1 Pressure development

In this section we present the experimental and modelling results of the experiment performed on the clay sample subjected to a concentration gradient of about 90 $\mathrm{mol}/\mathrm{m}^3$. For numerical modelling, we used the scripted finite element builder and numerical solver FlexPDE [26]. In Figure 6.6 the pressure buildup in the salt water reservoir is depicted. Obviously, in the short-circuited case, water flow is not hindered by electro-osmosis, and pressure reaches a higher point than in the non-shorted case. The graph breaks down at some point, for the shorted as well as the non-shorted case. This is probably due to temporary cracks in the clay, through which water can preferentially flow in the direction of the fresh water

reservoir. It is interesting to observe that in the non-shorted case, the pressure development continues after the degeneration in about the same way as before.

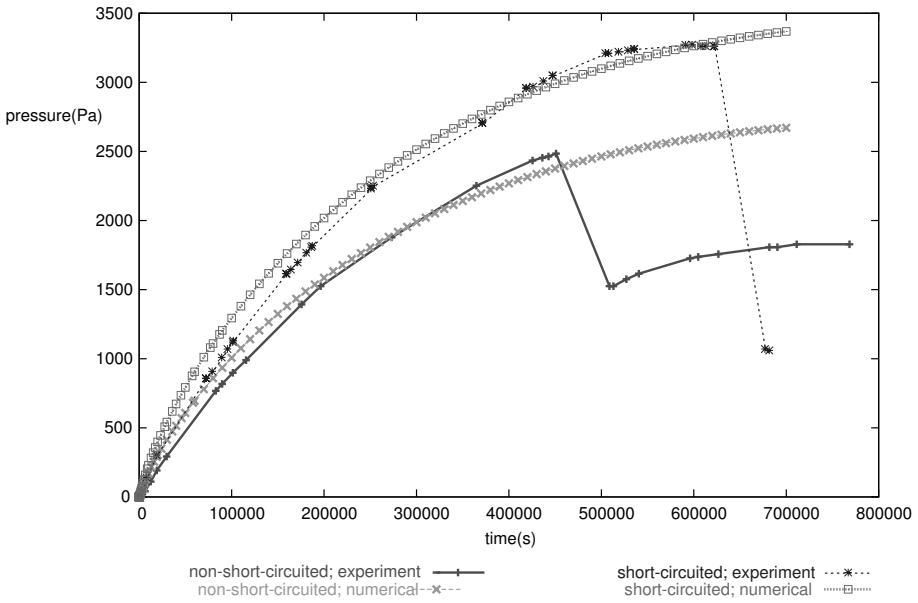

Figure 6.6: Pressure development for the shorted and non-shorted case; comparison of experimental and numerical results

6.9.2 Membrane potential development

In Figure 6.7 the dissipation of membrane potential is shown. The graph for the numerical and experimental results compare rather well, especially when the numerical graph is shifted to correspond with the initial membrane potential value, as is represented by the middle line.

The dissipation of membrane potential occurs somewhat faster in the experiment than in the simulation. This can be explained by a streaming potential development, that becomes significant for higher pressures. However, the streaming potential can be approximated by:

$$V_{sp} \approx -\frac{k_e}{\sigma_e} p \approx 7\mu V, \tag{6.56}$$

which is obviously much too small to contribute to the total potential. Other effects should therefore contribute to the dissipation of the potential.

6.9.3 Concentration development

In Figure 6.8 the development of the concentration in the salt water reservoir is shown for the non-shorted setup. Here, we corrected for the volume increase due to the inflow of water. Obviously, after $t = 180000$ s, something has happened during the experiment that 'degenerates' the diffusion. Using the shorted diffusion coefficient, we find for the shorted case the concentration evolution as depicted in Figure 6.9. In both cases, the agreement between numerical and experimental results is excellent, aside from the degeneration and the scattering of the concentration data in the shorted experiment.

6.9.4 Coefficients

During the experiments, the **permeability** was not measured directly, but was assumed to be equal to the permeability found in conductivity tests on similar samples of the same clay, under equal overburden pressures. Therefore, its value is assumed to be $k = 2.3{\cdot}10^{-18}$ m^2. From the results of the short-circuited experiment we can derive the value of the **reflection coefficient**. This can be calculated using van't Hoff's law, resulting in $\sigma = 0.024 \pm 0.005$. Van 't Hoff's law applies at the equilibrium flow conditions, and henceforth the concentration difference used in the expression for van 't Hoff's law was evaluated at the time of flow equilibrium. Obviously, it is smaller than the initial salt concentration difference. It is difficult to assess precisely the moment of flow equilibrium, resulting in the relatively large error.

The value of the **electro-osmotic permeability** is inferred from the difference between the water flux in the shorted and the non-shorted experiment. The difference corresponds to the counterflow of water induced by electro-osmosis, and equals the electro-osmotic permeability multiplied by the membrane potential gradient. This calculation, using the results of this experiment, yields a value of $k_e = 1.2{\cdot}10^{-9}$ m^2/Vs, which is on the low side of the spectrum of values $k_e \in (0.5, 5){\cdot}10^{-9}$ m^2/Vs, as reported by Bolt [9] for instance. As this value is directly correlated to the value of the reflection coefficient, which is apparently quite small as well, this is not a surprising result. Throughout this chapter, we assume the following:

$$\frac{k}{\mu} \gg \frac{k_e^2}{\sigma_e} \tag{6.57}$$

To check whether this is justified, we substitute the values of the parameters for this experiment: $\sigma_e = 0.12$ S/m, $k/\mu = 2.3 \cdot 10^{-15}$ m^2/s and $k_e = 1.2 \cdot 10^{-9}$ m^2/Vs. This leads to:

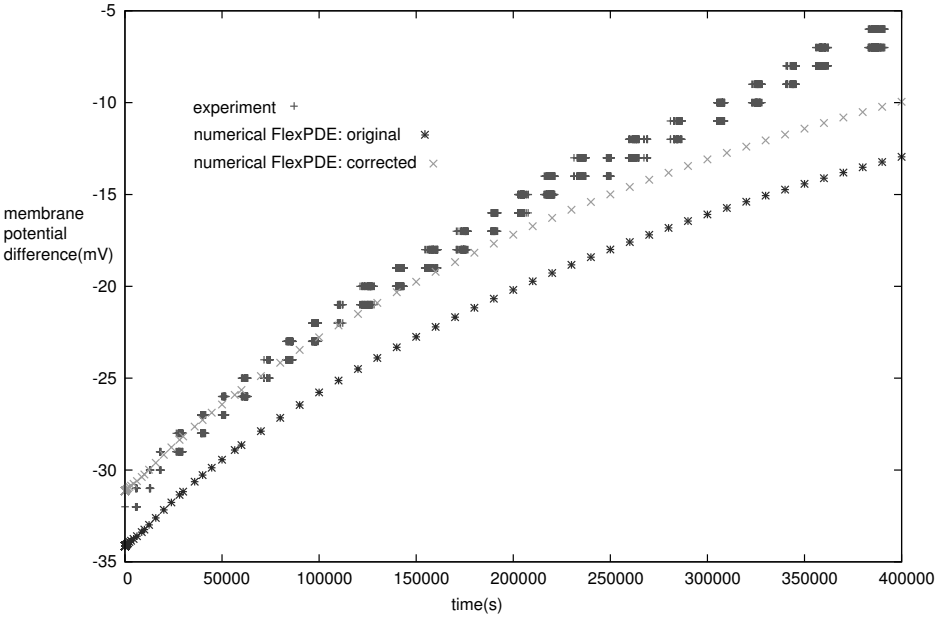

Figure 6.7: Membrane potential development for the non-shorted case; comparison of experimental and numerical results

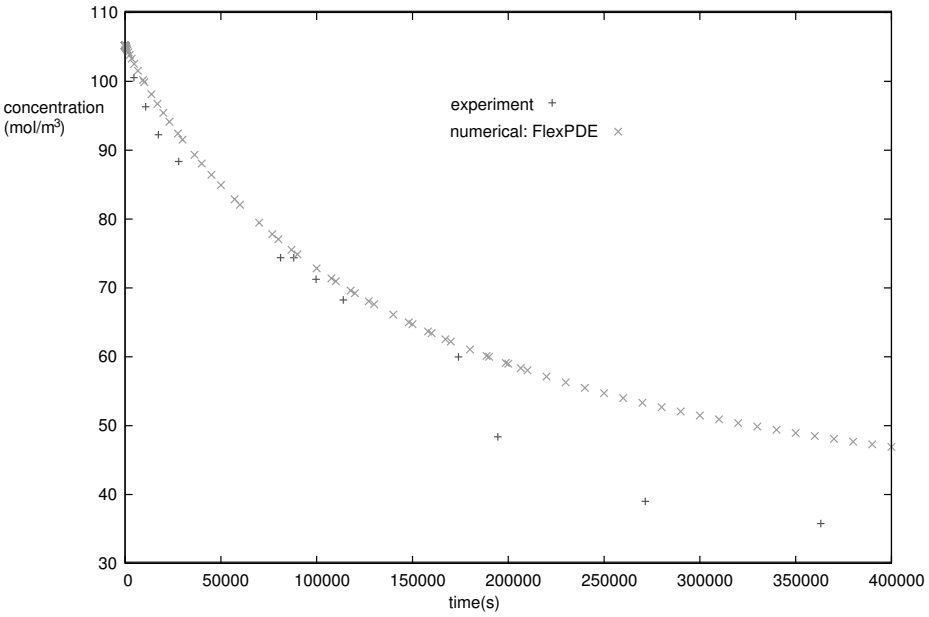

Figure 6.8: Concentration development for the non-shorted case; comparison of experimental and numerical results

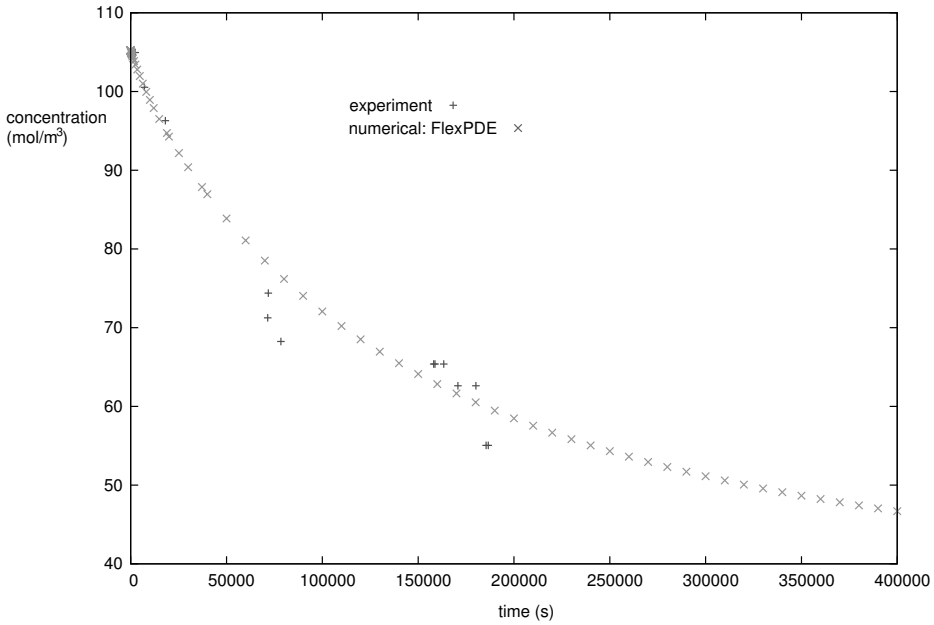

Figure 6.9: Concentration development for the shorted case; comparison of experimental and numerical results

$$\frac{k}{\mu} \approx 190 \cdot \frac{k_e^2}{\sigma_e}, \tag{6.58}$$

which seems an appropriate justification for the approximation. The **diffusion coefficient** for the non-shorted case is deduced from flow measurements and equals $D_{nsc} = 2.7 \cdot 10^{-10}$ m^2/s. The diffusion coefficient, from (6.25), has to be corrected for cation exchange, which may be represented by a retardation term $\mathcal{R}$ [76], as seen before in Chapter 2:

$$D = \frac{D_f \gamma}{\mathcal{R} F_0}. \tag{6.59}$$

This retardation parameter is inferred from the experimentally derived diffusion coefficient. It is subsequently used for the shorted case. Hence, the diffusion coefficient for the shorted experiment is about equal, viz.:

$$D = \frac{\mathcal{D}_-}{\mathcal{R} F_0} = 2.6 \cdot 10^{-10} \mathrm{m}^2/\mathrm{s}. \tag{6.60}$$

Finally, the **storativity** was chosen to fit pressure evolution. This value was subsequently used in all simulations, as it reflects a property of the clay which is not likely to be dependent on the salt concentration or cation occupation.

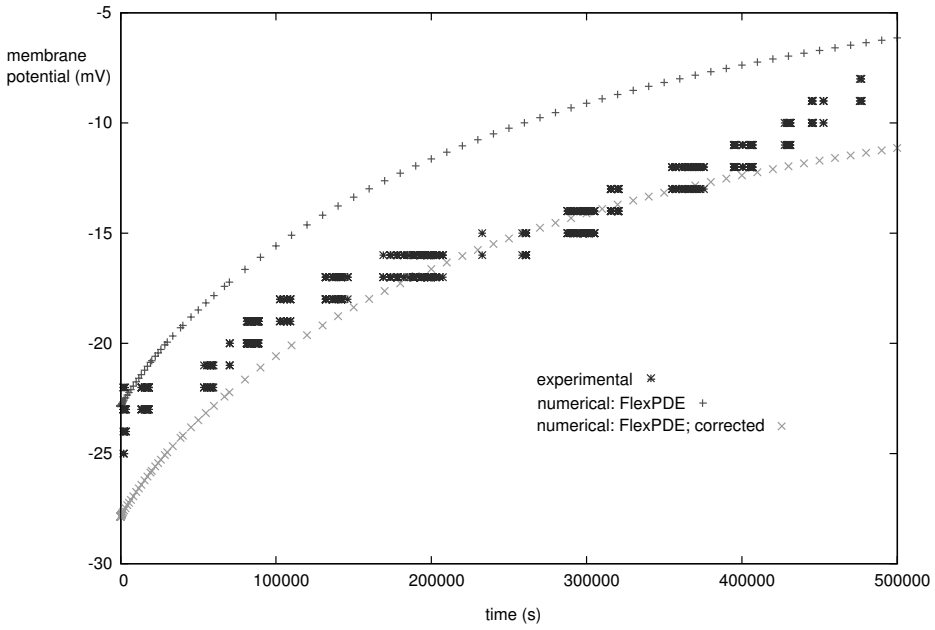

Figure 6.10: Membrane potential development for the non-shorted case of experiment be_{05}(n)sc; comparison of experimental and numerical results

6.10 Modelling results for bentonite: low Δc

A similar experiment was performed with a smaller concentration gradient, to assess the consistency of the results. Most coefficients were equal to the ones in the previous experiment, except for the diffusion coefficient, which, based on solute flux data, was seen to be slightly larger, i.e. $D = 4 \cdot 10^{-10}$ m^2/s. The reflection coefficient, which is expected to be larger for lower concentrations, equals $\sigma = 0.03 \pm 0.005$ in this setup. Actually, if we would calculate the reflection coefficient based on the values of the diffuse double layer thickness inferred from the σ in the high Δc-experiment, we would get a higher value, if we assume the concentration difference to be constant in the clay and equal to the mean of the concentrations in the reservoirs. However, as salt diffuses into the clay, the reflection coefficient becomes quite position dependent, and prediction of σ becomes very difficult.

The membrane potential was calculated using the same theory as in Section 6.7. The concentrations, as measured in the non-shorted experiment, are $0.055M$ and $0.014M$ for the salt and the fresh reservoir, which translates to activities of $0.051M$ and $0.013M$ respectively, yielding

$$E_{tot} = \frac{2RT}{F}\left(T_{1+}\ln 13.1 - T_{2+}\ln 51.4\right). \tag{6.61}$$

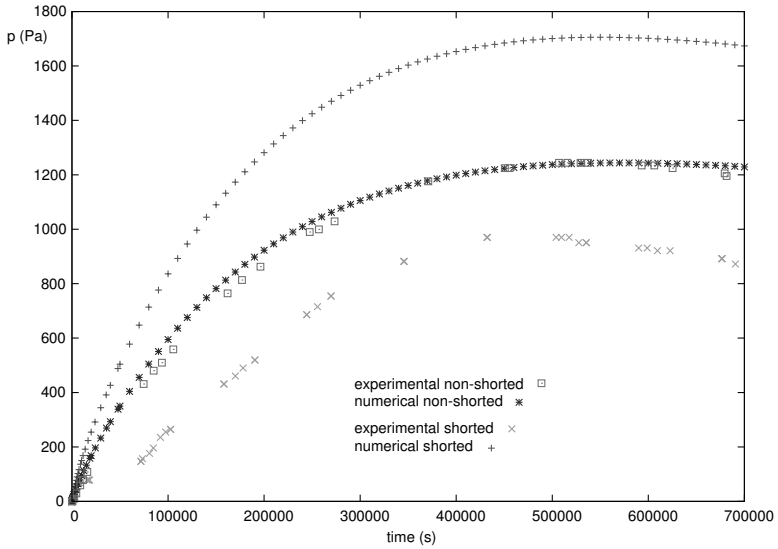

Figure 6.11: Pressure development for the non-shorted and the shorted case of experiment be_{05}(n)sc; comparison of experimental and numerical results

The corresponding Hittorf transport numbers are $T_{1+} = 0.52$ and $T_{2+} = 0.45$, and therefore the calculated, total membrane potential turns out to be -23 mV. This is in excellent agreement with the experimental result $E_{tot} = -23 \pm 3$ mV. The development of the membrane potential is displayed in Figure 6.10. The numerical result was shifted to a lower initial membrane potential value to obtain a better comparison of the evolution. It is remarkable to observe that, in the experiment, the development is apparently more linear than in the simulations.

The pressure development was simulated and the results are displayed in Figure 6.11. Unfortunately, the shorted experiment suffered a fate comparable to what had happened in the previous experiment, but now in the initial stage: the pressure drops unexpectedly, or evolution of pressure is somehow slowed down. However, from the results of the simulations, we may observe what most likely would have happened without this mishap.

Finally, in Figure 6.12 the evolution of concentration in the fresh water reservoir is shown.

6.11 Results with homo-ionic clay

In a second type of experiment, the results of **be_1(n)sc** (see Table 6.1) where shown to be reproducible. The experiment was performed with a homo-ionic clay to assess the influence of cation occupation on the clay platelets. In Table 6.3,

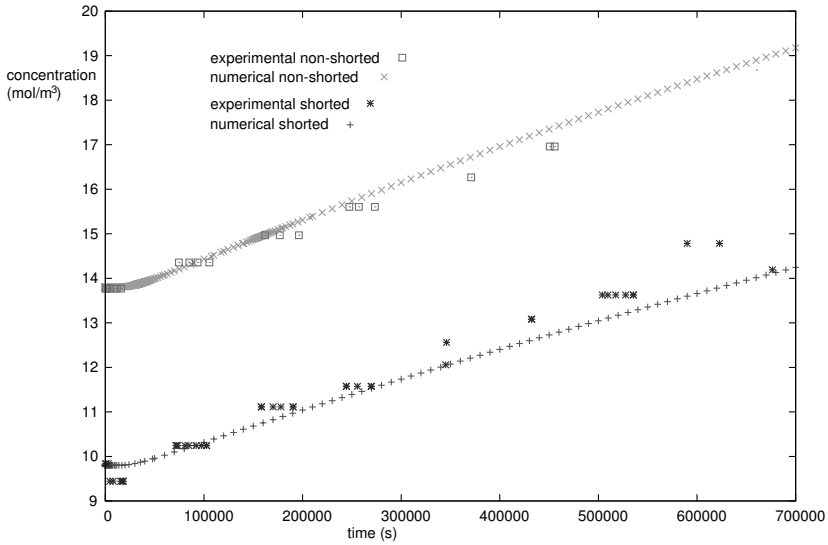

Figure 6.12: Concentration development in the fresh water reservoir for the shorted and non-shorted cases of the experiment be_{05}(n)sc; comparison of experimental and numerical results

the differences in coefficients between the two experiments are shown. The only differences are the initial concentrations, the cation occupation and hence the surface conductivity.

From the table we see that the homo-ionicity of the clay does not influence the values of membrane potential and reflection coefficient much: the initial concentration in the salt water reservoir is somewhat higher in the homo-ionic experiment compared to the hetero-ionic experiment. This should imply a somewhat smaller reflection coefficient, such as is observed in Table 6.3.

The initial membrane potential difference is nearly equal, and differences could be the result of different cation occupation. However, all values lie within the margin of error. From Figure 6.13 we observe that the evolution of pressure is rather similar compared to the experiment with the hetero-ionic clay, although the non-shorted pressure 'degenerates' in the homo-ionic experiment.

An interesting deviation from the first experiment can be seen in Figure 6.14: the (unknown) effect responsible for the divergence of numerical and experimental results in Figure 6.7, is seen to be even stronger here. Again, we could attribute this to streaming potential, although this effect is probably too small.

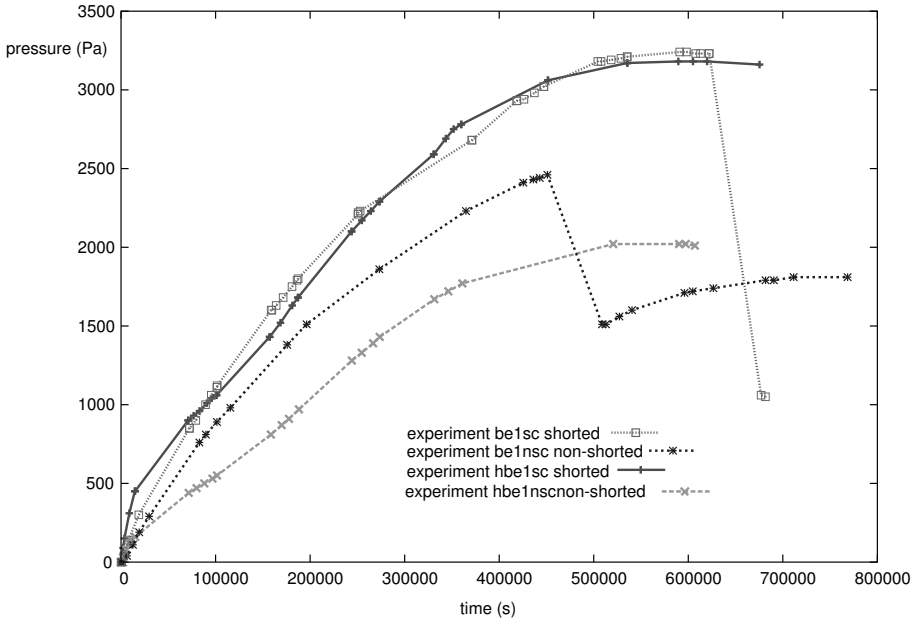

Figure 6.13: Comparison of pressure evolution for experiment $\mathbf{be_1(n)sc}$ and experiment $\mathbf{2be_1(n)sc}$

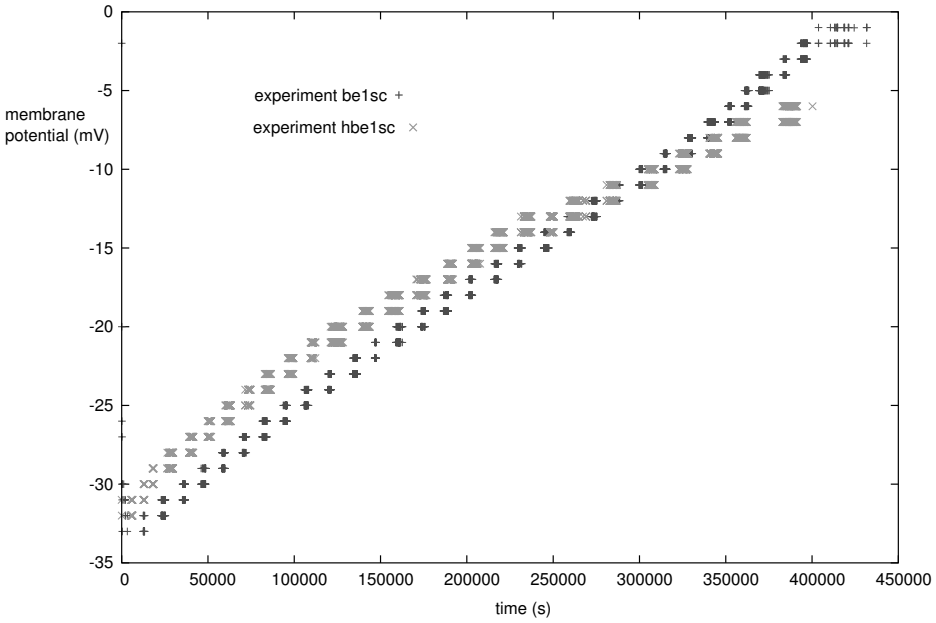

Figure 6.14: Comparison of membrane potential evolution for $\mathbf{be_1(n)sc}$ and experiment $\mathbf{2be_1(n)sc}$

parameter	exp. **2be$_1$(n)sc**	exp. **be$_1$(n)sc**
low concentration [mol/m^3]	12.9	12.2
high concentration [mol/m^3]	90.4	105
low activity [mol/m^3]	12.6	11.6
high activity [mol/m^3]	81.4	94.1
cation exchange capacity $\mathcal{C}$ meq/g	53	53
porosity n [-]	0.80	0.80
rock density ρ_s [kg/m^3]	2650	2650
excess of charge Q_v [C·m^3]	$5.1 \cdot 10^7$	$3.4 \cdot 10^7$
surface conductivity σ_χ [S/m]	0.178	0.118
membrane potential: measured [mV]	-33	-32
membrane potential: calculated [mV]	-32	-34
reflection coefficient [-]	0.025	0.024

Table 6.3: Comparison between parameters of the experiment with hetero-ionic clay and the one with homo-ionic clay

6.12 Conclusions

We have adapted the model of Revil [98] and validated it with results from laboratory experiments on bentonite clay. The model was shown to be quite suitable to predict membrane potential values. Also, it is shown how the model equations are perfectly able to simulate the transient development of pressure, concentration and membrane potential for shorted as well as for non-shorted conditions. As expected, when turning off the electrical terms in the equations, the numerical results agree with the experimental findings for the shorted experiment.

The model was shown to be applicable for homo-as well as hetero-ionic clays. However, there doesn't seem to be much difference between the results of the experiments on the two types of clay. As the cation occupation is the significant difference between the homo-ionic and hetero-ionic clay, this is apparently not of great influence on processes such as membrane potential development and chemical osmosis.

Some questions, however, remain unanswered: how can we come to an interpretation of the result for membrane potential that can agree with the interpretation of Revil? How can we explain the divergence of the development of membrane potential difference for numerical and experimental results, other than by streaming potential? And finally, does the cation occupation on the clay perhaps influence this development, and if so, in what way?

Chapter 7

Modelling osmosis with METROPOL

7.1 Introduction

Disposal of nuclear and other highly toxic wastes has become an increasingly important subject in hydrological modelling. Possible ways of storage are in subsurface salt formations, or in regions that are screened by clay liners. It is known that flow of groundwater is the main mechanism for transport of radionuclides from these regions into the environment [100]. The transport of radionuclides is subject to a number of processes. For example, in the vicinity of salt domes, high salt concentration gradients may occur, in general large heterogeneities and liquid density gradients may be present, and in clay layers, osmotic effects may play a significant role. High salt concentrations also alter fluid viscosity, diffusion, chemical osmosis. All these coupled processes give rise to three-dimensional flow fields, that have to be determined to accurately describe the flow of groundwater and transport of dissolved species. To accomplish this, in the eighties, a finite element code was developed by RIVM (the Rijksinstituut voor Volksgezondheid en Milieu), containing most transport processes mentioned above. Later on, this model code, called METROPOL, which is an acronym for **ME**thod for **TR**ansport **O**f **POL**lutants, was extended with various features, most notably with the factors accounting for the influence of temperature gradients on water flow and solute transport.

In this study, the code is extended with chemical and electro-osmosis. The original METROPOL code contained terms accounting for salt-gradient-driven water transport and hydraulically-induced solute transport. However, the osmosis term was represented by a bulk parameter and electrical effects were not included. In this chapter, a brief introduction to the code will be given. In Section 7.2, some

essential parts of the METROPOL code are presented. In Section 7.3 some numerical details of the code are explained. Section 7.4 includes the full set of equations applicable for osmotically induced groundwater flow. The next section deals with a simple one-dimensional application and a comparison with a laboratory experiment. Finally, in the last section the results of a three-dimensional numerical experiment are presented.

7.2 The program

7.2.1 Routines

METROPOL consists of a series of different subroutines, for tasks such as mesh generation, algebraic equation solving and postprocessing. The METROPOL manual [100] lists them all, but here we present the routines that were used, and in some cases modified, in this study:

- **METROMESH** a three-dimensional mesh generator
- **METROREF** a program for automatic mesh refinement
- **METROPOL-3** the default program that solves the equations for transient groundwater flow and transport of dissolved salt
- **METROHEAT** idem, but effects of temperature variations in the soil are included
- **METROSMO** idem, but extended with chemically and electrically coupled transport
- **METROPLOT** a program that plots the results of the calculation as contours, velocity vectors and/or particle trajectories in two-dimensional cuts
- **METROREAD** a program that delivers output files for inspection and that plots time profile graphs; the formatted output files can be used as input for professional plotting programs such as Tecplot and Gnuplot

7.2.2 Numerical method: description

The numerical method to solve the differential equations describing groundwater flow and solute transport which is used in METROPOL is the Finite Element Method. Compared to Finite Difference Methods, the main advantages are that it allows for irregular, non-rectangular boundaries, and moreover, that the solutions

are in general more accurate than those of finite difference methods. This study follows the approach of [60] in setting up a finite element problem. The first step in this procedure involves defining an appropriate mesh, i.e. distributing the nodes and selecting the size and shape of the elements. A number of evident rules [60] should be obeyed, such as conservation of topology of the domain and application of symmetry wherever possible. In addition, one should aim for elements that are as regularly shaped as possible to minimize computation time and numerical errors.

The second step is the derivation of an integral formulation for the governing groundwater flow and solute transport equations. Aside from the variational method, the method of weighted residuals is quite often used and is actually a more general approach. An approximate solution is substituted into the governing equations, and the weighted averages of all errors or residuals in each node over the domain is forced to equal zero. In some more detail, this procedure works as follows.

Consider a differential equation of the form

$$\mathcal{L}(\phi(x,y,z)) - F(x,y,z) = 0, \tag{7.1}$$

where $\mathcal{L}$ is a differential operator, ϕ is the field variable, such as pressure or concentration, and F is a known function. Define an approximate solution for ϕ, denoted by $\hat{\phi}$:

$$\hat{\phi}(x,y,z) = \sum_{i=1}^{m} N_i(x,y,z)\phi_i, \tag{7.2}$$

where ϕ_i are the variables at the nodes and N_i are so-called interpolation functions. Substitution of (7.2) in (7.1) yields:

$$\mathcal{L}(\hat{\phi}) - F = R, \tag{7.3}$$

where $R(x,y,z)$ is the vector containing the residuals of the solution. The weighted average of the residuals at the nodes is now forced to equal zero:

$$\int_{\Omega} W(x,y,z)R(x,y,z)d\Omega = 0, \tag{7.4}$$

where W is a weighing function, and Ω denotes the computational domain. Different choices are possible for choosing the weighing functions. In METROPOL,

Galerkin's method is used for the choice of the weighing function. In this method, the weighing function is chosen to be the same as the aforementioned interpolation function.

The next step involves the choice of interpolation functions. A suitable choice of interpolation functions improves the accuracy of the approximate solution. In METROPOL, tri-linear basis functions are chosen, i.e. functions that are 1 in nodal point i, zero in all other points and linear in x, y and z.

Choosing the interpolation function and weighing function yields a set of equations that can be written in matrix form.

Time derivatives are dealt with using standard algorithms. In METROPOL-3, mainly the Euler implicit or backward difference method is used. So, if F, C and K are indicated as the flow vector, capacitance matrix and conductivity matrix respectively, and h is the hydraulic head vector, the backward difference method implies

$$[C]\dot{h} + [K]h = F \rightarrow ([C] + \Delta t[K])h_{t+\Delta t} = [C]h_t + \Delta t F_{t+\Delta t}. \tag{7.5}$$

The matrix equations contain spatial integrations, for which in METROPOL-3 the method of Gauss quadrature is used, according to the following formula:

$$\iiint f(\mathbf{x})dx = \frac{1}{8}\sum_{k=1}^{8} J_k f_k, \tag{7.6}$$

where f is the function to be integrated, J_k is the Jacobian of the $k-$th Gauss point and f_k is the corresponding value of f in the Gauss point. Gauss points are located at the local $x, y, z-$coordinates $\frac{1}{2} \pm \frac{1}{6}\sqrt{3}$ which implies exact numerical integration for polynomials of degree three or less.

The final step is the solution of the equations. Picard iteration is employed to solve a set of non-linear equations: a sequence of solutions is constructed, in which each solution is calculated from the previous solution with a linear set of equations, until a certain convergence criterion is satisfied. For solving the linear equations, the Conjugate Gradient Method was used [54], specifically the code Bi-CGSTAB [117].

7.2.3 Numerical method: drawback

The major problem with respect to METROPOL for our purposes is related to the equation solving procedure: in the code, the inner iterations are the Picard iterations for separate variables within a time step, and outer iterations are the iterations that deal with the coupling between the salt mass fraction equations

and the pressure equations. Now, the inner iterations only apply to the salt mass fraction equations in METROPOL, whereas the 'inner' pressure equation is solved only once per outer iteration. This is because in METROPOL it is assumed that the pressure equations are 'nearly' linear. In our case, the role of the mass fraction gradient in the pressure equations is quite significant because of the chemical osmosis term. As we shall see, this has important consequences for the accuracy and convergence properties of the numerical solver.

7.3 The adapted METROPOL equations

The equations used in this adapted version of METROPOL are basically the same as presented in Chapter 3, but now extended with a number of features, such as a gravity term, source terms, non-linear flux parameters and most importantly, thermal energy terms. The original equations are taken from the METROPOL and METROHEAT manuals and are based on work presented in [73], [49]. The nomenclature, as presented in Tables 7.1 7.2 is slightly different from the general nomenclature defined in this thesis, because much of the terminology has been copied from the METROPOL manual.

The equations presented here contain all temperature related terms as given in the METROHEAT code. As we adapted this particular version of METROPOL, we do list these equations, without any comments, although much of the terms are based rather on analogy than on fact. This also means that the thermal energy terms have not been adapted for osmotic effects as they are never considered to be significant in this study.

In METROHEAT, the following **mass and energy balance equations** are presented for the total liquid phase, the dissolved salt and thermal energy respectively:

$$\begin{aligned}
\frac{\partial}{\partial t}(n\rho) + \nabla\cdot(\rho\mathbf{q}) &= \rho_i I_i - \rho I_e \\
\frac{\partial}{\partial t}(n\omega\rho) + \nabla\cdot(\rho\omega\mathbf{q}) + \nabla\cdot\mathbf{J} &= \rho_i\omega_i I_i - \rho\omega I_e \\
\frac{\partial}{\partial t}((\rho c)_{\text{eff}}T) + \nabla\cdot(\rho c_f T\mathbf{q}) + \nabla\cdot J_H + T\frac{\beta_T}{\beta}\nabla\cdot\mathbf{q} &= \rho_i c_f T_i I_i - \rho c_f T I_e.
\end{aligned}$$

Subsequently, modified Darcy's, Fick's and Fourier's law are used as the coupled flow equations for pressure, mass fraction and temperature. The equations adapted for chemical and electrical effects have been presented in this study in Chapter 3, the non-linear flux parameters f_i are derived from [49] and most of the temperature terms are constructed from analogy with the other equations.

Modified **Darcy's law**:

$$(1 + f_q|\mathbf{q}|)\,\mathbf{q} \;=\; -K_e\,(\nabla p - \rho\mathbf{g}) + \Lambda_e\rho\nabla\omega - T^f\cdot\nabla T \tag{7.7}$$

Modified **Fick's law**:

$$(1 + f_j|\mathbf{J}|)\,\mathbf{J} \;=\; -\Sigma_e\rho\omega\nabla p - \mathbf{D}\rho\nabla\omega - T^s\cdot\nabla T \tag{7.8}$$

Modified **Fourier's law**:

$$(1 + f_{J_H}|\mathbf{J}_H|)\,\mathbf{J}_H \;=\; -H\cdot\nabla T - L^T\cdot\nabla\omega - K^T\cdot\nabla p \tag{7.9}$$

The **liquid density** is assumed to depend on the pressure, mass fraction and temperature [111]:

$$\rho = \rho_0 e^{\beta(p-p_r)+\gamma\omega-\beta_T(T-T_r)}$$

The **liquid viscosity** μ and the **intrinsic permeability** depend on the salt mass fraction according to [73]

$$\mu \;=\; \mu_0 e^{\gamma_v\omega}.$$

$$k \;=\; k_r e^{\gamma_k\omega}$$

The **porosity** is assumed to depend on temperature and pressure [6]:

$$n = 1 - (1 - n_0)e^{-C_r(p-p_r)+C_{\mathrm{T,eff}}(T-T_r)}$$

The **dispersion tensor** is taken from Bear [5]:

$$\mathbf{D} = D_m\mathbf{I} + (\alpha_L - \alpha_T)\frac{\mathbf{q}\cdot\mathbf{q}}{|\mathbf{q}|} + \alpha_T|\mathbf{q}|\mathbf{I} \tag{7.10}$$

The **molecular diffusion coefficient** should be adapted for electrophoresis and semi-permeability, but as the former measure implies that we consider anion flux

	nomenclature 1	
roman	name	unit
b	double layer thickness	m
c_f	specific heat of fluid	J/kg ^{o}C
c_s	specific heat of rock	J/kg ^{o}C
C_{eff}	porous medium compressibility	ms^2/kg
C_{rock}	rock compressibility	ms^2/kg
$C_{\text{T,eff}}$	porous medium poro-elasticity	ms^2/kg
$C_{\text{T,rock}}$	rock poro-elasticity	ms^2/kg
$\mathbf{D}$	dispersion tensor	m^2/s
D_m	diffusion coefficient	m^2/s
D_0	reference diffusivity	m^2/s
$\mathbf{E}$	heat flux dispersion tensor	J/ms ^{o}C
f_q	non-linear flow factor	s/m
f_j	non-linear dispersion factor	m^2 s/kg
f_j	non-linear temperature factor	m^2 s/kg
F	Faraday constant	As/mol
$\mathbf{g}$	gravity vector	m/s^2
$\mathbf{H}$	heat flux tensor	J/ms ^{o}C
I_{ex}	extraction rate	–
I_{in}	injection rate	–
$\mathbf{J}$	dispersive mass flux	kg/(m^2 s)
$\mathbf{J}_H$	dispersive heat flux	kg/(m^2 s)
$\mathbf{k}$	intrinsic permeability	m^2
k_e	electro-osmotic permeability	m^2/Vs
K_e	electric/hydraulic conductivity tensor	m^2/Vs
K^T	heat transfer coefficient	Js/kg
$\mathbf{k}_r$	reference permeability	m^2
L_T	Dufour coefficient	J/ms
M_s	molar mass	kg/mol
n	porosity	–
n_0	reference porosity	–
p	pressure	kg/(ms^2)
p_0	reference pressure	kg/(ms^2)
$\mathbf{q}$	Darcy velocity	m/s
R	gas constant	Jmol/K
T	temperature	^{0}C
T_f	thermal osmosis coefficient	m^2/s ^{o}C
T_r	reference temperature	^{o}C
T_s	Soret coefficient	kg/(ms ^{o}C)
u	mobility	m^2/Vs

Table 7.1: Nomenclature METROPOL equations

	nomenclature 2	
greek	name	unit
α_L	longitudinal dispersivity in mass flux	m
α_T	transversal dispersivity in mass flux	m
$\alpha_{L,T}$	longitudinal dispersivity in heat flux	m
$\alpha_{T,T}$	transversal dispersivity in heat flux	m
β	liquid compressibility at constant T	$\mathrm{ms}^2/\mathrm{kg}$
β_T	liquid compressibility at constant p	$\mathrm{ms}^2/\mathrm{kg}$
β_{vis}	constant relating T and μ	$1/^o\mathrm{C}$
Δ_e	electric correction on the dispersion	S/m
γ	constant relating ρ and ω	–
γ_ν	constant relating μ and ω	–
γ_k	constant relating $\mathbf{k}$ and ω	–
Λ_e	electrochemical osmosis term	J/ms ^{o}C
λ_f	fluid thermal conductivity	J/ms ^{o}C
λ_s	rock thermal conductivity	J/ms ^{o}C
μ	liquid viscosity	kg/(ms)
ν	dissociation constant	–
ρ	liquid density	$\mathrm{kg/m}^3$
ρ_0	reference liquid density	$\mathrm{kg/m}^3$
$(\rho c)_{\mathrm{eff}}$	porous media effective heat capacity	$\mathrm{J}/^o\mathrm{Cm}^3$
ρ_s	rock density	$\mathrm{kg/m}^3$
σ	reflection coefficient	–
σ_e	electric conductivity	S/m
Σ_e	(electric) salt sieving term	S/m
ω	salt mass fraction	–
ω_0	reference salt mass fraction	–

Table 7.2: Nomenclature METROPOL equations

separately from cation flux, as was shown in Chapter 6, we merely consider a dependence on the reflection coefficient and introduce an effective molecular diffusivity D_{eff}:

$$D_m = D_{\mathrm{eff}}(1-\sigma)$$

The **heat conductivity tensor** is defined as

$$\mathbf{H} = (n\lambda_f + (1-n)\lambda_s)\mathbf{I} + \rho_f c_f \alpha_{L,T} - \alpha_{T,T})\frac{\mathbf{q}\cdot\mathbf{q}}{|\mathbf{q}|} + \alpha_{T,T}|\mathbf{q}|\mathbf{I} \tag{7.11}$$

The **salt sieving** term is corrected for the streaming potential, as presented in Chapter 3.

$$\Sigma_e = \sigma\frac{k}{\mu} + \frac{(T_+ - T_-)k_e M_s}{F\rho\omega} \tag{7.12}$$

At this point, we introduce a new coefficient K_e, which is a correction of the streaming potential on the **hydraulic mobility** k/μ:

$$K_e = \frac{k}{\mu} + \frac{k_e^2}{\sigma_e} \tag{7.13}$$

The **coefficient of chemical osmosis** is extended with the membrane potential term as follows:

$$\Lambda_e = \frac{k}{\mu}\sigma\frac{RT\nu}{M_s} \quad - \quad \frac{k_e u_{\text{eff}} RT}{\sigma_e} \tag{7.14}$$

or

$$\Lambda_e = \frac{k}{\mu}\sigma\frac{RT\nu}{M_s} \quad - \quad \frac{k_e(T_+ - T_-)RT}{F\rho\omega} \tag{7.15}$$

The first term of these equations was present in the original METROPOL code, however all dependencies were represented by a single lumped parameter. Here, two versions are given: a simple one, with constant (effective) mobility and electrical conductivity and one with a mass fraction dependent electrical conductivity.

The **reflection coefficient** is represented by three different descriptions. The first expression assumes the reflection coefficient to be constant throughout the domain, the second option is based on the simple description of Katchalsky and Curran and the third version is the approximate formula derived by Bolt and Groenevelt, valid for moderate to high concentrations. These expressions have been discussed in detail in Chapter 2.

$$\begin{aligned}
\sigma &= \sigma_0 \\
\sigma &= 1 - \frac{\omega}{\omega_0} \\
\sigma &= \sigma_{bolt} = \frac{12 M_s \ln 2}{\beta\rho\omega b^2} - \frac{\pi^2}{(\sqrt{\beta\rho\omega/M_s}\, b)^3}
\end{aligned}$$

7.4 Test cases

7.4.1 Simple computational domain

In order to validate the adapted code, a number of numerical experiments was conducted. In the first experiment, a rather simple domain was chosen, to allow us to compare the numerical results with a simple closed form solution. Then, a somewhat more complex, yet theoretical set-up was used to test the model. Finally, the aforementioned experiment of Keijzer was numerically simulated.

In the first numerical experiment, we define a simple geometry that consists of a one-dimensional, homogeneous clay soil with a certain length b. With c_0 and c_a the initial and ambient concentrations, and zero initial pressure and no-flow conditions at the boundaries, the analytical solution reads

$$c = c_0 - \frac{c_0 - c_a}{2} \sum_{i=0}^{\infty} (-1)^i \left[\text{erfc} \frac{-(x + 2b(i+1))}{2\sqrt{Dt}} + \text{erfc} \frac{x - 2bi}{2\sqrt{Dt}} \right], \tag{7.16}$$

for the concentration, and

$$p = \frac{a(c_0 - c_a)}{2} \left(\sum_{i=0}^{\infty} (-1)^i \left[\text{erfc} \frac{-(x + 2b(i+1))}{2\sqrt{\varepsilon t}} + \text{erfc} \frac{x - 2bi}{2\sqrt{\varepsilon t}} \right] - \right. \tag{7.17}$$

$$\left. \sum_{m=0}^{\infty} (-1)^m \left[\text{erfc} \frac{-(x + 2b(m+1))}{2\sqrt{Dt}} + \text{erfc} \frac{x - 2bm}{2\sqrt{Dt}} \right] \right), \tag{7.18}$$

for the pressure. Here, the following definitions were introduced:

$$p_0 = \sigma \nu RT(c_0 - c_a) \tag{7.19}$$

$$\varepsilon = \frac{DnS\mu}{k} \tag{7.20}$$

$$a = \frac{\lambda}{\frac{k}{\mu} - SD} \tag{7.21}$$

$$\lambda = \sigma \nu RTk/\mu, \tag{7.22}$$

where D is a diffusivity, σ is the reflection coefficient, ν a dissociation constant, R the gas constant, T temperature, n is porosity, S is storativity, k is permeability, μ is viscosity and i and m are dummy variables.

Table 7.3 lists the values for the model parameters and Figure 7.1 shows the development in space and time of the concentration and the pressure. A particularly low value for the reflection coefficient has been adopted to assure convergence. The graphs for the analytical solution of concentration and pressure are depicted in Figure 7.1.

Now, in METROPOL, we set up a domain as before, subdivided in 200 grid blocks in the x-direction and one grid block in the y- as well as the z-direction. More grid blocks did not improve the results and slowed down computations. The finite domain extends for 5 meters, as in the analytical model. In the Appendix listings of three METROPOL input files are shown used for this problem. On

parameter	symbol	value
initial concentration	c_0 (mol/m^3)	60
ambient concentration	c_a (mol/m^3)	6
porosity	$n(-)$	1
intrinsic permeability	k (m^2)	$1 \cdot 10^{-16}$
diffusion coefficient	D(m^2/s)	$1 \cdot 10^{-9}$
temperature	T(^{o}C)	20
storativity	S(1/Pa)	$1 \cdot 10^{-8}$
reflection coefficient	$\sigma(-)$	0.0001
gas constant	R (Jmol/K)	8.314
dissociation constant	ν (-)	2
dynamic viscosity	μ (kg/ms)	$1.004 \cdot 10^{-3}$
length of domain	L (m)	5

Table 7.3: *Values of the model parameters, simple analytical model*

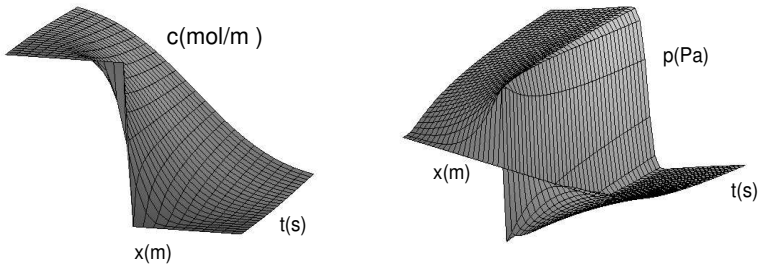

Figure 7.1: Space-time plot of analytical solutions of pressure and concentration

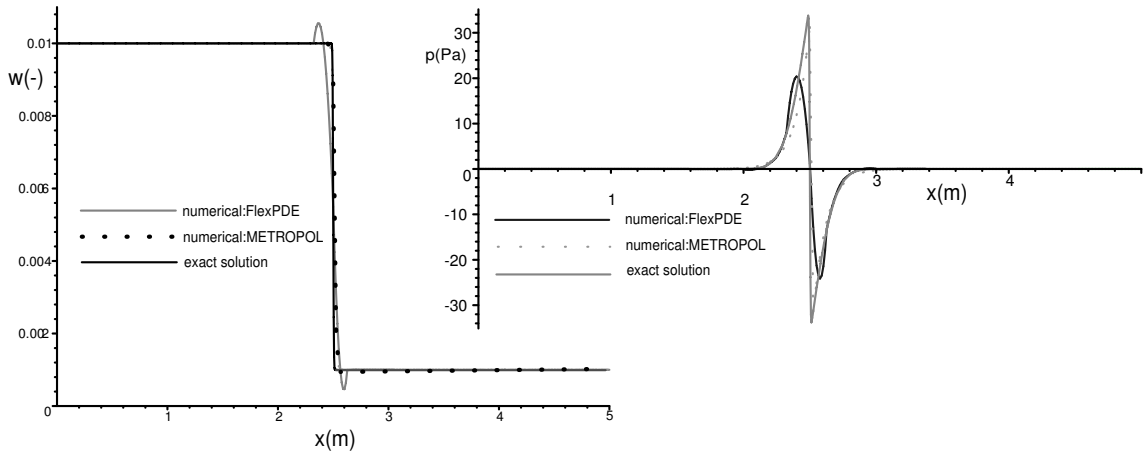

Figure 7.2: Concentration and pressure profiles; comparison of METROPOL results with exact solution and numerical results of FlexPDE; time is $10^4 s$

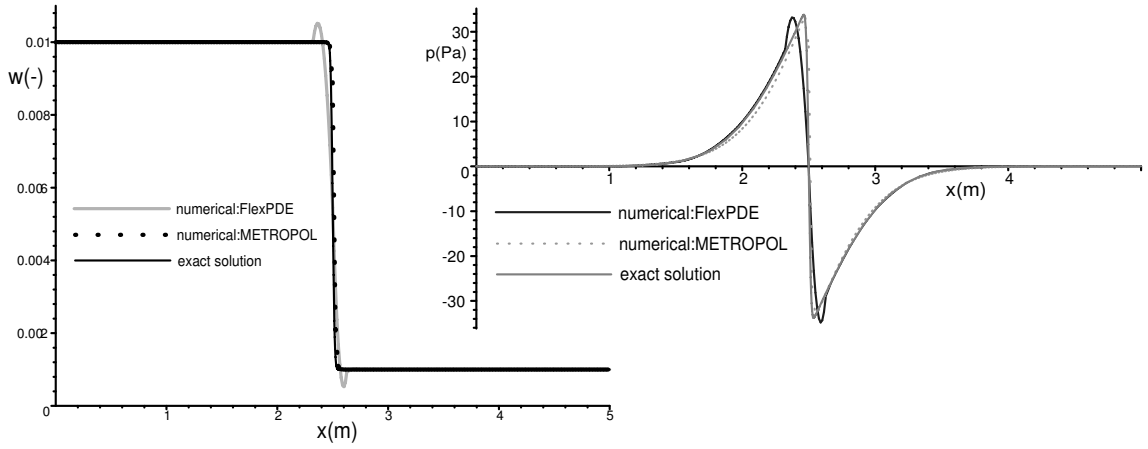

Figure 7.3: Concentration and pressure profiles; comparison of METROPOL results with exact solution and numerical results of FlexPDE; time is $10^5 s$

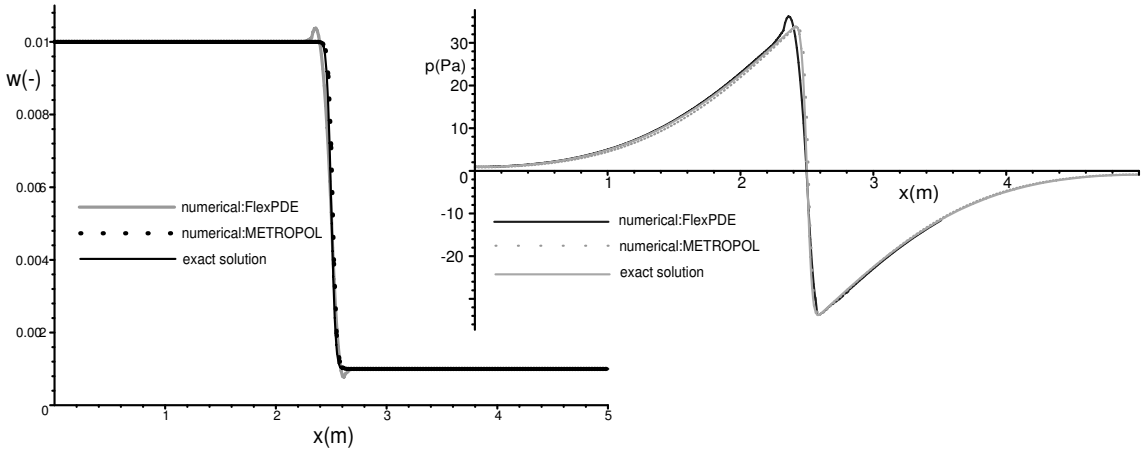

Figure 7.4: Concentration and pressure profiles; comparison of METROPOL results with exact solution and numerical results of FlexPDE; time is $5 \cdot 10^5 s$

the first page of the Appendix, the general script (USEFIL) file used is shown, as well as the mesh input file. The second page shows the general input file. In Figures (7.2), (7.3), (7.4) and (7.5), the comparison of the exact solution with the numerical results of METROPOL and the numerical results of FlexPDE are depicted. The output times are $t = 10^4 s$, $t = 10^5 s$, $t = 5 \cdot 10^5 s$ and $t = 10^6 s$ respectively.

From these graphs we observe that the results of the numerical modelling with FlexPDE are not entirely satisfactory for small times. This is because the initial salt profile implies a large salt concentration gradient. The pressure profile shows an obvious anomaly at the location of the initial salt concentration gradient. However, the FlexPDE results show somewhat better correspondence with the exact solution than the METROPOL results for larger times.

We also show the influence of electro-osmosis in this numerical experiment. For a somewhat higher reflection coefficient $\sigma = 0.0015$, a constant electrical conductivity $\sigma_e = 0.1$ S/m, and an electro-osmotic permeability of $k_e = 6.3 \cdot 10^{-10} \mathrm{m}^2/\mathrm{Vs}$, the pressure development by combined chemical and electro-osmosis is shown in Figure 7.6. For completeness, the numerical solution for the situation without electro-osmosis and the comparison with the exact solution are shown. The FlexPDE results are, again, not exact near the location of the salt concentration gradient. The METROPOL results compare not as well with the exact solution as the previous results. This is attributed to the fact that the reflection coefficient is higher, and hence the non-linear term in the pressure equations is more significant.

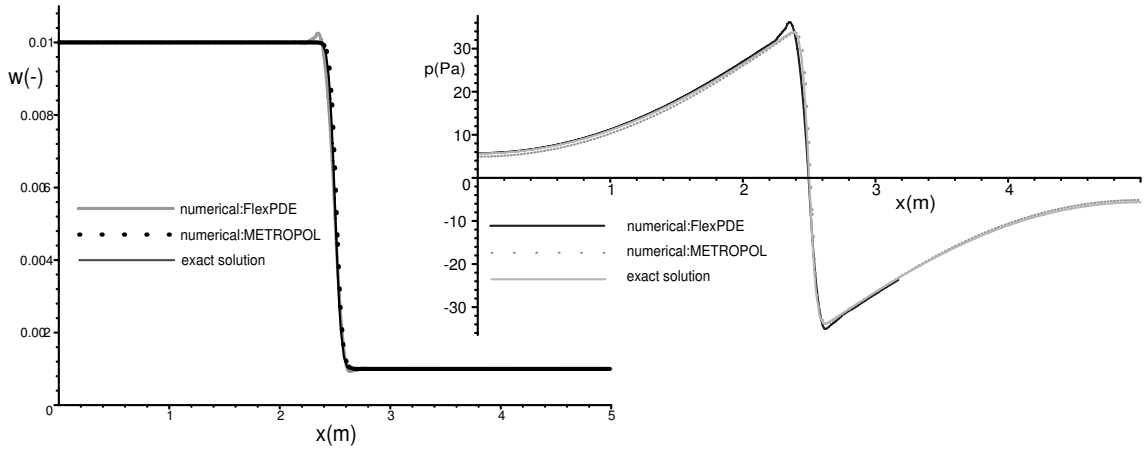

Figure 7.5: Concentration and pressure profiles; comparison of METROPOL results with exact solution and numerical results of FlexPDE; time is $10^6 s$

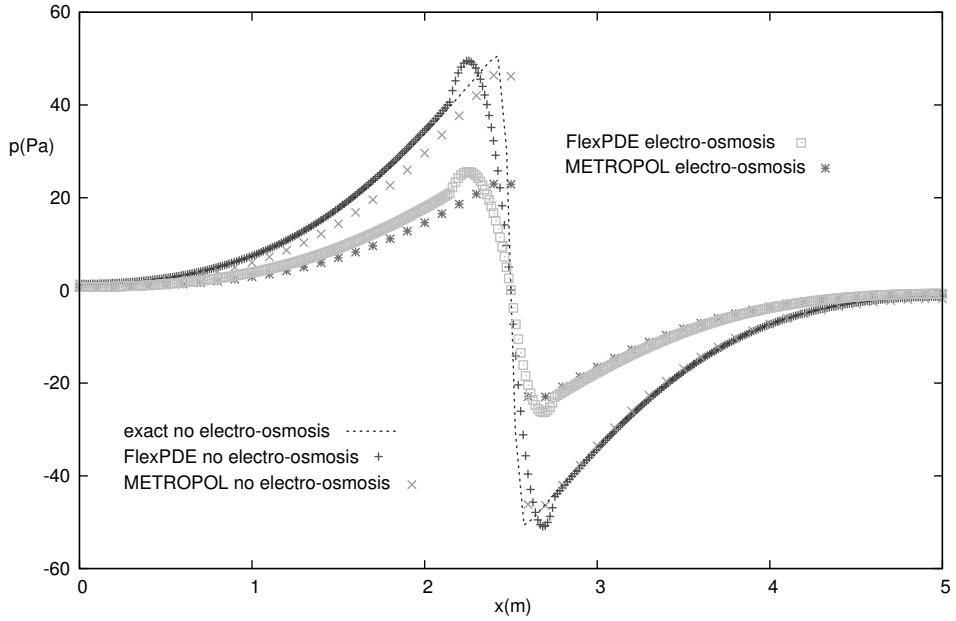

Figure 7.6: Electrochemical osmosis; comparison of numerical methods

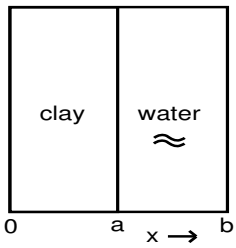

parameter	value in clay	value in water
$n(-)$	0.5	1
$T(K)$	298	298
$k(\mathrm{m}^2)$	$1 \cdot 10^{-19}$	$1 \cdot 10^{-13}$
$D(\mathrm{m}^2/\mathrm{s})$	$1.9 \cdot 10^{-12}$	$1.5 \cdot 10^{-9}$
$S_s(1/\mathrm{Pa})$	$1 \cdot 10^{-8}$	$4.6 \cdot 10^{-10}$
σ(-)	0.024	0
length (m)	$a = 0.05$	$b = 0.1$

Figure 7.7: *Simple composite domain and relevant parameters*

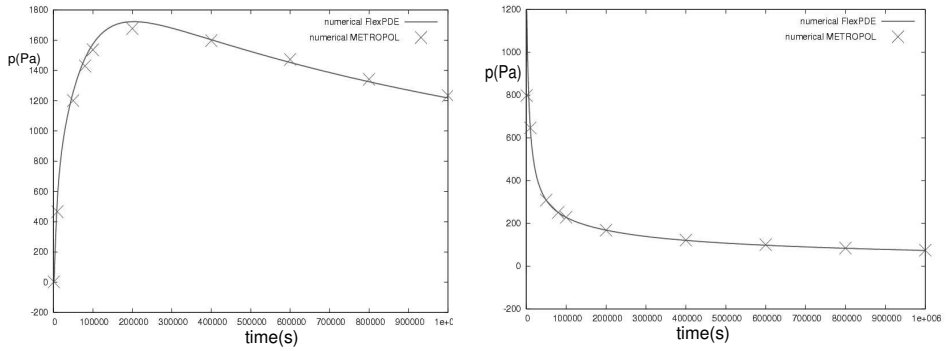

Figure 7.8: Pressure profile simple composite domain at x=0.03m (left) and x=0.05m (right)

7.4.2 Simple composite domain

The second model consists of the domain, shown in Figure 7.7, i.e. composed of a saturated clay region and a water region. The graphs in Figure 7.8 show the comparisons between the results of the numerical calculations of the time profiles for pressure in the middle of the clay and at the interface. The comparison with the FlexPDE results is very good.

7.4.3 Keijzer domain

The third model is called the Keijzer model, referring to experiments performed by Keijzer [63], where a bentonite clay under an overburden pressure of 4 bar, was subjected to a salt concentration gradient; the model setup is identical to the one presented in chapter 5, except for some slightly alterated values of the reflection coefficient, the diffusion coefficients and the compressibilities. The corresponding domain is shown in Figure 7.9.

Figures (7.10) and (7.11) show the correspondence of the numerical results

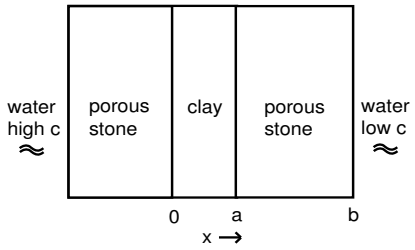

parameter	value in clay	value in porous stone
c_i (mol/l)	0.1	0.1 (l), 0.01 (r)
$n(-)$	0.5	0.56
$k(\mathrm{m}^2)$	$1.2 \cdot 10^{-19}$	$1 \cdot 10^{-13}$
$D(\mathrm{m}^2/\mathrm{s})$	$2.6 \cdot 10^{-13}$	$1.2 \cdot 10^{-10}$
$T(^oC)$	25	25
$S_s(1/\mathrm{Pa})$	$1 \cdot 10^{-8}$	$2 \cdot 10^{-6}$
σ(-)	0.024	0
length (mm)	$a = 2.3$	$b - a = 7.2$

Figure 7.9: *Modelling domain Keijzer experiment and relevant parameters*

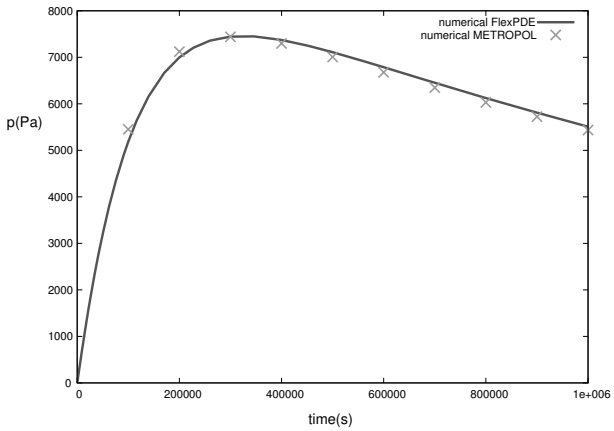

Figure 7.10: Time profile pressure for Keijzer experiment; comparison FlexPDE and METROPOL

generated with METROPOL and those generated with FlexPDE. Although this correspondence is not perfect, this graph shows that it is possible to model a real experiment with METROPOL. Choosing the time step and the convergence parameters, however, turned out to be quite a nuisance, which makes this a very inconvenient method of modelling an osmosis problem, especially if we compare this to the ease of use of FlexPDE. The sharp incline of pressure in time, the aforementioned high initial salt concentration gradients and the large difference between, for example, permeability between regions, are factors that complicate numerical matters greatly. But most problems arise because of the relatively high non-linearity of the pressure equations.

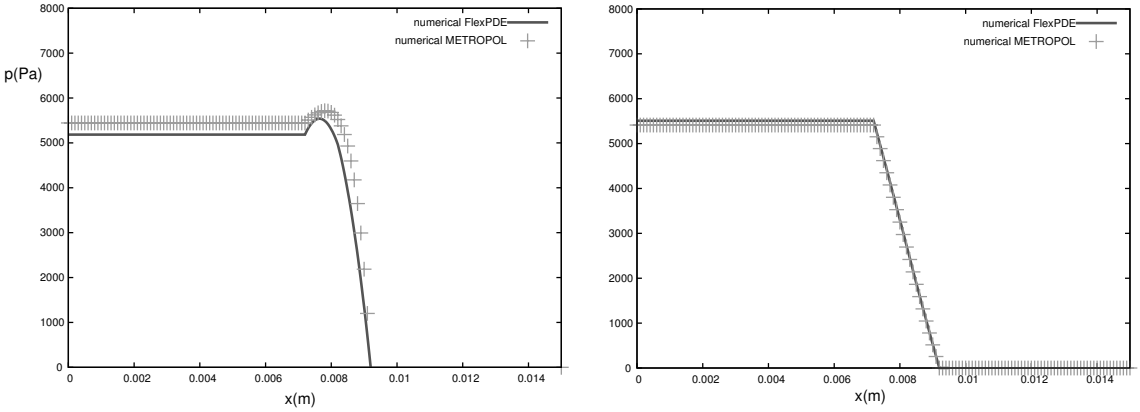

Figure 7.11: Pressure profile across setup for Keijzer experiment; comparison FlexPDE and METROPOL; $t = 10^5 s$ and $t = 10^6 s$

7.5 Using METROPOL: conclusions

In this chapter, three distinct chemical osmosis problems were simulated to show the applicability of the adapted METROPOL code for modelling the influence of osmosis on groundwater flow and solute transport. The METROPOL code was adapted for chemical and electro-osmosis, and a dependence of the reflection coefficient of concentration was introduced.

Generally speaking, simple models without any extremities such as sharp transitions or high salt concentration gradients, can be modelled without major problems with METROPOL. However, because of the nature of the solver in the code, coupled effects can be modelled correctly only to a certain extent. The pressure equations are assumed to be nearly linear. Consequently, the non-linear pressure equations are solved only once per coupling iteration. This was evidently done to limit the computational time. However, strong coupling behaviour will therefore be difficult to simulate accurately. As the chemical osmosis term, in the problems under consideration, is relatively large, this is a major disadvantage. It is therefore only recommended to use the code for osmosis problems if the coupling term is relatively small. To make the code really suitable for dealing with problems of osmosis, there is no other option than to rewrite the solver code to make the pressure equations go through the full inner iterative scheme as well.

```
METROMESH INPUT
MESH ID: meshos_ex8
PROJECT: test
mesh for simple example
END HEADING
NUMBER OF POINTS
201 2 2
CORNERS
0.0 0.0 0.0
50 0.0 0.0
50 0.1 0.0
0.0 0.1 0.0
0.0 0.0 0.1
50 0.0 0.1
50 0.1 0.1
0.0 0.1 0.1
EDGE 1
1
EDGE 2
1
EDGE 3
1
EDGE 4
1
EDGE 5
1
EDGE 6
1
EDGE 7
1
EDGE 8
1
EDGE 9
1
EDGE 10
1
EDGE 11
1
EDGE 12
1
SURF 1
1
SURF 2
1
SURF 3
1
SURF 4
1
SURF 5
1
SURF 6
1
VOLUME
1
OUTPUT OPTIONS
1 1 0 0 0 0
```

```
USEFIL
MESH INPUT: 2iosm_ex.in
MESH: 2iosm_ex11.mes
MESH PRINT: 2iosm_ex.prn
METROPOL-3 INPUT: 2ios_ex.in
METROPOL-3 PRINT: test.prn
METROPOL-3 UNFORMATTED OUTPUT: 2ios_ex.unf
```

```
METROPOL-3 INPUT
MESH ID: meshos_ex8
PROJECT: osmosis simple example 2
test run
END HEADING
0
002
51 150000 1e-4 1e-4
151 150000 1e-2 1e-2
151 150000 1e-2 1e-2
1e-4 1e-4 1e-2 1e-2 1e-2 1e-2 500 1e10 1e5
0 0 0 0
998.2 0 0 0 0 0
1 1.004e-3
0 0
0.58 4186
DISTRIBUTED DATA
startcos2_ex.in
startpos_ex.in
starttos2_ex.in
cmat.in
densm.in
kxos_ex.in
kxos_ex.in
kxos_ex.in
zero.in
zero.in
zero.in
poros_ex.in
compros_ex.in
zero.in
zero.in
diffmos_ex.in
zero.in
zero.in
2dfxos_ex.in
2dfxos_ex.in
2dfxos_ex.in
zero.in
zero.in
zero.in
zero.in
zero.in
zero.in
zero.in
zero.in
zero.in
zero.in
zero.in
zero.in
zero.in
zero.in
zero.in
zero.in
BOUNDARY CONDITIONS
SURFACE 1
1
1,200,1,1
SURFACE 2
1
1,200,1,1
SURFACE 3
1
200,200,1,1
SURFACE 4
1
1,200,1,1
SURFACE 5
1
1,1,1,1
SURFACE 6
1
1,200,1,1
OVERWRITE
0
INTERNAL PRESSURE
0
INTERNAL SALT MASS FRACTION
0
INTERNAL TEMPERATURE
0
PROFILE POINTS
0 0 0
ELEMENTS FOR SUBROSION
0 0 0
OUTPUT TIMES
6
1e5
1 1 1 1 1 1
5e5
1 1 1 1 1 1
1e6
1 1 1 1 1 1
2.5e6
1 1 1 1 1 1
5e6
1 1 1 1 1 1
1e7
1 1 1 1 1 1
```

Summary

In problems of groundwater flow and solute transport in clayey soils subject to salt concentration gradients, chemical and electro-osmosis can be too important to disregard, as is commonly done in geohydrology. In this thesis, we consider the quantification of these coupled effects to be able to simulate experiments and natural situations involving possible chemically and electrically driven water flow.

After a general introduction in **Chapter 1**, in **Chapter 2** we follow the route from clay structure to chemical osmosis: the building blocks of clay are negatively charged platelets that, when compacted in soil, impose electrical restrictions on charged particles that migrate through the clay under a variety of gradients. This means that the clay can be considered to be a semi-permeable membrane, and when a salt concentration gradient is present, all the conditions for chemical osmosis are met. The water flux, under these circumstances, is therefore dependent on the pressure gradient as well as the salt concentration gradient. It is shown that it can depend on gradients of electrical potential as well, in which case we speak of electro-osmosis. Assuming we may extend Darcy's law linearly with a salt concentration and an electrical potential gradient, the corresponding coupling parameters are called the reflection coefficient in the case of chemical osmosis and the electro-osmotic permeability in the case of electro-osmosis. After a review of some of the occurrences and applications of these processes, we list different expressions available for the reflection coefficient and the electro-osmotic permeability. For the former, the different formulas are compared; in the case of the latter coefficient, it is shown how certain assumptions can reduce all expressions to one particular formula. Finally, some aspects of two additional parameters, i.e. the electrical conductivity and the diffusion coefficient are discussed.

To obtain a full model for simulating osmotic processes in groundwater, the equations that follow from non-equilibrium thermodynamics are derived in **Chapter 3**. The equations are partly based on existing formulas. A number of aspects however, have been adapted because of serious shortcomings in equations appearing in literature. Along with some general mass balance equations, we are now equipped with the relevant modelling tools.

In **Chapter 4**, the complete set of equations is presented and utilized, where we derive analytical solutions for simplified, general situations. These solutions clearly show the simultaneous development of pressure and concentration profiles due to osmosis. The simplified setup is then used to gain some insight in issues that relate to osmosis. For example, we present the different timescales involved with modelling osmosis in groundwater, and we justify some assumptions introduced in this study. The influence of osmosis on molecular diffusion of a tracer is investigated, and the importance is shown of the choice of the dependence of the reflection coefficient on salt concentration. In addition, we show how our model correctly describes the limiting behaviour of the reflection coefficient.

Chapter 5 puts the model to the test: two chemical osmosis experiments from literature - one performed in the laboratory and one in a field situation - are modelled, where the emphasis is on the applicability of assumptions used to obtain (semi-)analytical solutions. It is shown by dimensional analysis how the storage parameters of the system determine this applicability. Furthermore, the frequently applied Boussinesq approximation is shown not too hold for problems involving osmosis in groundwater.

The real challenge is to apply the extension of Darcy's law including chemical as well as electrical effects. In **Chapter 6** the influence of the membrane potential on the osmotic pressure and concentration development is studied. The value of the membrane potential found in a particular experiment is derived from theoretical first principles. Furthermore, the membrane potential induces an electro-osmotic counterflow, that can be turned off by (virtual) shortcircuiting the experimental setup. The model of Chapter 5, extended with electro-osmosis, is shown to be able to simulate the transient buildup and decline of pressure, as well as the evolution of concentration and electrical potential. The effect of shortcircuiting is shown to correspond with letting the electrical parameters pass to zero.

In **Chapter 7**, the results are presented of adapting an existing finite element groundwater code with chemical and electro-osmosis. This code, called METROPOL, is used to model groundwater flow and solute transport in, for example, conditions of high salt concentration gradients. The existing, incorrect term for salt concentration driven water flow was adapted and electrical coefficients were added. To test the code, some sample problems were constructed. First, a simple setup for comparison with analytical and other numerical results was used. This showed that METROPOL produced better results for situations with high salt concentration gradients than some other (simple) numerical codes. As the models were made more complicated however, METROPOL turned out to be more and more unsuitable for our purposes. The solver assumes the pressure equations to be nearly linear: when chemical osmosis becomes considerable, this leads to convergence and accuracy problems.

- Chapter 2 and parts of Chapter 4 form the basis of a review paper on aspects the reflection coefficient, to be submitted to a journal yet unknown
- Parts of Chapters 3 and 5 have appeared as the article: **S. Bader**, H. Kooi 2005 *Modelling of solute and water transport in semi-permeable clay membranes: comparison with experiments* Advances in Water Resources **28** 203-214
- Parts of Chapter 4 have appeared as a paper in the (refereed) proceedings of Symposium on the mechanics of physicochemical and electromechanical interactions in porous media 2003
- Chapter 6 is a transcription of the paper **S. Bader, K. Heister** *The effect of membrane potential on development of chemical osmotic pressure in compacted clay* Submitted to Transport in Porous Media

Samenvatting

De gebruikelijke manier om grondwaterstroming modelmatig te beschrijven is met behulp van de wet van Darcy. Het is echter bekend dat in bepaalde situaties, zoals die veelvuldig voorkomen in Nederland, deze vergelijking niet altijd voldoet. Namelijk, in kleibodems kan de stroming van grondwater ook beïnvloed worden door aanwezige zoutgradienten. Dit komt door een proces dat we kennen als chemische osmose: een semi-permeabel membraan, zoals klei, laat geladen deeltjes in beperkte mate door terwijl het geen belemmering vormt voor water. Dit betekent dat, wanneer een zoutgradient aanwezig is, chemische osmose verantwoordelijk zal zijn van het stromen van water van de zoete kant naar de zoute kant van het membraan. Nu blijkt dat dit wiskundig beschreven kan worden door de wet van Darcy uit te breiden met een term gerelateerd aan de zoutgradient. Sterker nog, dit geldt evenzeer voor elektrische potentiaalgradienten, waar we het elektro-osmose noemen en temperatuurgradienten (thermo-osmose).

In dit proefschrift hebben we een wiskundig model opgesteld om de rol van chemische en elektro-osmose in grondwaterstroming te beschrijven om zo de gelijktijdige ontwikkeling van druk, zoutconcentratie en elektrische potentiaal te kunnen voorspellen. Dit is met name gedaan om de uitkomsten van experimenten te verklaren, die uitgevoerd zijn in laboratoria en in het veld om deze effecten aan te tonen.

Na de introductie in **Hoofdstuk 1**, zien we in **Hoofdstuk 2** hoe uit de interne structuur van klei volgt, waarom osmose een rol kan spelen: klei bestaat uit negatief geladen plaatjes, die bij het samendrukken van klei, elektrische restricties opwerpen voor ionen die door de klei bewegen. Dit betekent dat klei gezien kan worden als een semi-permeabel membraan. Als nu ook een zoutgradient aanwezig is, gaat chemische osmose een rol spelen. We nemen aan dat de wet van Darcy uitgebreid kan worden met chemische osmose en elektro-osmose door de Darcy flux lineair af te laten hangen van de zoutgradient en de potentiaalgradient. De zogenaamde koppelingsparameters die hiermee samenhangen zijn de coefficienten die de relatie tussen stroming van water en deze gekoppelde processen weergeven. In het geval van chemische osmose is dit de reflectiecoefficient, die de mate van semi-permeabiliteit weergeeft, en de zg. elektro-osmotische permeabiliteit in het

geval van elektro-osmose. Behalve een uitgebreid overzicht van het voorkomen en toepassingen van de processen, worden in een groot deel van het tweede hoofdstuk deze parameters onder de loep genomen. Er wordt gekeken naar beschikbare theoriën in de literatuur en deze worden vergeleken, en waar nodig, gecorrigeerd. Ook andere parameters die van belang zijn in dit werk, passeren de revue, zoals daar zijn de diffusiecoefficient en de coefficient voor elektrische geleiding.

Om een volledig model voor het simuleren van osmose in grondwater op te stellen, worden de vergelijkingen afgeleid in **Hoofdstuk 3**. Hoewel voor een deel gebaseerd op bestaande formuleringen, worden belangrijke tekortkomingen daarin gecorrigeerd. Verder worden algemene vergelijkingen voor behoud van massa van water en opgeloste stoffen gegeven.

In **Hoofdstuk 4** passen we deze vergelijkingen toe. Door schaling houden we een een simpele set van vergelijkingen over waarvoor we betrekkelijk eenvoudige oplossingen kunnen bemachtigen waaruit algemene eigenschappen van osmose in grondwater kunnen worden gededuceerd. Zo kijken we bijvoorbeeld naar de verschillende tijdschalen die van belang zijn en beschouwen we het loslaten van een tracer onder invloed van osmose.

In **Hoofdstuk 5** beschrijven we hoe twee experimenten uit de literatuur, één uitgevoerd in het laboratorium en één in het veld, zijn gemodelleerd, en kijken we of de opbouw van druk en het verval van concentratie, zoals waargenomen in deze experimenten, gesimuleerd kan worden. De nadruk ligt hier op de toepasbaarheid van de aannames die we gebruiken om tot de versimpeling van de vergelijkingen te komen. Het blijkt dat de parameter die samendrukbaarheid van de bodem en het water combineert het belangrijkste is in deze analyse. Een bepaalde eigenschap blijkt er ook voor te zorgen dat de zogenaamde Boussinesq aanname, die vaak wordt gebruikt, in ons geval taboe is.

Wanneer ook elektrische effecten worden meegenomen in het modelleren, gaan aanzienlijk veel meer processen een rol spelen. Dit wordt aangetoond in **Hoofdstuk 6**. Hier wordt verslag gedaan van experimenten aan de zogenaamde membraanpotentiaal en zijn invloed op de opbouw van osmotische druk. De membraanpotential ontstaat wanneer ionen migreren door een poreus medium. Positief en negatief geladen ionen blijken onder invloed van bijvoorbeeld een geladen poreuze medium, niet allemaal even snel te bewegen. Omdat ze toch als één zout 'opereren', ontstaat een elektrische potentiaal die zorgt dat de verschillende ionen bij elkaar blijven. Deze membraanpotentiaal is gemeten in een experiment waar, zoals in vorige beschreven experimenten, klei wordt blootgesteld aan een zoutgradient, en met behulp van een geavanceerd model blijkt de waarde van deze potentiaal te volgen uit theoretische overwegingen. Nu wekt de membraanpotentiaal op zijn beurt ook weer een elektro-osmotische waterstroming op die de stroming door chemische osmose tegenwerkt. Dit blijkt nu niet alleen geobserveerd te zijn tijdens

het experiment, maar kan ook worden verklaard met behulp van het model. Een belangwekkend resultaat is dat het kortsluiten van de opstelling om het effect van de membraanpotentiaal te duiden, overeen blijkt te komen met het 'op nul zetten' van een parameter in de vergelijkingen.

In **Hoofdstuk 7** ten slotte, wordt verteld hoe de bestaande computercode METROPOL is aangepast, opdat simulaties met chemische en elektro-osmose gedaan kunnen worden. Deze grondwatercode, gebaseerd op de eindige elementenmethode, wordt normaliter gebruikt om bijvoorbeeld verval van radio-actieve stoffen in een zeer zoute bodem te voorspellen. In dit werk laten we zien hoe de code nu ook geschikt wordt om experimenten te modelleren waar osmose een rol speelt. Hiertoe zijn drie verschillende modeldomeinen opgesteld: een zeer simpele, om vergelijking met analytische oplossingen mogelijk te maken, een wat meer realistischer domein, en één domein waarmee een in Hoofdstuk 5 eerder genoemd experiment wordt nagebootst. Het blijkt echter dat de solver die aan de basis ligt voor METROPOL ongeschikt is om met grote niet-lineaire effecten in de drukvergelijkingen om te gaan: *a priori* is het namelijk een veronderstelling in de code dat deze effecten klein zijn, dit om rekentijden te verkorten. Wanneer chemische osmose een aanzienlijke rol speelt, steken onvermijdelijk convergentie- en nauwkeurigheidsproblemen de kop op. Bij kleine 'osmotische aberraties' is de code echter zeer geschikt en geeft betere resultaten dan andere programma's.

- Hoofdstuk 2 en delen van Hoofdstuk 4 vormen de basis van een overzichtsartikel over verschillende aspecten van de reflectiecoefficient; dit wordt opgestuurd naar een nader te bepalen tijdschrift

- Delen van Hoofdstukken 3 en 5 zijn verschenen als het artikel: **S. Bader**, H. Kooi 2005 *Modelling of solute and water transport in semi-permeable clay membranes: comparison with experiments* Advances in Water Resources **28** 203-214

- Delen van Hoofdstuk 4 zijn verschenen als een artikel in de (peer reviewed) proceedings van het Symposium on the mechanics of physicochemical and electromechanical interactions in porous media 2003

- Hoofdstuk 6 is een betrekkelijk directe transcriptie van het artikel **S. Bader, K. Heister** *The effect of membrane potential on development of chemical osmotic pressure in compacted clay* hetgeen is opgestuurd naar het tijdschrift Transport in Porous Media

Glossary

- **abnormal osmosis** The flow of water due to a concentration difference in the opposite direction as expected by chemical osmosis; explained by electro-osmosis induced by a membrane potential [71]
- **anion exclusion** The restrictions imposed by the double layers on anions meaning to migrate through a clay sample, also called Donnan exclusion or negative adsorption
- **anomalous osmosis** According to Gu, Lai (a49), Mow the flow rate of solvent in a charged porous membrane is not proportional to the concentration difference; this flow rate is called anomalous osmosis
- **bi-ionic potential** The counterpart of membrane potential for solutions of different ionic composition
- **capillary osmosis** Additional osmotic water flux due to slipping of solute particles near the surface of clay platelets; when the size of the particles is larger than the roughness of the surface, there is a phase-separation at the surface, such that a layer that can act as a lubricant will develop [21]
- **cataphoresis** See electrophoresis
- **chemical osmosis** Water flow due to a gradient of chemical potential/concentration; chemical osmosis is strictly connotated with the presence of a semi-permeable membrane (like clay), that permits the passage of solvent, whereas it omits the passage of solute; the word *osmosis* is derived from the greek word $\omega\sigma\mu o\sigma$, meaning 'to push'
- **chemico-osmosis** See **chemical osmosis**
- **chemico-osmotic mobility** The coefficient relating the salt concentration gradient gradient to the specific discharge
- **counter-advection** The advection induced by the chemico-osmotic flux

- **diffuse double layer** A clay surface and the ionic distribution in its vicinity due to surface negative electric charge
- **diffusion osmosis** water transport due to diffusion of dissolved solutes/clay particles [94]; electro-osmosis could be seen as a special case of this, because diffusion-osmosis also deals with the dragging along of water by the cations
- **diffusion potential:** according to Bolt [9], diffusion potential is the electrical potential due to a salinity gradient, caused by different ionic transport numbers; it is built up of a liquid-junction potential (the fluid) and a membrane potential (the membrane)
- **diffusiophoresis** The transport of particles in a concentration field due to the formation of diffuse (and mobile) adsorption layers of neutral molecules or ions formed at the surface of the particles [21]
- **disjoining pressure** The additional pressure in a thermodynamically equilibrium interlayer compared to the pressure in the bulk solution [21]
- **DLVO theory** Theory of stability of lyophobic colloids; Derjaguin Landau Verwey Overbeek theory
- **Donnan exclusion** Negative adsorption of anions due to the repulsion of these ions near the negatively charged surface
- **Donnan osmosis** water flow due to concentration difference between cations in a clay solution and in a salt solution on one hand and anions in a clay solution and in a salt solution on the other hand [59]
- **Donnan potential** Difference between clay solution potential and salt solution potential [59]
- **Dorn effect** See migration potential
- **Dufour effect** Heat flow due to an chemical potential difference
- **electro-endosmosis** See electro-osmosis
- **electro-migration** The transport of ions in the pores under the influence of an electric field
- **electro-osmosis** Water flow due to an electrical gradient; if an electric potential is applied across a clay mass, cations are attracted to the cathode. There is an excess of cations in the (wet) clay, due to the net negative charge on the clay particles. As these cations migrate to the cathode, they drag water with them, causing water movement towards the cathode [80]

- **electro-osmosis permeability** Coefficient representing electro-osmosis: k_e m^2/Vs
- **electrophoresis** When an electrical potential gradient is applied, charged double layer particles are attracted electrostatically to one of the electrodes and repelled from the other; electrophoresis involves discrete particle transport through water (electro-osmosis involves water transport) [80]
- **electrosedimentation** See migration potential
- **exclusion potential** The electrical potential difference, according to Revil [98], caused by the electrical restrictions of the membrane, see membrane potential
- **filtration efficiency** See reflection coefficient
- **Gouy Chapman theory** Theory of the diffuse double layer [115]
- **Hittorf transport number** Relative mobility of an ion: ratio of ion mobility and sum of mobilities of all ions
- **hyperfiltration** See salt-sieving
- **iontophoresis** Movement of (large) ions due to an electrical potential gradient, used in medicine
- **liquid junction potential** A potential in an electrolyte needed to compensate different transport numbers of ionic constituents
- **membrane potential** Electrical potential (difference) equal to the liquid-junction potential plus the exclusion potential [98] or merely the potential caused by the restrictions of the membrane itself [9]
- **microfiltration** Designates a membrane separation process similar to ultrafiltration but with even large membrane pore size allowing particles in the range of 0.2 to 2 micrometers to pass through. The pressure used is generally lower than that of ultrafiltration processes.
- **membrane efficiency** See reflection coefficient
- **migration potential** When charged colloidal particles dispersed in a liquid phase sink to the bottom due to gravity, a potential difference is generated known as migration of sedimentation potential
- **nanofiltration** Same as ultrafiltration, but with much smaller pores, hence a finer form of filtration; not as fine as reverse osmosis though.

- **negative adsorption** In a diffuse double layer, anions are repelled from the surface, as if they are negatively adsorbed
- **negative (anomalous) osmosis** The osmotic flow of electrolyte solutions through a charged porous membrane that occurs from the concentrated side to the dilute side (K and C)
- **normal osmosis** See **chemical osmosis**
- **osmosis** In general the name for water flow caused by a salt concentration gradient in the presence of a semi-permeable membrane. In this study, and often in soil science, the general name for non-hydraulic water transport. The former process then is called chemical osmosis. Other examples are electro-osmosis and thermo-osmosis
- **osmotic selectivity coefficient** See reflection coefficient
- **osmotic pressure** The pressure π that must be applied to stop the flow caused by osmosis
- **Peltier effect** Heat flow due to an electrical potential difference
- **reflection coefficient** Parameter that expresses the extent of semi-permeability of a membrane
- **reverse osmosis** Hydraulically driven water transport in the presence of a counteracting osmotic gradient [63]; reverse osmosis, hyperfiltration and salt-sieving are the same phenomenon; it is the 'finest' form of filtration; as with ultrafiltration, nanofiltration and microfiltration, selection of particles is based on charge an size properties.
- **salt sieving** When salt water is pushed trough a clay, solutes may be sieved through the clay because of geometrical restrictions (reverse osmosis, ultrafiltration etc.) or because of electrical restrictions; the latter effect is called hyperfiltration of salt-sieving
- **Saxen's law** Denotes the equivalence between streaming potential and electro-osmosis
- **sedimentation potential** See migration potential
- **Seebeck effect** Electrical current due to a temperature gradient.
- **self potential** Sum of potentials measured in soils: consist of streaming and membrane potential

- **Soret effect** See thermophoresis
- **streaming current** Electrical current as well as current of discrete charged particles due to water transport [80]
- **streaming potential** Electrical potential difference due to water flow: a hydraulic head difference induces a migration of double layer charges that make for a potential difference [80]
- **thermo-electricity** See Seebeck effect
- **thermo-osmosis** Flow of liquid, driven by a temperature gradient
- **thermophoresis** Flow of ions due to a temperature gradient [21]
- **ultrafiltration** movement of solute relative to solvent, induced by a mechanical pressure [62]
- **zeta potential** Electrokinetic potential in the double layer at the interface between a particle which moves in an electric field and the surrounding liquid [91]

Nomenclature

b	double layer thickness	m
$\bar{c}_i$	ion concentration within the membrane	mol/m^3
c_f	salt concentration	mol/m^3
c_i	ion concentration	mol/m^3
c_s	concentration of solute	mol/m^3
f_i	friction coefficient	$-$
g	acceleration of gravity	m/s^2
g_f	parameter relating σ_f and concentration	S/m
h	hydraulic head	m
k	intrinsic permeability	m^2
k_T	thermo-osmotic permeability	m^2/Ks
k_e	electro-osmotic permeability	m^2/Vs
l_t	water film thickness	$\mathring{A}$
m	cementation exponent	-
n	porosity	-
n_i	number of moles of i	-
n_0	reference porosity	-
p	pressure	Pa
p_0	reference pressure	Pa
q	energy per volume element	J/m^3
q_i	ion concentration on solid	mol/m^3
$\mathbf{q}$	specific discharge	m/s
s	non-dimensional DDL quantity	-
s	entropy of a volume element	J/(K m^3)
s	mass of absorbed solute per unit area of solid matrix	kg/m^2
t	time	s
t_i^0	free solution ionic transport number	-
t_i	microscopic Hittorf transport number of an ion	-
u	mobility	m^2/Vs
u	double layer parameter	-
u	internal energy per unit volume element	J/m^3

u_i	mobility of ion i	m^2/Vs
v	volume element	m^3
v_i	velocity of constituent i	m/s
w	relative thickness mobile layer DDL	-
x	position	m
x_m	molar fraction	-
y	relative thickness immobile layer DDL	-
A	area	m^2
B	counter-ion surface mobility	m^2/Vs
C	capacitance	F
$\mathcal{C}$	cation exchange capacity	meq/g
C_s	capacitance of porous medium	F
C_f	capacitance of fluid	F
D	effective diffusion coefficient of porous medium	m^2/s
D_0	free diffusion coefficient of salt in water	m^2/s
D_f	free diffusion coefficient of salt in water	m^2/s
$\mathcal{D}_i$	microscopic diffusion coefficient of ion	m^2/s
D_i	diffusion coefficient of ion	m^2/s
D_r	effective diffusion coefficient corrected for retardation	m^2/s
E	cation exchange capacity	mol/kg
F_0	formation factor	$-$
F	Faraday constant	C/mol
F_l	driving force on liquid phase	N
$\mathcal{H}$	parameter used in the calculation of k_e	m^2/Vs
I_i	production of i	$kg/(m^3s)$
$\mathbf{I}$	electrical current density	A/m^2
$\mathbf{J}_m$	solute mass flux relative to the porous medium	kg/m^2s
$\mathbf{J}_n$	solute molar flux relative to the porous medium	mol/m^2s
$\mathbf{J}_q$	energy flux	$J/(m^2\ s)$
$\mathbf{J}_s$	entropy flux	$J/(K\ m^2\ s)$
$\mathbf{J}_m^d$	diffusive solute mass flux relative to the solution	kg/m^2s
$\mathbf{J}_n^d$	diffusive solute molar flux relative to the solution	mol/m^2s
K_c	chemico-osmotic parameter	$Jm^3s/(kg\ mol)$
K_e	electro-osmotic parameter	m^2/Vs
K_e	hydraulic mobility corrected for electro-osmosis	m^3s/kg
K_d	distribution coefficient	m^3/kg
K_{ij}	selectivity coefficient	var.

L	typical length	m
L_D	Debye length	m
L_e	typical length of tortuous path	m
$L_{\ddot{\imath}\ddot{\jmath}}$	coupling coefficient	var.
M_s	molar mass	kg/mol
P	pressure	Pa
Q	charge density	C/m^2
Q_v	excess surface charge density	C/m^2
R	gas constant	J/(mol K)
$\mathcal{R}$	retardation parameter	-
R_m	ratio of ion–membrane friction coefficients	-
R_w	ratio of ion–water friction coefficients	-
R_{wm}	ratio of ion–water friction coefficients	-
S	entropy	J/K
S	macroscopic adsorbed mass fraction	-
S_s	effective storativity of porous medium	1/Pa
T	temperature	K or ^{o}C
T_i	macroscopic Hittorf transport number of an ion	-
U	relative mobility corrected for k_e	-
U	internal energy	J
$\bar{U}$	macroscale adsorption term	mol/ms
V	electrical potential	V
V_i	volume of i-th reservoir	m^3
$\bar{V}_s$	molar salt volume	m^3/kg
X	excess surface charge	mol/m^3
$\mathbf{X}_i$	driving forces	var.
α	soil compressibility	1/Pa
β	liquid compressibility	1/Pa
β_s	mobility of counter-ions	m^2/Vs
β_T	coefficient of thermal expansion	1/K
γ	parameter that relates fluid density to mass fraction	-
γ	relative thickness of double layer	-
γ	constant relating $\mathcal{C}$ and K_d	-
γ_f	solute activity coefficient	m^3/mol
γ_t	ratio of macroscopic and microscopic Hittorf number	-
δ	position of imaginary plane in double layer	m
ε	perturbation parameter	-
ε_r	electrical permittivity	$C^2/(Nm^2)$

ζ	zeta potential	V
η	kinematic viscosity	m^2/s
θ	water content	-
θ	effective mobility coefficient	-
κ_0	reciprocal Debye length	$1/m$
κ_e	dielectric constant	-
λ	chemico-osmotic mobility	$m^5/(mol\ s)$
Λ	effective mobility	m^2/Vs
Λ_i^e	chemico-osmotic mobility corrected for electro-osmosis	$m^5/(mol\ s)$
μ	dynamical viscosity	kg/ms
μ_i	chemical potential of i-th constituent	kg/m^4s
ν	dissocation coefficient	-
ξ	ratio of σ_s and σ_f	-
ξ	non-dimensional DDL quantity	-
π	osmotic pressure	Pa
ρ	charge density	C/m^3
ρ_f	density of fluid phase	kg/m^3
ρ_s	density of solid phase	kg/m^3
σ	reflection coefficient	-
σ_{ent}	entropy source strength	$J/(K\ m^3\ s)$
σ_e	bulk electrical conductivity	S/m
σ_f	electrical conductivity of fluid	S/m
σ_i	reflection coefficient corrected for electrical effects	-
σ_χ	surface electrical conductivity	S/m
σ_s	surface electrical conductivity	S/m
Σ	surface charge density	C/m^3
τ	tortuosity	-
ϕ	electrical potential	-
Φ	dissipation function	$J/(m^3\ s)$
ψ	(local) electrical potential	-
ψ_a	(local) wall electrical potential	-
ω	mass fraction	-
ω	solute permeability coefficient	m^2mol/Js

Bibliography

[1] Archie, G.E. 1942 *The electrical resistivity log as an aid in determining some reservoir characteristics* AIME **146** 54-67

[2] Auriault, J.L., Strzelecki, T. 1981 *On the electro-osmotic flow in a saturated porous medium* International Journal of Engineering Sciences **19** 915-928

[3] Bader, S., Kooi, H. 2005 *Modelling of solute and water transport in semi-permeable clay membranes: comparison with experiments* Advances in Water Resources **28** 203-214

[4] Barbour, S.L., Fredlund, D.G. 1989 *Mechanisms of osmotic flow and volume change in clay soils* Canadian Geotechnical Journal **26** 551-562

[5] Bear, J. 1972 *Dynamics of fluids in porous media* Dover Publications, New York.

[6] Bear, J. and Corapcioglu, Y., 1981 *A mathematical model for consolidation in a thermo-elastic aquifer due to hot water injection or pumping* Water resources Research, **17(3)** 723-736

[7] Benzel, W.M., Graf, D.L. 1984 *Studies of smectite membrane behaviour: importance of latter thickness and fabric at 20°C* Geochimica et Cosmochimica Acta **48** 1769-1778

[8] Bird, R.B., Stewart, W.E., Lightfoot, E.N. 1960 *Transport phenomena* J. Wiley and Sons, New York

[9] ed. Bolt, G.H., 1982 *Soil Chemistry B. Physical-Chemical Models* Elsevier, Amsterdam

[10] Bolt, G.H. 1955 *Analysis of the Validity of the Gouy-Chapman theory of the Electric Double Layer* Journal of Colloid Science **10** 206

[11] Bresler, E. 1973 *Non-steady transport through unsaturated soils* Soil Science Society of America Proceedings **37** 663-669

[12] Brun, T.S., Vaula, D. 1967 Ber. Bunsenges. Physik. Chem. **71** 824

[13] Carslaw, H.S., Jaeger, J.C. 1959 *Conduction of heat in solids* Oxford University Press, New York

[14] Casagrande, L. 1948 *Electro-osmosis in soils* In: Proc. 2nd ICSMFE Rotterdam **1** 218-223

[15] Casagrande, L. 1949 *Electro-osmosis in soils* Geotechnique **1(3)** 159-177

[16] Cey, B.D., Barbour, S.L., Hendry, J.L. 2001 *Osmotic flow through a Cretaceous clay in southern Saskatchewan, Canada; Cey* Canadian Geotechnical Journal **38** 1025-1033

[17] Charbeneau, R.J. 1981 *Groundwater Contaminant Transport with Adsorption and Ion Exchange Chemistry: Method of Characteristics for the Case Without Dispersion* Water Resources Research **17(3)** 705-713

[18] Corapcioglu, M.Y., 1991 *Formulation of Electro-Chemico-Osmotic Processes in Soils* Transport in Porous Media **6** 435-444

[19] Cornell, D., Katz, D.L. 1953 *Flow of gases through consolidated porous media* Ind. Eng. Chem. **45** 2145-2152

[20] Cussler, E.L. 1992 *Diffusion-Mass Transfer in Fluid Systems* Cambridge University Press, Cambridge

[21] Derjaguin, B.V. 1989 *Theory of Stability of Colloids and Thin Films* Consultants Bureau, New York

[22] Dirksen, C. 1969 *Thermo-Osmosis Through Compacted Saturated Clay Membranes* Proceedings of the Soil Science Society of America **33(6)** 821-826

[23] Domenico, P.A., Schwartz, F.W. 1990 *Physical and Chemical Hydrogeology*, J. Wiley and Sons, New York

[24] Esrig, M.I. 1968 *Pore pressures, consolidation and electrokinetics* Journal of the Soil Mechanics and Foundations Division **94** 899-921

[25] Fitts, D.D. 1962 *Nonequilibrium thermodynamics* Mc-Graw Hill, New York

[26] FlexPDE Version 2.20e1-Scripted finite element model builder and numerical solver. `http://www.pdesolutions.com`

[27] Fritz, S.J 1986 *Ideality of Clay Membranes in Osmotic Processes* Clays and Clay Minerals **34** 214-223

[28] Fritz, S.J., Eady, C.D. 1985 *Hyperfiltration-induced precipitation of calcite* Geochimica et Cosmochimica Acta **49** 761-768

[29] Fritz, S.J., Marine, I.W. 1983 *Experimental support for a predictive osmotic model of clay membranes* Geochimica et Cosmochimica Acta **47** 1515-1522

[30] Garavito, A.M., Bader, S., Kooi, H., Richter, K., Keijzer, T.J.S. 2002 *Numerical modelling of chemical osmosis and ultrafiltration across clay membranes* Developments in Water Sciences. Proceedings of the International Conference in Computational Methods in Water Resources **1** 647-653

[31] Garavito, A.M., Kooi, H, Neuzil, C. 2005 *Numerical Modeling of field experimental data concerning chemical osmosis in the Pierre Shale - South Dakota* submitted to Advances in Water Resources

[32] Ghassemi, A., Diek, A. 2003 *Linear chemo-poroelasticity for swelling shales; theory and application* Journal of Petroleum Science and Engineering **38** 199-212

[33] Ghassemi, A., Diek, A. 2002 *Porothermoelasticity for swelling shales* Journal of Petroleum Science and Engineering **34** 123-135

[34] Gray, D.H. 1966 *Coupled Flow Phenomena in Clay-water Systems* University of California, Berkeley

[35] Gray, D.H., Mitchell, J.K. 1967 *Fundamental aspects of electro-osmosis in soils; Gray, Mitchell* J. Soil Mech. Found. Div. Proc. ASCE **93** 209-236

[36] Greenberg, J.A., Mitchell, J.K., Witherspoon, P.A. 1973 *Coupled Salt and Water Flows in a Groundwater Basin* Journal of Geophysical Research **78(27)** 6341-6353

[37] Grim, R.E., Güven, N. 1978 *Bentonites. Geology, mineralogy, properties and uses* Elsevier, Amsterdam, the Netherlands

[38] Groenevelt, P.H., Bolt, G.H. 1969 *Non-equilibrium thermodynamics of the soil-water system* Journal of Hydrology **7** 358-388

[39] Groenevelt, P.H., Bolt, G.H. 1972 *Permiselective properties of porous materials as calculated from diffuse double layer theory* First Symposium of Fundamental Transport Phenomena, Haifa, Israel 241-255

[40] de Groot, S.R. and Mazur, P. 1962 *Non-equilibrium thermodynamics* North Holland, Amsterdam

[41] Gross, R.J., Osterle, J.F. 1968 *Membrane Transport Characteristics of Ultrafine Capillaries* The Journal of Chemical Physics **49(1)** 228-234

[42] Gu, W.Y., Lai, W.M., Mow, V.C. 1997 *A Triphasic Analysis of Negative Osmotic Flows through Charged Hydrated Soft Tissues* Journal of Biomechanics **30(1)** 71-78

[43] Hanshaw, B.B. 1962 *Membrane properties of compacted clays* Ph.D. thesis, Harvard University, USA

[44] Hanshaw, B.B., Coplen, T.B. 1973 *Ultrafiltration by a compacted clay membrane: II. Sodium ion exclusion at various ionic strengths* Geochimica et Cosmochimica Acta **37** 2311-2327

[45] Hanshaw, B.B., Zen, E. 1965 *Osmotic equilibrium and overthrust faulting* Geol. Soc. Amer. Bull. **76** 1379-1387

[46] Hassanizadeh, S.M. 1986 *Derivation of the Basic Equations of Mass Transport in Porous Media, Part 1. Macroscopic Balance Laws* Advances in Water Resources **9** 196-206

[47] Hassanizadeh, S.M. 1986 *Derivation of the Basic Equations of Mass Transport in Porous Media, Part 2. Generalized Darcy's and Fick's laws* Advances in Water Resources, **9** 207-222

[48] Hassanizadeh, S.M., 1999 *Upscaling equations of solute transport and biodegradation in soils* Technical report, Dept. of Civil Engineering and Geosciences, TUDelft, the Netherlands

[49] Hassanizadeh, S.M. Leijnse, A. 1995 *A non-linear theory of high-concentration-gradient dispersion in porous media* Advances in Water Resources **18(4)** 203-215

[50] Heidug, W.K., Wong, S.W. 1996 *Hydration swelling of water-absorbing rocks: a constitutive model* International Journal for Numerical and Analytical Methods in Geomechanics **20** 403-430

[51] Heister, K., Kleingeld, P.J., Loch, J.P.G. 2005 *Quantifying the effect of membrane potential in chemical osmosis across bentonite membranes by virtual short-cicuiting* Journal of Colloid and Interface Science, in press

[52] Helfferich, F. 1962 *Ion Exchange* Mc-Graw Hill, New York

[53] Helmholtz, H. 1879 Wiedemanns Annalen d. Physik **7** 137

[54] Hestenes, M.R., Stiefel, E. 1952 *Methods of conjugate gradients for solving linear systems*, J. Res. Nat. Bur. Stand. **49(1)** 409-436

[55] Hillel, D. 1998 *Environmental Soil Physics* Academic Press, San Diego

[56] van 't Hoff, J. H. 1887 *The role of osmotic pressure in the analogy between solutions and gases* Z. phys. Chem. **1** 481-508

[57] Hollenbeck, K.J., 1998 *INVLAP.M: A Matlab function for numerical inversion of Laplace transforms by the de Hoog algorithm*, `http://www.isva.dtu.dk/staff/karl/invlap.htm`

[58] Hornung, U. 1997 *Homogenization and porous media* Springer Verlag, New York

[59] Huyghe, J.M., Janssen, J.D., 1997 *Quadriphasic mechanics of swelling incompressible porous media* International Journal of Engineering Science **35(8)** 793-802

[60] Istok, J. 1989 *Groundwater modelling by the Finite Element Method* American Geophysical Union

[61] Kargol, A. 2000 *Modified Kedem-Katchalsky equations and their applications* Journal of Membrane Science **174** 43-53

[62] Katchalsky, A., Curran. P.F. 1965 *Nonequilibrium thermodynamics in biophysics* Harvard University Press, Cambridge, Ma.

[63] Keijzer, T.J.S. 2000 *Chemical osmosis in natural clayey materials* Ph.D. thesis, University of Utrecht

[64] Keijzer, T.J.S., Kleingeld, P.J., Loch, J.P.G. 1999 *Chemical osmosis in compacted clayey material and the prediction of water transport*, Engineering Geology **53** 151-159

[65] Kemper, W.D. 1961 *Movement of water as affected by free energy and pressure gradients: II. Experimental analysis of porous systems in which free e nergy and pressure gradients act in opposite directions* Proceedings of the Soil Science Society of America **25** 260-265

[66] Kemper, W.D., Evans, N.A. 1963 *Movement of water as effected by free energy and pressure gradients. II. REstriction of solutes by membranes* Soil Science Society of America Proceedings **27** 485-490

[67] Kemper, W.D., Quirk, J.P. 1972 *Ion mobilities and electric charge of external clay surfaces inferred from potential differences and osmotic flow* Proceedings of the Soil Science Society of America **36** 426-433

[68] Kemper, W.D. Rollins, J.B. 1966 *Osmotic efficiency coefficients across compacted clays* Soil Science Society of America, Proceedings **30** 529-534

[69] Kharaka, Y.K., Berry, F.A.F. 1973 *Simultaneous flows of water and solutes through geological membranes: I. Experimental Investigation* Geochimica et Cosmochimica Acta **37** 2577-2603

[70] Kooi, H., Garavito, A.M., Bader, S. 2003 *Numerical modelling of chemical osmosis and ultrafiltration across clay formations* Journal of Geochemical Exploration **78-79** 333-336

[71] Kruyt, H.R., 1952 *Colloid Science* Elsevier, Amsterdam

[72] Lakshminarayanaiah, N. 1969 *Transport phenomena in membranes* Academic Press, New York

[73] Leijnse, A. 1992 *Three-dimensional modeling of coupled flow and transport in porous media* Ph.D. thesis, University of Notre Dame

[74] van Loon, L.R., Soler, J.M., Bradbury, M.H., 2003 *Diffusion of HTO,* $^{36}Cl^-$ *and* $^{125}I^-$ *in Opalinus Clay samples from Mont Terri; Effect of Confining pressure* Journal of Contaminant Hydrology **61** 73-83

[75] Loret, B., Hueckel, T., Gajo, A. 2002 *Chemo-mechanical coupling in saturated porous media: elastic-plastic behaviour of homo-ionic expansive clays* International Journal of Solids and Structures **39** 2773-2806

[76] Malusis, M.A., Shackelford, C.D. 2002 *Chemico-osmotic efficiency of a geosynthetic clay liner* Journal of Geotechnical and Geoenvironmental Engineering **97-106**

[77] Marine I. W., Fritz S. J. 1981 *Osmotic model to explain anomalous hydraulic heads* Water Resources Research **17** 73-82

[78] Mason, E.A., Wendt, R.P., Bresler, E.H. 1972 *Test of the Onsager relation for ideal gas transport in membranes* Faraday Trans. II **68** 1938-1959

[79] Milne, I.H., McKelvey, J.G., Trump, R.P 1964 *Semi-permeability of bentonite membranes to brines* Bulletin of the American Association of Petroleum Geologists **48** 103-105

[80] Mitchell, J.K. 1976 *Fundamentals of soil behavior*, J. Wiley and Sons, New York.

[81] Mitchell, J.K. 1991 *Conduction phenomena: from theory to geotechnical practice* Geotechnique **41** 299-340

[82] Mitchell, J.K., Greenberg, J.A., Witherspoon, P.A. 1973 *Chemico-osmotic effects in fine-grained soils* Journal of the Soil Mechanics and Foundations Division 307-322

[83] Moyne, C., Murad, M.A. 2002 *Electro-chemo-mechanical in swelling clays derived from a micro/macro homogenization procedure* International Journal of Solids and Structures **32** 6159-6190

[84] Moyne, C., Murad, M. 2003 *Macroscopic Behaviour of Swelling Porous Media Derived from Micromechanical Analysis* Transport in Porous Media **50** 127-151

[85] Murad, M.A., Bennethum, L.S., Cushman, J.H. 1995 *A Multi-Scale Theory of Swelling Porous Media: I. Application to One-Dimensional Consolidation* Transport in Porous Media **19** 93-122

[86] Murad, M.A., Cushman, J.H. 1996 *Multi-scale flow and deformation in hydrophilic swelling porous media* Int. J. Engng Sci. **34(3)** 313-338

[87] Neuzil, C.E. 1982 *On Conducting the Modified 'Slug' Test in Tight Formations* Water Resources Research **18(2)** 439-441

[88] Neuzil, C.E. 1986 *Groundwater flow in low-permeability environments* Water Resources Research **22** 1163-1195

[89] Neuzil, C.E. 2000 *Osmotic generation of "anomalous" fluid pressures in geological environments* Nature **403** 182-184

[90] ed. Nielsen, D.R., Jackson, R.D., Cary, J.W., Evans, D.D 1972 *Soil water* ASA, Wisconsin

[91] van Olphen, H. 1977 *An Introduction to Clay Colloid Chemistry*, J. Wiley and Sons, New York

[92] Olsen, H.W., Giu S., Lu, N. 2000 *Critical Review of Coupled Flow Theories for Clay Barriers* Transportation Research Record **1714** 57-64

[93] Olsen, H.W. 1969 *Simultaneous fluxes of liquid and charge in saturated kaolinite* Soil Science Society of America, Proceedings **33** 338-344

[94] Olsen, H,W., Yearsley, E.N., Nelson, K.R. 1990 *Chemico-Osmosis Versus Diffusion Osmosis* Transportation Research Record **1288** Soils, geology and foundations, Washington D.C. 15-22

[95] Pamukcu, S. 1997 *Electro-chemical technologies for in-situ restoration of contaminated subsurface soils* **2** The Electronic Journal of Geotechnical Engineering

[96] Ravina, I., Zavlasky, D. 1968 *Non-linear electrokinetic phenomena: I. Review of literature* Soil Science **106** 60-66

[97] Ren, L., Chen, B., Hu, J.G. 1990 *Initial analysis on the law of reducing adhesion of soil animals* Transactions of the Chinese Society of Agricultural Engineering **6(1)** 13-20

[98] Revil, A. 1999 *Ionic Diffusivity, Electrical Conductivity, Membrane and Thermoelectric Potentials in Colloids and Granular Porous Media: A Unified Model* Journal of Colloid and Interface Science **212** 503-522

[99] Robinson, D.A. 2004 *Measurement of the Solid Dielectric Permittivity of Clay Minerals and Granular Samples Using a Time Domain Reflectometry Immersion Method* Vadose Zone Journal **3** 705-713

[100] Sauter, F.J, Leijnse, A., Beusen, A.H.W. 1993 *METROPOL user's guide* RIVM Bilthoven

[101] Saxen, U. 1892 in *"Electrokinetic Potentials", Textbook of Physical Chemistry* New York

[102] Schmid, G. 1911 *Zur Elektrochemie Feinporiger Kapillarsystems* Zhurnal fur Elektrochemie **54** 425, **55** 684

[103] Sen, P.N. 1989 *Ionic transport and membrane potential in porous media with interfacial charges* Physica A **157** 446-453

[104] Shackelford, C.D., Malusis, M.A., Olsen, H.W., 2001 *Clay membrane barriers for waste containment* Geotechnical News **19** 2-39

[105] Sherwood, J.D., Bailey, L. 1994 *Swelling of shale around a cylindrical wellbore* Proc. Roy. Soc. London A **444** 161-184

[106] Sherwood, J.D., Craster, B. 2000 *Transport of water and ions through a clay membrane* Journal of Colloid and Interface Science **230** 349-358

[107] Smoluchowksi, M. 1914 *Handbuch der Elektrizitat und Magnetismus (L. Graetz, Ed.)* **2** J.A. Barth, Leipzig

[108] Soler, J.M. 2001 *The effect of coupled transport phenomena in the Opalinus Clay and implications for radionuclide transport* Journal of Contaminant Hydrology **53** 63-84

[109] Spiegler, K.S. and Kedem, O. 1966 *Thermodynamics of hyperfiltration (reverse osmosis): criteria for efficient membranes*, Desalination **1** 311-326

[110] Staverman, A. J. 1951 *The theory of measurement of osmotic pressure* Rec. Trav. Chim. **70** 344

[111] Strauss, J.M. and Schubert, G., 1977 *Thermal convection of water in a porous medium: effects of temperature and pressure-dependent thermodynamic and transport properties* Journal of Geophysical Research **82** 2 325-333

[112] Tartar, L. 1980 *Incompressible fluid flow in a porous medium-convergence of the homogenization process* in: Non-homogeneous Media and Vibration Theory, E. Sanchez-Valencia, 368-377

[113] Tikhomolova, K.P. 1993 *Electro-osmosis* Ellis Horwood, New York

[114] Truesdell, C. 1984 *Rational Thermodynamics* Springer-Verlag, New York

[115] Verwey, E.J.W., Overbeek, J.Th.,G. 1948 *Theory of the Stability of Lyophobic Colloids* Elsevier, Amsterdam, the Netherlands

[116] Visser, G. 2002 *Reduction of adherence of clay by electro-osmosis under dynamic circumstances* M.Sc. thesis TU Delft

[117] van der Vorst, H.A. 1990 *Bi-CGSTAB: a fast and smoothly converging variant of Bi-CG for the solution of non-symmetric linear systems* preprint 633, Department of Mathematics, Utrecht University

[118] Waxman, M.H., Smits, L.J.M., 1968 *Electrical Conductivities in Oil-bearing Shaly Sands* Society of Petroleum Engineers Journal **8** 107-122

[119] Whitworth, T.M., DeRosa, G., 1997 *Geological membrane controls on saturated zone heavy metal transport* New Mexico Water Resources Research Institute, WRRI Technical Completion Report 303, Las Cruses, NM, USA

[120] Winsauer, W.O., Shearin, H.M., Masson, P.H., Williams, M. 1952 *Resistivity of brine saturated sands in relation to pore geometry* Bull. Amer. Ass. Petrol. Geol. **36** 253-277

[121] Wyllie, M.R.J., Gardner, G.H.F. 1958 *The generalized Kozeny-Carman equation II. A novel approach to problems of fluid flow* World Oil Prod. Sect. 210-228

[122] Wyllie, M.R.J., Spangler, M.B. 1952 *Application of electrical resistivity measurements to problems of fluid flow in porous media* Bull. Amer. Ass. Petrol. Geol. **36** 359-403

[123] Yeung, A.T. 1990 *Coupled flow equations for water, electricity and ionic contaminants through clayey soils under hydraulic, electrical and chemical gradients* Journal of Non-Equilibrium Thermodynamics **15** 247-267

[124] Yeung, A.T., Mitchell, K.J. 1993 *Coupled fluid, electrical and chemical flows in soil*, Geotechnique **43** 121-134.

[125] Yeung, A.T. 1994 *Electrokinetic flow processes in porous media and their applications* in Advances in Porous Media, Elsevier, Amsterdam, The Netherlands bf 2 309-395.

[126] Young A., Low P. F. 1965 *Osmosis in agrillaceous rocks* Bulletin of the American Association of Petroleum Geologists **49** 1004-1008

[127] `http://soils1.cses.vt.edu/MJE/pdf/soil/_chem/_props.pdf`

Curriculum Vitae

Samuel Bader werd geboren op 12 oktober 1977 in Breda. De middelbare school werd doorlopen op het Stedelijk Gymnasium in dezelfde stad en in 1995 werd de opleiding voortgezet aan de Universiteit Utrecht. Na zich eerst als sterrenkundige ingeschreven te hebben werd spoedig de richting natuurkunde gekozen. In 2000 studeerde hij af in de vakgroep Theoretische Natuurkunde op een onderwerp uit de hoge energiefysica. Drie maanden later, we schrijven inmiddels 2001, werd een aanvang genomen met het wetenschappelijk onderzoek waar dit proefschrift de uiteindelijke vrucht van is. De eerste drie jaar vond dit werk plaats in de vakgroep Hydrologie en Ecologie, faculteit Civiele Techniek en Technische Geowetenschappen aan de Technische Universiteit Delft, waarna hij zijn promotor en co-promotor volgde naar de Universiteit Utrecht, waar de promotie in 2005 werd afgerond in de vakgroep Environmental Hydrogeology, Faculteit Geowetenschappen. Per 5 juli is hij begonnen als onderzoeker bij het Laboratorium voor Stralingsonderzoek bij het Rijksinstituut voor Volksgezondheid en Milieu in Bilthoven.